REAL-TIME FPGA FIRMWARE FOR VGA RESOLUTION INFRARED CAMERA

A THESIS SUBMITTED TO
THE GRADUATE SCHOOL OF NATURAL AND APPLIED SCIENCES
OF
MIDDLE EAST TECHNICAL UNIVERSITY

BY

KAMİ ÇEVİK

IN PARTIAL FULFILLMENT OF THE REQUIREMENTS
FOR
THE DEGREE OF MASTER OF SCIENCE
IN
ELECTRICAL AND ELECTRONICS ENGINEERING

SEPTEMBER 2019

Approval of the thesis:

REAL-TIME FPGA FIRMWARE FOR VGA RESOLUTION INFRARED CAMERA

submitted by **KAMİ ÇEVİK** in partial fulfillment of the requirements for the degree of **Master of Science in Electrical and Electronics Engineering Department, Middle East Technical University** by,

Prof. Dr. Halil Kalıpçılar
Dean, Graduate School of **Natural and Applied Sciences** _____

Prof. Dr. İlkay Ulusoy
Head of Department, **Electrical and Electronics Eng.** _____

Prof. Dr. Tayfun Akın
Supervisor, **Electrical and Electronics Eng., METU** _____

Examining Committee Members:

Prof. Dr. Gözde Bozdağı Akar
Electrical and Electronics Engineering, METU _____

Prof. Dr. Tayfun Akın
Electrical and Electronics Engineering, METU _____

Prof. Dr. Aydın Alatan
Electrical and Electronics Engineering, METU _____

Prof. Dr. Haluk Külah
Electrical and Electronics Engineering, METU _____

Assist. Prof. Dr. Dinçer Gökçen
Electrical and Electronics Engineering, Hacettepe Uni. _____

Date: 09.09.2019

I hereby declare that all information in this document has been obtained and presented in accordance with academic rules and ethical conduct. I also declare that, as required by these rules and conduct, I have fully cited and referenced all material and results that are not original to this work.

Name, Surname: Kami Çevik

Signature:

ABSTRACT

REAL-TIME FPGA FIRMWARE FOR VGA RESOLUTION INFRARED CAMERA

Çevik, Kami
Master of Science, Electrical and Electronics Engineering
Supervisor: Prof. Dr. Tayfun Akın

September 2019, 82 pages

Infrared cameras generally require pre-processing on raw image data in order to improve the output image quality. Raw output of the infrared cameras occupies a narrow part of the available dynamic range. Contrast enhancement is one of the pre-processing operations and used for improving dynamic range of the low contrast images.

This thesis proposes an adaptive histogram equalization method for enhancing the contrast of long wavelength infrared camera output with 640×480 resolution and provides a FPGA implementation architecture of this method that operates in real-time. Proposed method aims to improve the contrast of the background and foreground details while avoiding from over-enhancement effects and preserving thermal characteristics of the frame. Design of the proposed contrast enhancement algorithm based on integration of Adaptive Double Plateaus Histogram Equalization and Weighting Mean-Separated Sub-Histogram Equalization algorithms which are two widely used contrast enhancement methods for infrared and grayscale images. Threshold calculation is rearranged in order to prevent the excessive enhancement effects. Since the proposed method is a modified version of these two methods, it named as Weighting Mean-Separated Double Plateaus Histogram Equalization.

Various contrast enhancement algorithms are implemented and compared quantitatively in MATLAB for evaluating the performance of the proposed method. FPGA implementation output is also compared with MATLAB output for testing the implementation process. Real-time image processing pipeline is designed as compatible for integration of the implemented design with targeted infrared imaging system. Test results show that the developed method improves background and foreground gray level intensity values with reducing excessive enhancement effects.

Keywords: Real-Time Image Processing, Contrast Enhancement, Histogram Equalization, Infrared Imaging, FPGA

ÖZ

VGA ÇÖZÜNÜRLÜKLÜ KIZILÖTESİ KAMERA İÇİN GERÇEK ZAMANLI FPGA YAZILIMI

Çevik, Kami
Yüksek Lisans, Elektrik ve Elektronik Mühendisliği
Tez Danışmanı: Prof. Dr. Tayfun Akın

Eylül 2019, 82 sayfa

Kızılötesi kameralar genellikle çıkış görüntüsünün kalitesini arttırmak amacıyla ham görüntü verisi üzerinde ön işleme gereksinimine ihtiyaç duymaktadır. Kızılötesi kameraların ham çıkışı mevcut dinamik aralığın dar bir kısmını kapsar. Kontrast iyileştirme, düşük kontrastlı görüntülerin dinamik aralıklarını geliştirmek için kullanılan ön işleme yöntemlerinden biridir.

Bu tez, 640×480 çözünürlüğe sahip uzun dalga boylu kızılötesi kamera çıkışının kontrastını iyileştirmek için adaptif bir histogram eşitleme yöntemi ve bu yöntem için gerçek zamanlı çalışan bir FPGA uygulaması mimarisi önermektedir. Önerilen yöntem, arka plan ve ön plan ayrıntılarının kontrastını, aşırı iyileştirme etkilerinden kaçınarak ve karedeki termal karakteristiği koruyarak iyileştirmeyi amaçlamaktadır. Önerilen kontrast iyileştirme tasarımı, kızılötesi ve gri seviyeli görüntülerin kontrastlarını iyileştirmede yaygın olarak kullanılan yöntemler olan Adaptif Çift Platolu Histogram Eşitleme ve Ağırlıklı Ortalama ile Ayrılmış Alt-Histogram Eşitleme algoritmalarının birleştirilmesine dayanmaktadır. Eşik değeri hesaplaması aşırı iyileştime etkilerini önlemek amacıyla yeniden düzenlenmiştir. Önerilen yöntem, bu iki yöntemin değiştirilmiş bir versiyonu olduğundan, Ağırlıklı Ortalama ile Ayrılmış Çift Platolu Histogram Eşitleme olarak adlandırılmıştır.

Çeşitli farklı kontrast eşitleme algoritmaları önerilen yöntemin performansını değerlendirmek için MATLAB üzerinde uygulanmış ve nicel olarak karşılaştırılmıştır. Önerilen yöntemin FPGA uygulamasının çıktıları, uygulama işleminin test edilmesi için MATLAB çıktıları ile ayrıca karşılaştırılmıştır. Gerçek zamanlı görüntü işleme hattı, uygulanan tasarımın hedeflenen kızılötesi görüntüleme sistemine entegrasyonu için, bu sistemle uyumlu olarak tasarlanmıştır. Test sonuçları, geliştirilen yöntemin, aşırı iyileştirme etkilerini azaltarak arka plan ve ön plan gri seviye yoğunluk değerlerini iyileştirdiğini göstermektedir.

Anahtar Kelimeler: Gerçek Zamanlı Görüntü İşleme, Kontrast İyileştirme, Histogram Eşitleme, Kızılötesi Görüntüleme, FPGA

To My Family

ACKNOWLEDGEMENTS

I would like to express my sincere gratitude and appreciation to my advisor Prof. Dr. Tayfun Akın for his guidance throughout my study and thesis work.

I also would like to thank Semih Genç, Ozan Kızıldağ and the other friends from Mikro-Tasarım.

Last but not least, I would like to thank my family for their continuous support and encouragement through all my life.

TABLE OF CONTENTS

LIST OF TABLES

TABLES

LIST OF FIGURES

FIGURES

CHAPTER 1

INTRODUCTION

Electromagnetic spectrum is distribution of electromagnetic radiation in terms of wavelength, frequency or energy. Electromagnetic radiation has a widely distributed spectrum from the radio waves to gamma rays. Within this wide range, human eyes can only detect wavelengths between 400 nanometers and 740 nanometers. This visible spectrum of light covers all the colors from the longest wavelength called red to shortest wavelength called violet. Visible spectrum is surrounded by ultraviolet (beyond violet) and infrared (below red) spectrums.

Infrared radiation is the part containing wavelengths from 0.74 micrometers to approximately 1000 micrometers. Infrared spectrum can be divided into five regions based on atmospheric transmittance as Near Infrared (NIR), Short Wavelength Infrared (SWIR), Medium Wavelength Infrared (MWIR), Long Wavelength Infrared (LWIR) and Very Long Wavelength Infrared (VLWIR). Human eyes are unable to see these regions because starting from the NIR region, photons do not have enough energy for triggering the chemical reaction in the eye for perceiving color of the light. Infrared detectors that include specific sensitive materials can perceive the incoming infrared radiation. These detectors are commonly used in military and civilian applications including night vision, biomedical imaging, thermography, fire detection and surveillance.

Thermal radiation is the electromagnetic wave emission made from all substances with temperature that above from absolute zero. At temperatures around room temperature, a significant portion of thermal radiation falls into the infrared spectrum. Emitted thermal radiation is collected, filtered and focused onto a detector array by thermal imaging systems. Detector array converts the incident thermal radiation into analog

signals. These signals are amplified, digitized and processed by sensor electronics for displaying the thermal image.

Thermal imaging systems vary according to the intended use. This variety can be arisen from structural requirements, such as cooling system or shutter requirements, or it can also be caused by functional requirements, such as image enhancement and/or image processing. Contrast enhancement is one of the important pre-processing operations in the infrared imaging systems. Optimal contrast enhancement varies according to the characteristics of the target and the environment to be viewed. This thesis focuses on contrast enhancement and proposes a method and its implementation for the minimizing artifacts while enhancing contrast of the thermal images.

The rest of this chapter is organized as follows: Section 1.1 provides information about infrared radiation. Section 1.2 explains acquisition techniques of the infrared images. Section 1.3 states the enhancement requirements of the infrared images. Section 1.4 emphasizes the advantages of the FPGAs on real-time image processing. Finally, Section 1.5 gives the research objectives and description of organization of the thesis.

1.1. Infrared Spectrum

Infrared radiation is the part containing wavelengths from 0.74 micrometers to approximately 1000 micrometers. Infrared spectrum can be divided into five zones according to the atmospheric transmittance of the various wavelengths as Near Infrared (NIR: 0.74 μm - 1 μm), Short Wavelength Infrared (SWIR: 1 μm - 3 μm), Medium Wavelength Infrared (MWIR: 3 μm - 5 μm), Long Wavelength Infrared (LWIR: 8 μm - 14 μm) and Very Long Wavelength Infrared (VLWIR: 14 μm – 1000 μm) as Figure 1.1 shows [1]. Note that, 5 μm - 8 μm wavelength band of the infrared spectrum is not permeable for infrared radiation due to very low atmospheric transmittance.

The NIR wavelength band was the first part of the electromagnetic spectrum outside the visible region to be discovered, by astronomer Sir William Herschel in 1800. He used an experiment setup which includes three blackened thermometers and a prism.

He measured the heat transfer of different colors of sunlight refracted by the prism with thermometers. The thermometers indicated a heat change even when placed in the dark region just beyond the red part of the rainbow pattern [2]. Herschel concluded that the cause of the heat increase in the thermometers was invisible light rays.

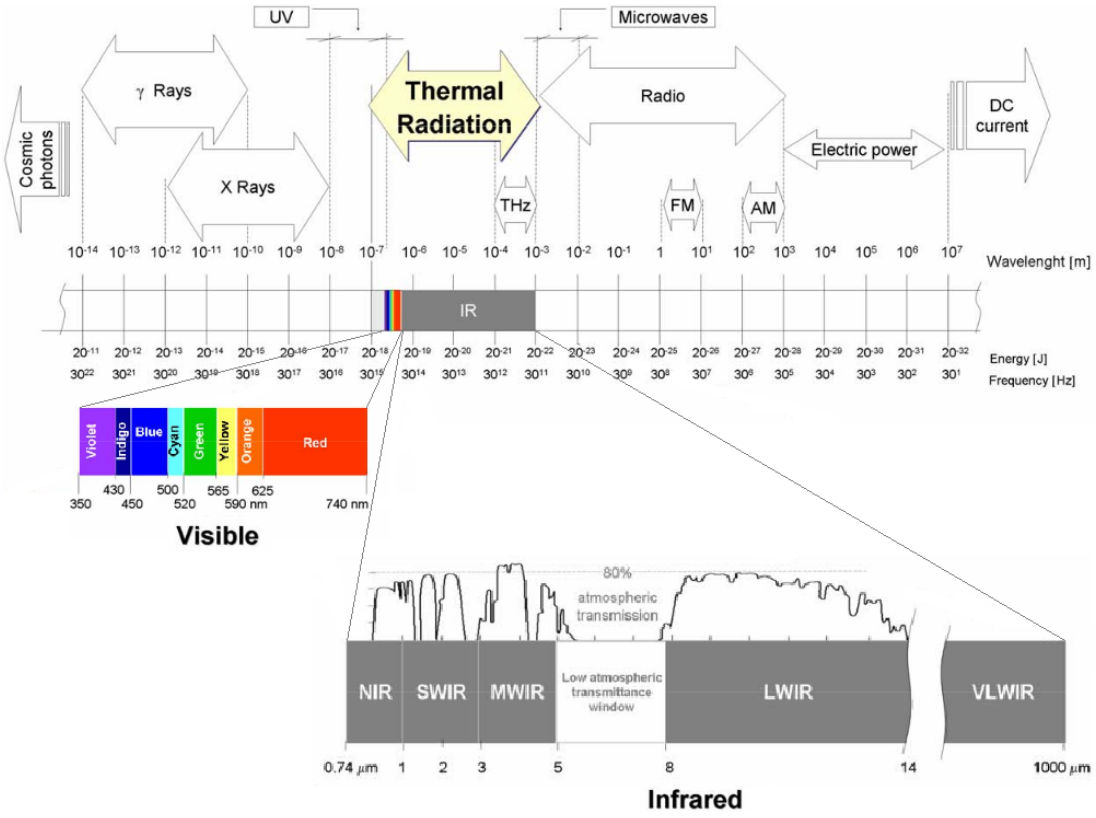

Figure 1.1. The electromagnetic spectrum [1]

Different wavebands of the infrared spectrum can be suitable for various applications. For example, NIR detectors can be used for vision systems which can operate at low-illuminated conditions or in space surveillance telescopes. SWIR detectors are suitable for detecting fluids for different purposes such as production quality tests or security. NIR and SWIR cameras are also be used for the identification of original or fake paintings as shown in Figure 1.2.

Figure 1.2. Visible image of Natura and two details in visible and NIR bands [2]

MWIR and LWIR detectors are mostly used for monitoring the thermal distribution for various purposes such as detection of thermal insulation leaks, failure detection in electrical and electronic systems, medical imaging, military surveillance and target detection and tracking systems, etc. Figure 1.3 shows the detection of unwanted high resistance connections in transformer substation with using LWIR camera.

Figure 1.3. Detection of unwanted high resistance connections in transformer substation with using LWIR camera [3]

1.2. Infrared Imaging Systems

Systems that collect radiant energy and generate an image of the subject without visible light are called infrared imaging systems. Infrared detection methods can be categorized into two main parts as photon detectors and thermal detectors. Many sensitive materials have been investigated for the increasing the performance of both detection methods. Figure 1.4 gives approximate dates of main developments for these materials.

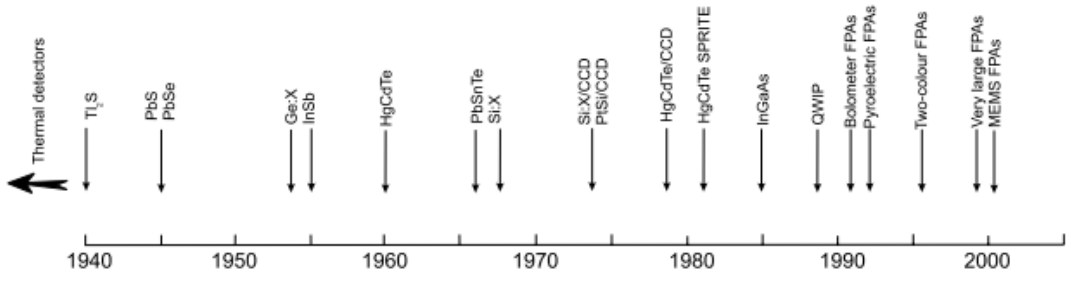

Figure 1.4. History of the development of IR detectors [4]

Incident radiation is absorbed within the material by interaction with electrons in photon detectors. Electrical output signal is observed with monitoring the changes in electronic energy distribution. Photon detectors offer both good signal-to-noise ratio (SNR) and fast response. But necessity of cryogenic cooling is main impediment that make them heavy and expensive for the common use of these detectors. In thermal detectors, electrical output signal is generated from the changes in some physical properties with respect to temperature change in absorber material which interacts with incident radiation. These detectors are more attractive devices comparing with photon detectors due to providing wider bandgap (electrical output signal depends on radiant power, but not depends on its spectral content) and lack of need of cryogenic cooling (they can operate at room temperature). Besides these advantages of the uncooled thermal detectors, their small size, reduced power consumption and lower cost make these detectors the most appropriate option for high volume applications that require relatively lower performance [4] [5].

Microelectromechanical systems (MEMS) allows the fabrication of sensitive bolometric infrared detectors on thermally isolated membranes. Figure 1.5 shows the structure of a microbolometer. Incident infrared radiation increases the temperature of the absorber material. Thermally sensitive material resistivity changes with the change of temperature related to its temperature coefficient of resistance (TCR). Resistance change is measured and electrical output signal is generated by readout circuitry (ROIC). Thermally sensitive material can also be utilized as a diode and the diode potential can also be monitored for achieving the thermal data.

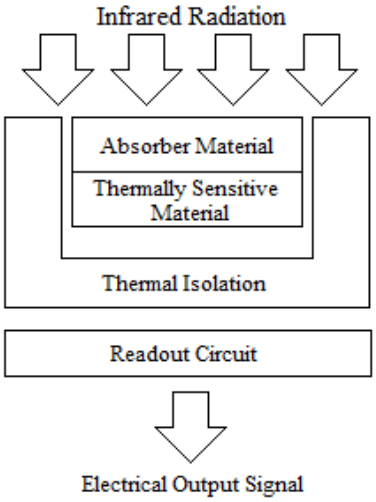

Figure 1.5. Structure of a microbolometer

METU MEMS Research and Applications Center specializes on infrared microbolometer detectors. Resistive and diode type microbolometers are designed and fabricated for a variety of applications that require a variety of performance [6-12].

1.3. Enhancement Requirements of Infrared Images

Image enhancement is an initial step of processing the digitally obtained image to an improved view of it in terms of brightness, smoothness and contrast, etc. Generally, raw infrared images are not meaningful to be understood by humans. Sensor defects (dead pixels, dead columns and dead rows), noise introduced by ROIC and non-uniformity of the sensors forms the requirement for image enhancement. Non-uniformity correction (NUC), contrast enhancement and dead pixel filtering can be done to get a better quality image.

Non-uniformity correction can be used for eliminating the fixed pattern noise which is caused by spatial and temporal non-uniformities between pixels in infrared focal plane array (IRFPA). Offset and gain corrections eliminate the offset and gain errors between pixels with using dark and flat-field frames. Dead pixel filtering is basically replacing a calculated pixel value or neighboring pixel itself with the dead pixel. There are many methods for the dead pixel correction. Median filtering is a common method for replacing the dead pixel in the raw image.

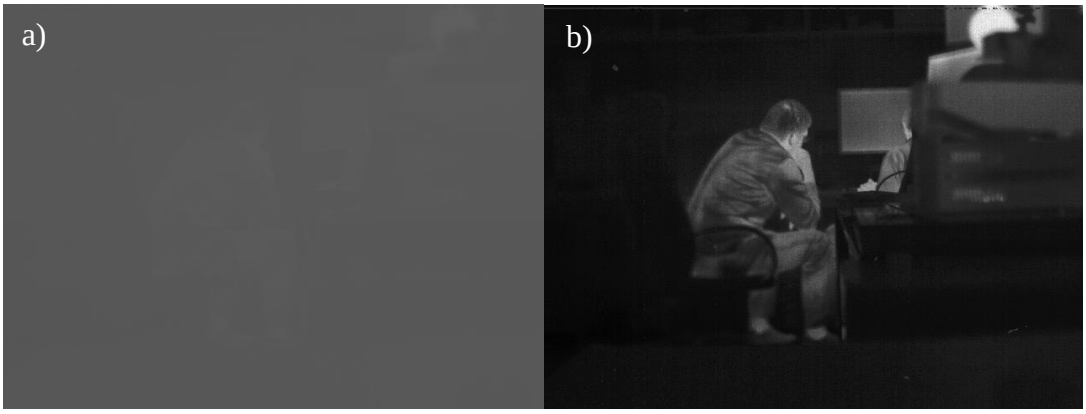

Figure 1.6. a) LWIR camera output before contrast enhancement b) Contrast enhanced image

Raw output of the infrared cameras generally occupies a very narrow part of dynamic range of the available gray levels that ROIC can generate as seen in the Figure 1.6. These low-contrast output images generally include a highly dark background and brighter detailed foreground information for white-hot infrared images. In order to enhance the low contrast infrared images, a suitable contrast enhancement method must be selected to enhance the background and foreground contrast while suppressing the noise and other artifacts of the incorrect over-enhancement.

1.4. Advantages of FPGAs on Real-Time Image Processing

Field Programmable Gate Arrays (FPGAs) are specific type of integrated circuits that offer the possibility of developing reconfigurable, custom hardware. FPGAs allow designers both rapid prototyping before the manufacturing and modifying the design even after the end-product is deployed in the field. Basic architecture of the most FPGAs is shown in Figure 1.7. Logic blocks, interconnections and input/output pins form the basic structure of FPGA. Reconfiguration capability of the interconnect matrix blocks provides implementation of custom hardware with arranging logic blocks and input/output pins. Modern FPGAs contain large internal block memories, sophisticated DSP blocks and millions of logic gates. Advanced ones contain several Central Processing Units (CPU) and Graphical Processing Units (GPU) in System on a Chip (SoC) architecture.

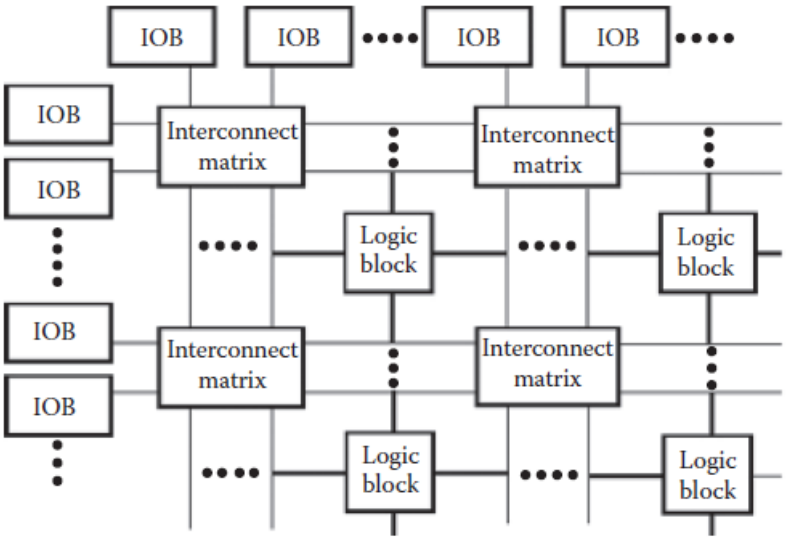

Figure 1.7. Basic structure of FPGA [13]

Since the FPGAs implement the logic required by a process by configuring separate hardware for each function, they can operate in parallel by their nature. This advantage makes FPGAs well suited to real-time image processing applications. Large chunks of image data can be processed in a pipelined structure. A synchronous image processing pipeline is given in Figure 1.8. Frames of the real-time video processed one by one without any buffer between image processing modules. Note that, Frame 1 is displayed while Frame 2 is being filtered and Frame 3 is being buffered. If this system designed as asynchronous pipeline, there must be memories between the image processing modules.

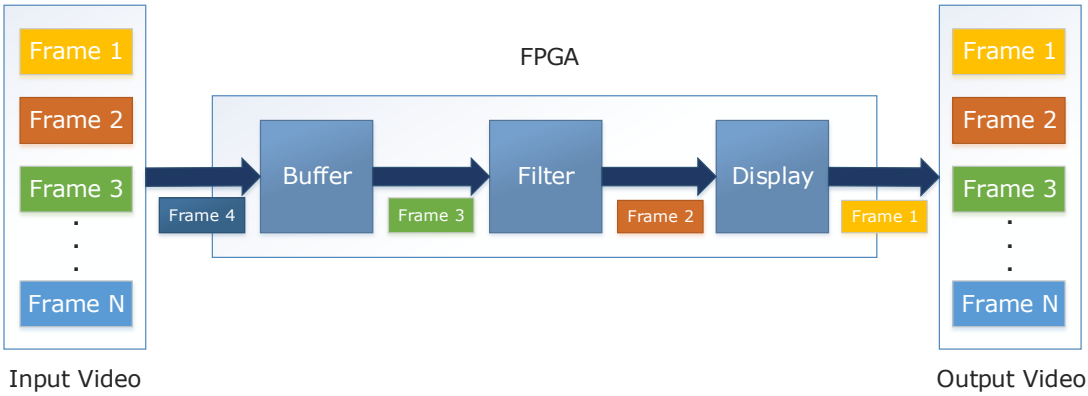

Figure 1.8. Image processing pipeline

1.5. Research Objectives and Thesis Organization

The goals of this research are;

1. To develop an adaptive contrast enhancement algorithm that enhances the offset corrected video stream input with 640×480 resolution which comes from the output of LWIR uncooled microbolometer camera in real-time.
2. To implement the developed contrast enhancement algorithm on FPGA.

LWIR uncooled microbolometer camera core and electronics are designed in Mikro-Tasarım Elektronik San. ve Tic. A.Ş. in Ankara, Turkey. Camera core that contains MT6417BA ROIC and MTAS1410X4 ASIC connected to the camera electronics. Camera electronics include MTPCB1725 FPGA Board that contains Xilinx Artix-7 XC7A100T-1CSG324C FPGA and a carrier board that includes GPIOs, power input and Camera Link output connectors. Camera electronics connected to a computer via Camera Link interface. On the computer side, there is a software that responsible for controlling the camera core and displaying the thermal video stream. Note that, developed contrast enhancement firmware will be integrated into the whole firmware that operates deserialization, offset correction and Camera Link transmission. Internal line or frame buffer is not used in the design to ensure minimum FPGA resource utilization in the contrast enhancement module. External memory is not used because of hardware limitation of the imaging system. For reducing the logic element utilization and for simplicity, mathematical operations such as multiplication and division are implemented as fixed-point operations.

Contrast enhancement module is designed with using same video controlling ports as the other modules in the whole firmware for reusability and modularity. In addition to this, all camera and enhancement variables such as frame size and dynamic range bit length are designed parametrically. IPs that performs the arithmetic operations are used from default IP catalog of the FPGA manufacturer, so it can be updated for using in the other FPGA families of Xilinx.

This thesis is organized as follows:

Chapter II discusses the contrast enhancement methods. This chapter investigates advantages and disadvantages of widely used contrast enhancement methods which target the infrared and grayscale images.

Chapter III introduces the proposed contrast enhancement method for the thermal images. This chapter also explains architecture of the FPGA implementation in depth.

Chapter IV presents the results of the implemented contrast enhancement firmware and discusses the performance of implementation by using figures of merit from similar researches. It gives performance comparison of the developed algorithm with commonly used infrared contrast enhancement methods.

Finally, Chapter V summarizes this research and presents a road map for future improvements.

CHAPTER 2

AN OVERVIEW OF CONTRAST ENHANCEMENT METHODS FOR INFRARED IMAGES

Captured raw infrared images are generally require some pre-processing operations such as contrast enhancement for increasing the dynamic range and improving the image visibility for human observers.

Contrast enhancement plays a key-role in various applications that require high dynamic range imaging such as thermography and driver assistance systems. For example, even the smallest details in the thermography images must be visible or distinguishable in order to diagnose the diseases correctly [14]. Similarly, it is vital to detect the objects on the road or on the side of the road at similar temperatures to the background in driving assistance systems. Proper contrast enhancement is again important for achieving a visible image in fog or haze [15].

Contrast stretching and histogram equalization methods are well-known methods for contrast enhancement. There are a number of different histogram equalization algorithms exist in the literature, but in order to achieve the optimum contrast, appropriate methods to the wavelength must be investigated. In addition to wavelength, methods that are used for similar characteristics to the infrared image characteristics can also be useful for the infrared contrast enhancement. For example, deep underwater raw grayscale images generally have a low contrast like raw infrared images. Investigation of the contrast enhancement methods for these images may also be useful for the infrared images.

This chapter discusses the contrast enhancement and selected contrast enhancement methods that can be suitable for infrared images. Section 2.1 introduces contrast stretching method. Section 2.2 presents histogram equalization and commonly used

histogram equalization methods: Plateau Histogram Equalization, Adaptive Double Plateaus Histogram Equalization, Weighting Mean-Separated Sub-Histogram Equalization and Contrast Limited Adaptive Histogram Equalization. Section 2.3 examines the advantages and disadvantages of the investigated contrast enhancement methods.

2.1. Contrast Stretching

Contrast stretching is the simplest technique that is used to stretch the gray level spectrum of an image between the minimum and maximum available gray levels (intensity values) so that the dynamic range of the image is filled completely. Gray level reconstruction is done by using below equation

$$G_{out} = \frac{(G_{in} - G_{min})}{(G_{max} - G_{\min})} \times G_{dmax} \qquad (2.1)$$

where G_{out} is the stretched output gray level, G_{in} is the unstretched input gray level, G_{max} and G_{min} are the maximum and minimum gray levels of the input image and G_{dmax} is the maximum available gray level of the dynamic range.

Histogram is the representation of probability distribution of the discrete valued data. A grayscale image histogram indicates the occurrence values of each gray level in available dynamic range.

Infrared image histograms generally consist of a peak region and a few pixels which are far from this region. This situation limits the stretching of the histogram and reduces efficiency of the contrast enhancement operation. Histogram clipping can be done around the minimum and maximum gray levels of the original histogram for achieving a better enhancement. Contrast stretching results from the MATLAB implementation can be seen in below figures. Raw image and its original histogram are given in Figure 2.1. Contrast stretching on non-clipped and clipped histograms are given in Figure 2.2 and Figure 2.3, respectively.

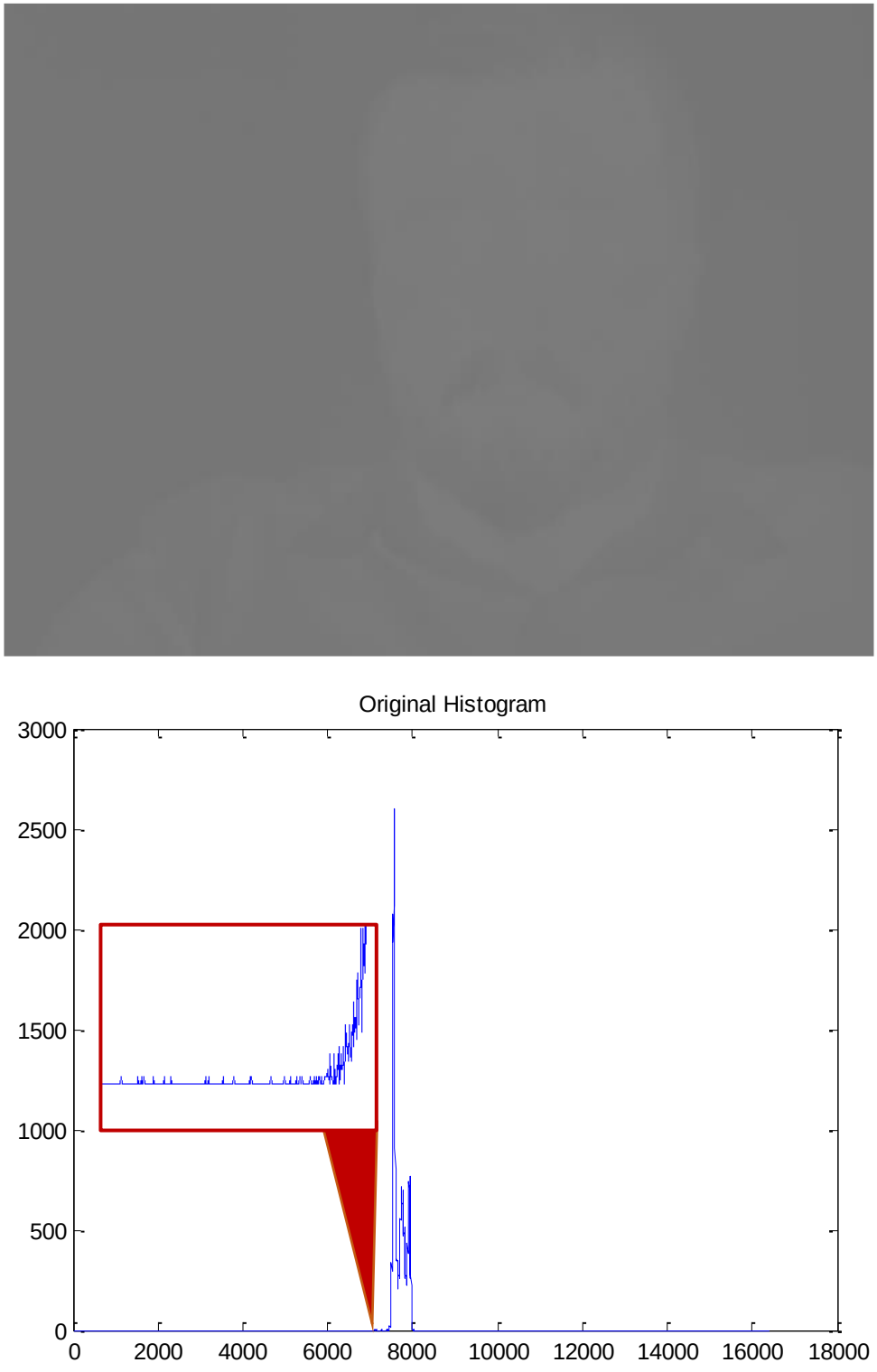

Figure 2.1. Raw infrared image and its histogram. Gray level values of some pixels are far from the meaningful histogram range.

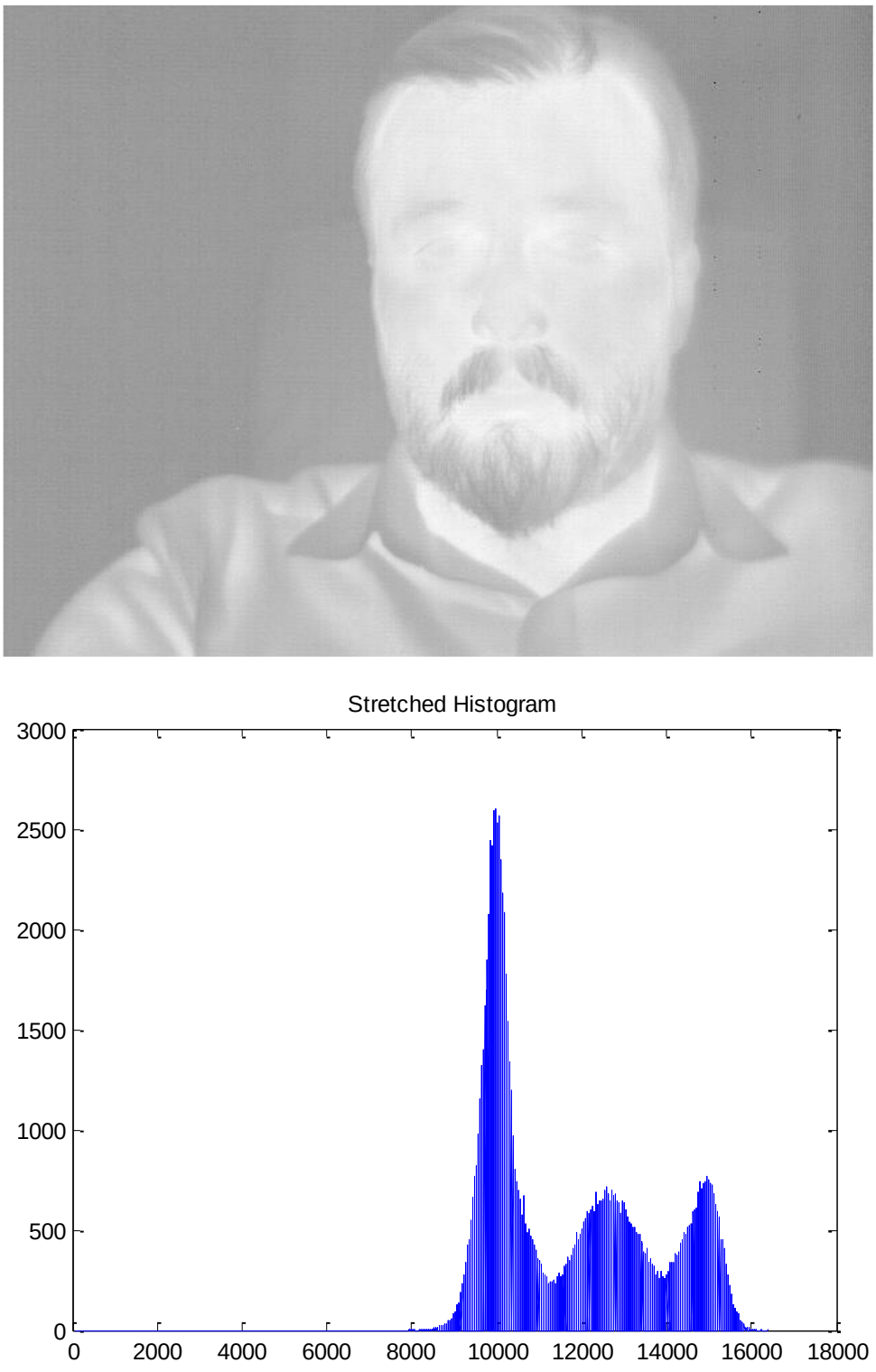

Figure 2.2. Contrast stretched image (from non-clipped original histogram) and its histogram. Pixels that far from the meaningful histogram range have limited the contrast stretching

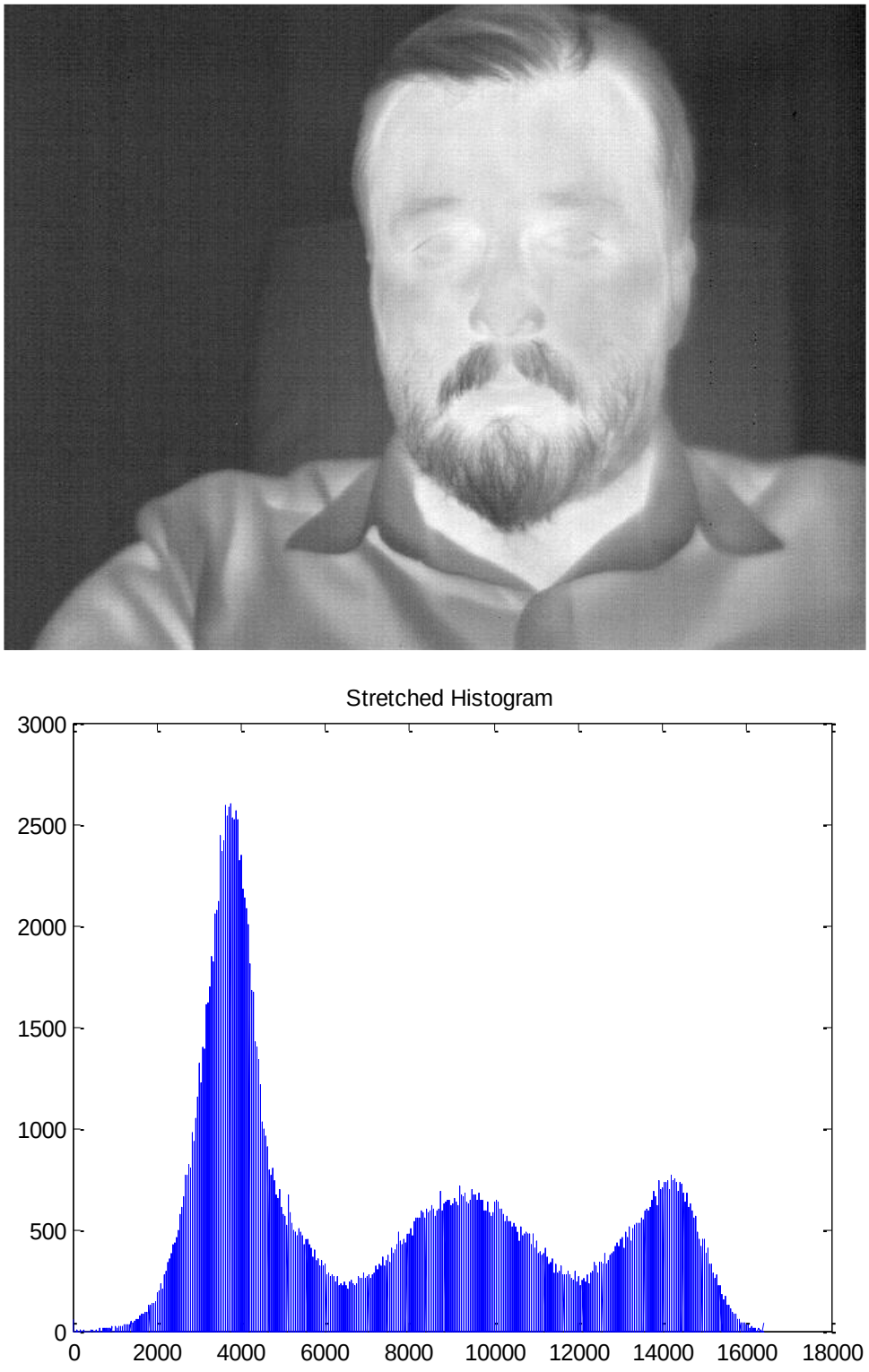

Figure 2.3. Contrast stretched image (from clipped original histogram) and its histogram. Pixels with gray levels less than 5 were clipped

2.2. Histogram Equalization

Histogram equalization is the most common method for the contrast enhancement. Frequency of appearance of the intensity values in the grayscale image can be analyzed easily with using the image histogram. Original histogram is used for constructing a monotonic mapping that results in a nearly flattened equalized histogram.

Definition of the well-equalized histogram may vary depending on the purpose of the application. From the contrast enhancement perspective, a good histogram must cover all the possible intensity values for visible spectrum gray scale images. On the other hand, this can cause the over-enhancement for the thermal images. Over-enhancement can corrupt the temperature information and cause objects to look hotter than they actually are. But if the visibility has the priority over the temperature accuracy, wide dynamic range will be more convenient. Block diagram of the histogram equalization is presented in Figure 2.4.

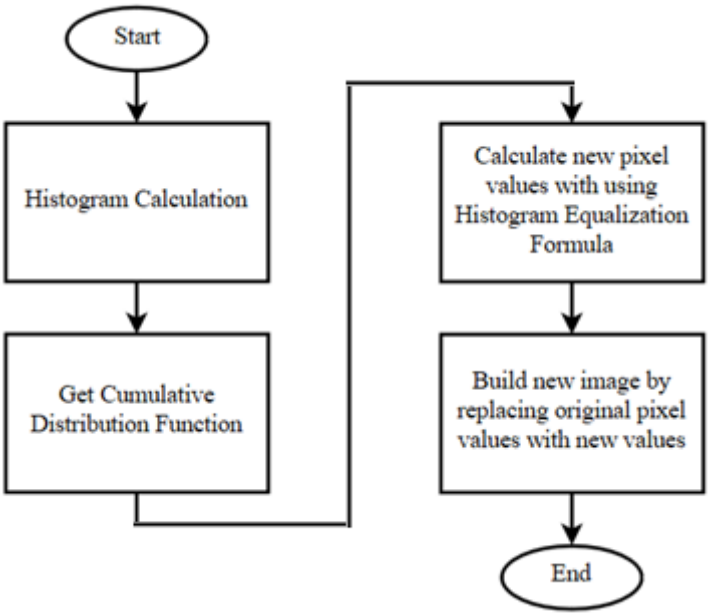

Figure 2.4. Block diagram of the histogram equalization

Probability density function (pdf) of a digital image can be calculated with

$$pdf(i) = \frac{n_i}{n_{TOTAL}} \qquad (2.2)$$

where n_i is the number of pixels in ith gray intensity level and n_{TOTAL} is the total number of the pixels in the image. After finding pdf values for each gray intensity level, cumulative distribution function (cdf) of the digital image can be calculated with

$$cdf(i) = \sum_{k=1}^{i} pdf(k) \qquad (2.3)$$

Finally, using with the histogram equalization expression, new image can be built.

$$G_{out} = round(\frac{cdf(G_{in})}{n_{TOTAL}} \times (G_{dmax} - 1)) \qquad (2.4)$$

Histogram equalization results from the MATLAB implementation are presented in Figure 2.5 (Raw image in Figure 2.1 was used as the input image). As discussed in the previous chapter, thermal images generally have two parts as background and foreground scenes. Raw image histograms also have this characteristic. Background and foreground parts can easily distinguishable from the histogram. Enhancement of these scenes must be done using the suitable methods to prevent the unwanted artifacts on images.

There are various histogram equalization algorithms that separate the raw histogram into sub-histograms exist in the literature. This separation can be done on both occurrence values and gray level values. Statistical properties such as weighting mean of the gray level values are used for dividing the histogram into vertical parts. Plateaus or thresholds are used for the grouping horizontally the particular parts of the histogram by limiting the occurrence values.

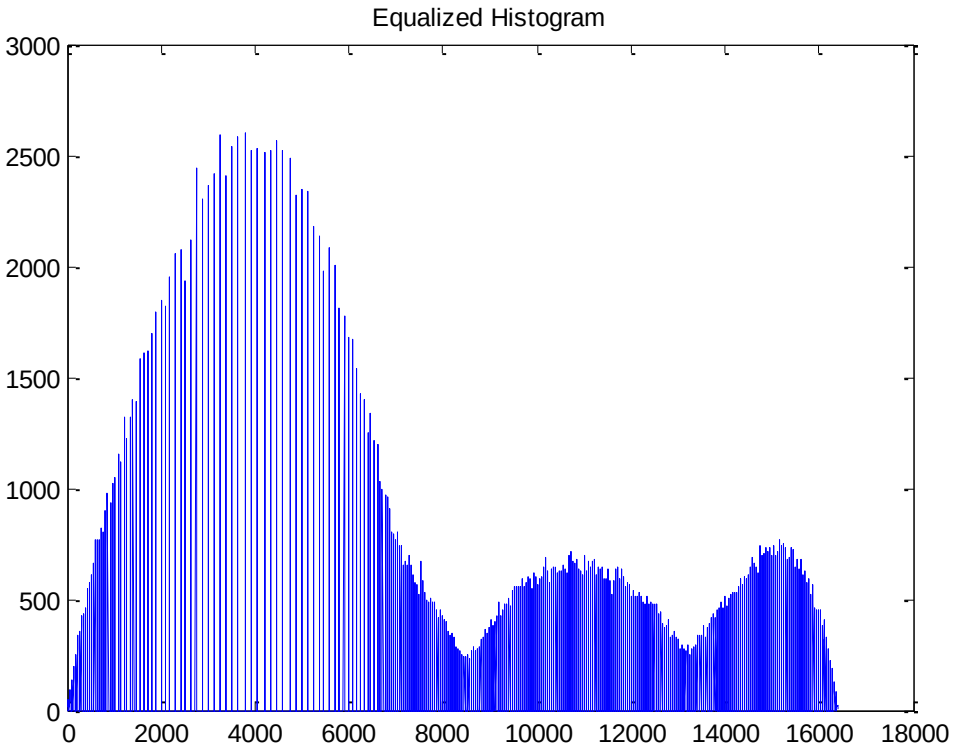

Figure 2.5. Histogram equalized image and its histogram

2.2.1. Adaptive Double Plateaus Histogram Equalization

Plateau or threshold-based histogram equalization methods are frequently used for contrast enhancement of the infrared images. Virgil E. Vickers [16] proposed the Plateau Histogram Equalization method to suppress the over-enhancement of background part of the infrared images. The drawback of this algorithm is that it uses a fixed and empirical plateau level and this limits the usage for different scenarios. Wang et al. [17] and Lai et al. [18] proposed adaptive plateau level calculation-based algorithms and hardware implementations for both methods to overcome the fixed threshold drawback of Plateau Histogram Equalization method. Adaptive threshold level is calculated by using median of local and global maximum values of the non-zero valued histogram. Enhanced image is generated with implementation of this threshold into whole histogram, and then global histogram equalization is done in the method of Wang et al. Plateau level is calculated adaptively by scaling the histogram with using the maximum value of the histogram and an empirical value for exponent, in the algorithm of Lai et al. Both methods targeted for constraining the enhancement of background scene of the infrared images with using one adaptive plateau level that calculated in different properties of the histogram. However, some detailed foreground information with improper gray intensity values can still be combined with other gray levels, as a result the details of the foreground cannot be fully enhanced with these histogram equalization methods.

Liang et al. [19] proposed Adaptive Double Plateaus Histogram Equalization (ADPHE) method as an improvement of Plateau Histogram Equalization. Figure 2.6 shows the steps of the ADPHE algorithm. Up and down threshold levels are calculated with

$$T_{UP} = \frac{POLAR(1) + \ldots + POLAR(P)}{\mathrm{P}} \quad (2.5)$$

$$T_{DOWN} = \frac{\min\{N_{total}, T_{UP} \times L\}}{\mathrm{M}} \quad (2.6)$$

where POLAR is the set of local maximum values and P is its size, N_{total} is total pixel number of original image, L is total number of non-zero statistic and M is total number of the original gray levels.

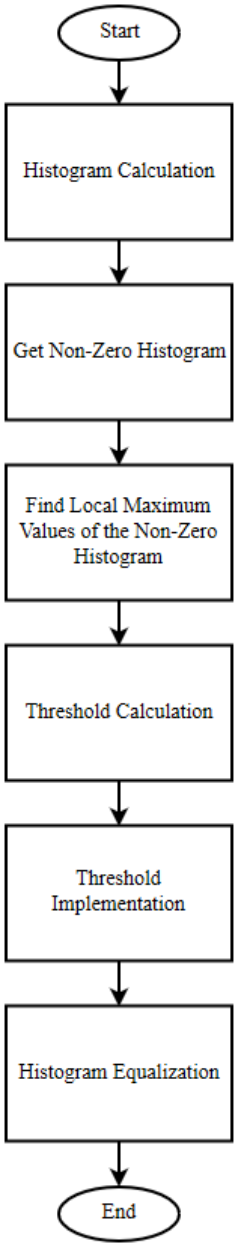

Figure 2.6. Block diagram of the ADPHE method

ADPHE results from the MATLAB implementation are presented in Figure 2.7. (Raw image in Figure 2.1 was used as the input image.)

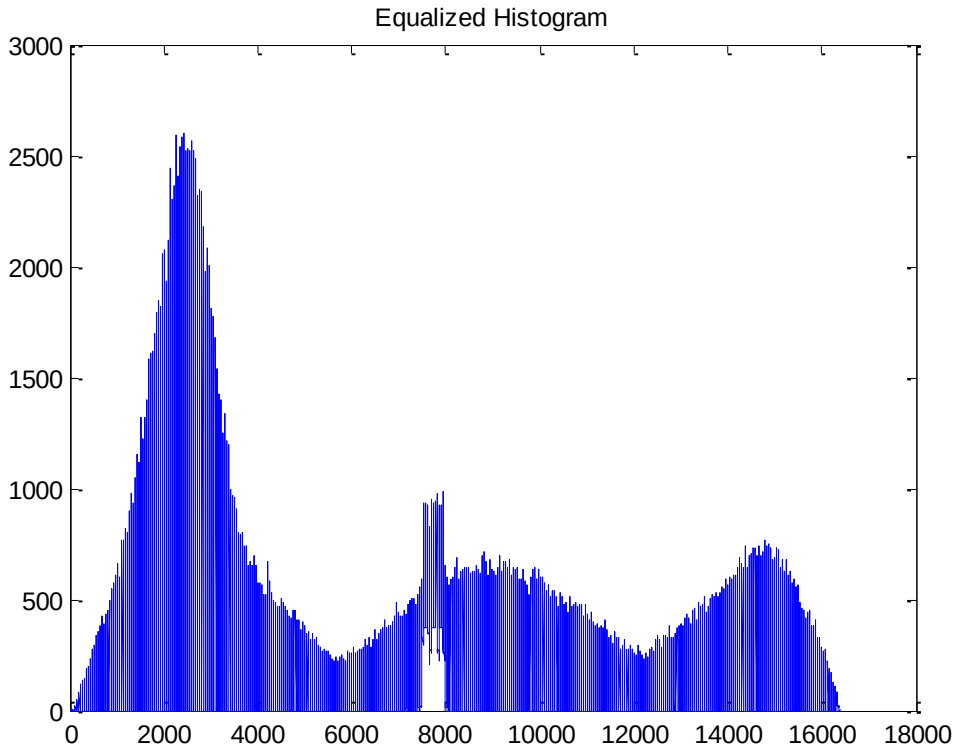

Figure 2.7. Contrast enhanced image with ADPHE method and its histogram

2.2.2. Weighting Mean-Separated Sub-Histogram Equalization

The main advantage of plateau-based contrast enhancement methods is that one or more thresholds are applied to the entire histogram before the histogram equalization. However, applying the threshold values to the entire histogram may prevent optimal enhancement of the contrast of sections with different characteristics within the image. In order to overcome this situation, it would be useful to examine the algorithms that can adaptively separate the histogram into parts with different characteristics.

Wu et al. [20] proposed Weighting Mean-Separated Sub-Histogram Equalization (WMSHE) method for enhancing the contrast with keeping the original histogram characteristics. Instead of global-based histogram equalization method, this method works local-based.

Hariprasat et al. [21] also proposed a novel WMSHE method for underwater images which has similar algorithm of Wu et al. Since the contrast of the underwater images may reduce due to behavior of the light, this case has similarities with infrared low-contrast images. Therefore, by examining the effects of this method on infrared images, a field of application for contrast enhancement for the infrared images can be developed.

Both methods adaptively divide the original histogram by two with using first calculated weighting mean value of whole histogram. Then two more weighting mean values are calculated for upper and lower sub-histograms. In Hariprasat et al.'s algorithm, each sub-histogram's threshold values are calculated as

$$T_1 = \frac{1}{G_{ml}+1}\sum_{i=0}^{G_{ml}} n_i \qquad (2.7)$$

$$T_2 = \frac{1}{G_m-1-G_{ml}}\sum_{i=G_{ml}+1}^{G_m} n_i \qquad (2.8)$$

$$T_3 = \frac{1}{G_{mu}-1-G_m}\sum_{i=G_m+1}^{G_{mu}} n_i \qquad (2.9)$$

$$T_4 = \frac{1}{G_{dmax}-1-G_{mu}}\sum_{i=G_{mu}+1}^{G_{dmax}-1} n_i \qquad (2.10)$$

where T_1, T_2, T_3 and T_4 are the threshold values of the separated histogram regions and G_{ml}, G_m and G_{mu} are the lower, middle and upper mean values, respectively.

There is no threshold in the Wu et al.'s algorithm. Finally, a piecewise histogram equalization is carried out on each sub-histogram individually in both methods. Block diagram of the Hariprasat et al.'s method is presented in Figure 2.8.

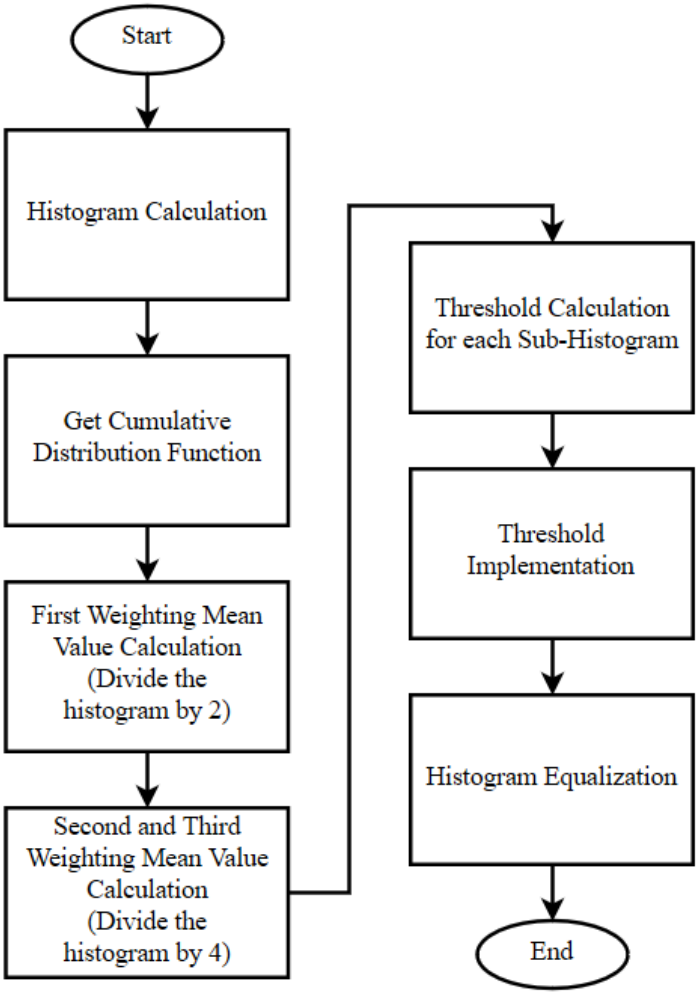

Figure 2.8. Block diagram of the WMSHE method for underwater images

WMSHE algorithm for underwater images is implemented in MATLAB to investigate whether the method is useful for infrared images. Implementation and results are presented in Figure 2.9 and Figure 2.10, respectively.

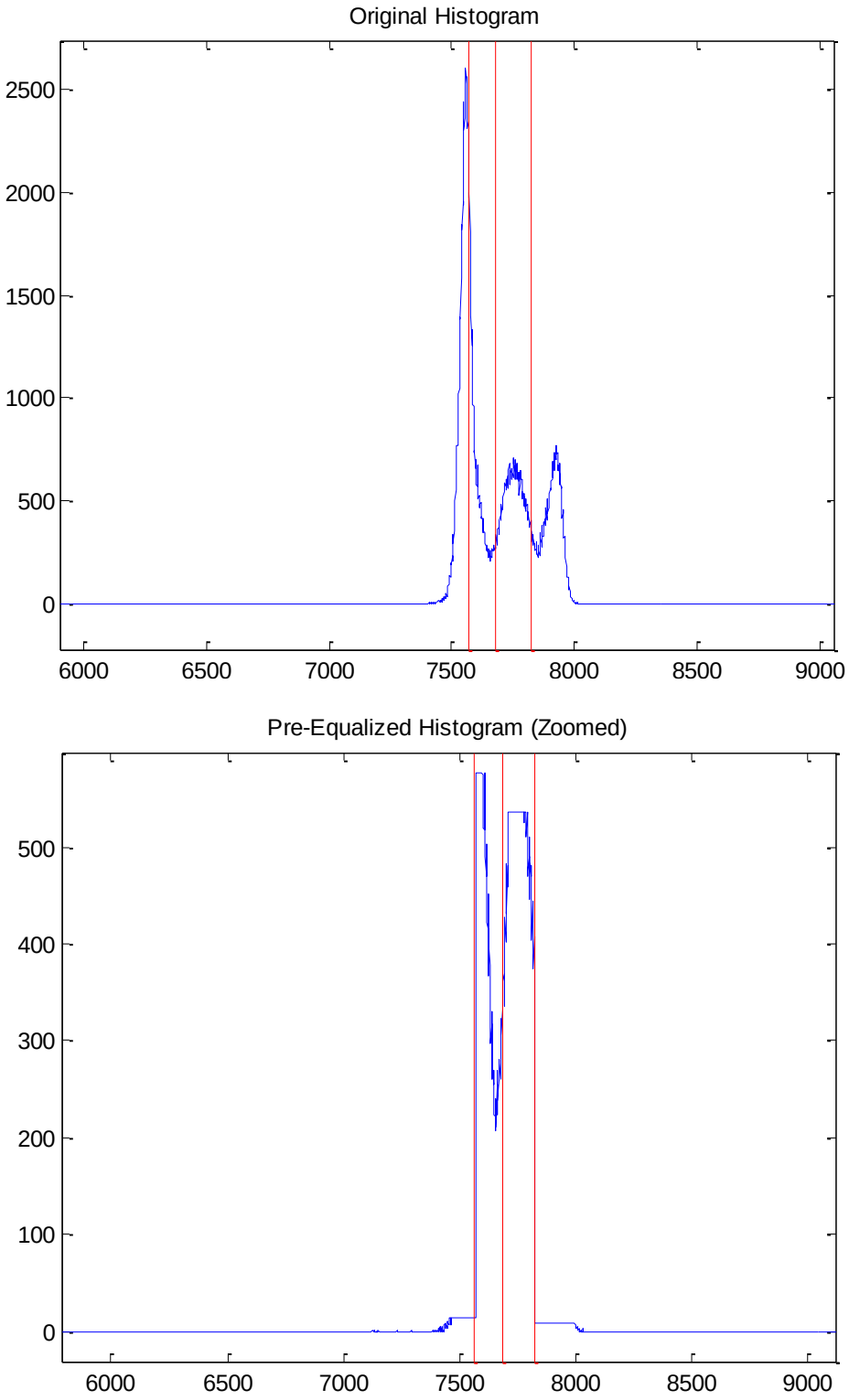

Figure 2.9. Separation of the original histogram by calculated weighted mean values and implementation of the thresholds

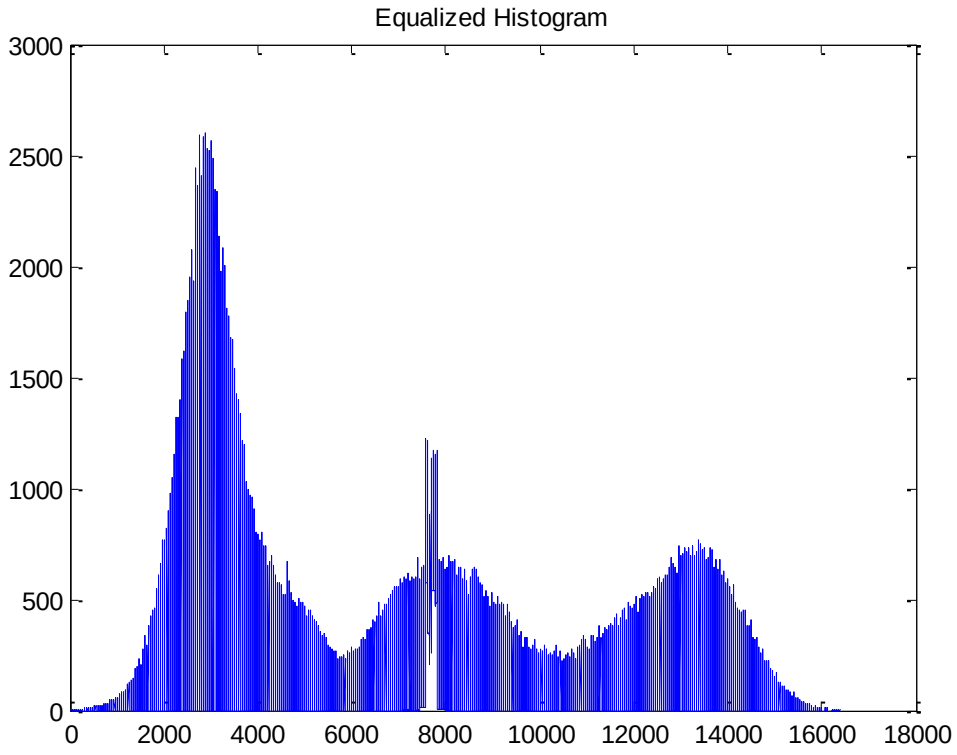

Figure 2.10. Contrast enhanced image with Hariprasat et al.'s WMSHE method and its histogram

2.2.3. Contrast Limited Adaptive Histogram Equalization

Pizer et al. [22] proposed another method for the contrast enhancement that provides equalization by limiting the contrast in the separated sub-regions of the low-contrast image. Schatz [23] also proposed a hardware implementation method for Contrast Limited Adaptive Histogram Equalization (CLAHE) on FPGA. Sub-histograms are calculated for each sub-regions of the image and intended enhancement is achieved with contrast limiting in CLAHE. Unlike the plateau-based histogram equalization and Hariprasat et al.'s WMSHE methods, excess pixels which are above the threshold limit are distributed into neighboring pixels of the sub-regions. The amount of excess pixel redistribution is adjusted by according to the pixel distribution values below the threshold value as shown in Figure 2.11.

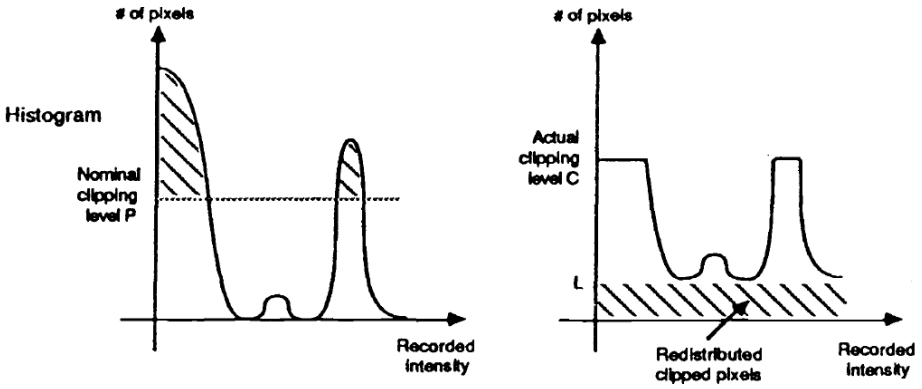

Figure 2.11. Histogram clipping in CLAHE method [22]

Variations in number of separated tiles, threshold limitation and redistribution of the excess pixels are affecting the performance of the contrast enhancement in CLAHE method. Table 2.1 shows the variations of the parameters and Figure 2.12 presents results of MATLAB prototype, obtained with different values of these variables on the raw image of Figure 2.1. Enhancement results are highly scene-depended in CLAHE and selection of proper parameter values is critical for achieving a successful contrast enhancement. From the Figure 2.12, both 2^{nd} and 5^{th} implementation results have better enhancement than the others. Uniform and exponential distributions achieved similar results for this raw image.

Number of tiles and clipping limit adjustments are selected empirically and results show that the higher the number of columns dividing the image, the better enhancement is achieved for this image.

Table 2.1. *Values of the CLAHE parameters in different implementations*

Image	*Tiles*	*Clipping Limit*	*Distribution*
1	4x2	0.01	Uniform
2	2x4	0.01	Uniform
3	2x4	0.005	Uniform
4	2x4	0.025	Uniform
5	2x4	0.01	Exponential
6	2x4	0.01	Rayleigh

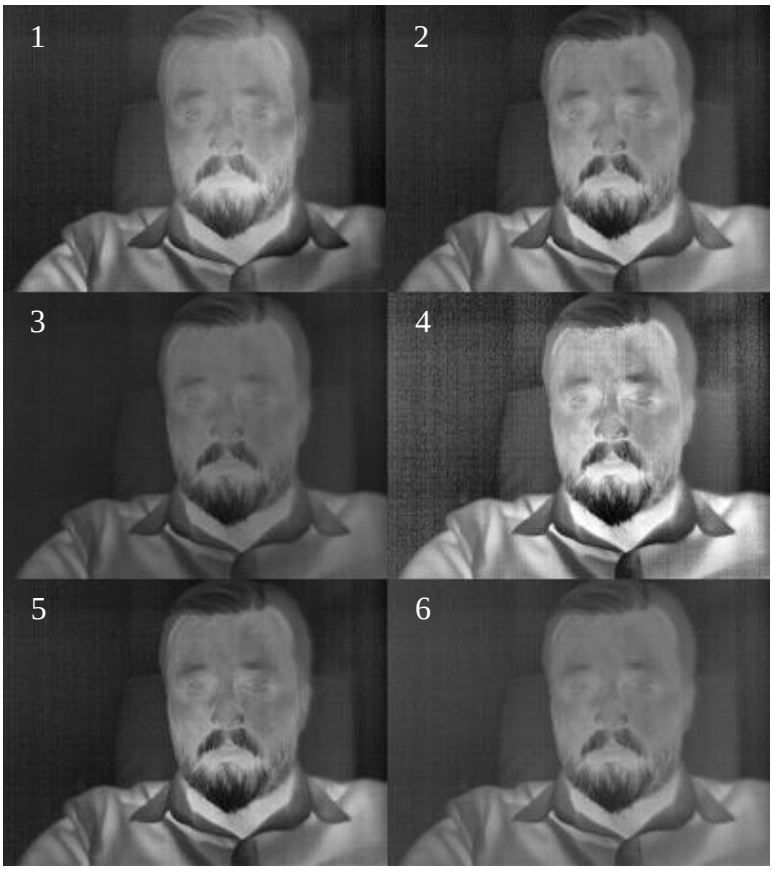

Figure 2.12. Contrast enhanced images with CLAHE method by using various parameter values in Table 2.1

CHAPTER 3

PROPOSED CONTRAST ENHANCEMENT METHOD FOR INFRARED IMAGES

Characteristics of the images taken from infrared cameras are different from the usual gray level images. When the methods used to improve grayscale images are used for improving the infrared images, background noise may be over-enhanced or detailed temperature information may be lost. For this reason, a more appropriate method should be used for enhancing the low-contrast infrared images.

A new method has been developed with the arrangement of Hariprasat et al.'s Weighting Mean-Separated Sub-Histogram Equalization method which is used for enhancing the contrast of gray level underwater images and Adaptive Double Plateaus Histogram Equalization which is used for enhancing the contrast of the infrared images. Adaptive threshold calculation of both methods is rearranged to achieve the optimal performance on the enhancement of background and foreground regions. Since the proposed method is a modified version of WMSHE and ADPHE, this method is named as Weighting Mean-Separated Double Plateaus Histogram Equalization (WMDPHE).

This chapter presents the algorithm of WMDPHE and its implementation on FPGA. Section 3.1 provides theoretical information about the proposed method, and then presents the implementation results of this method. Section 3.2 describes the firmware architecture and examines the functions of submodules in detail.

3.1. Weighting Mean-Separated Double Plateaus Histogram Equalization

WMDPHE is an improvement that is designed by approaching to the ADPHE method from the WMSHE perspective. Global background and foreground enhancement of the ADPHE algorithm is adaptively localized with separation of the original histogram into sub-histograms by using image characteristics. Since the localization of

enhancement is implemented by using original histogram characteristics, instead of portions of the image itself, infrared image integrity is protected and avoided from the enhancement differences between infrared image parts unlike the CLAHE method. Rearrangement of the adaptive threshold values based on weighted mean and local extremum calculations aims to better limitation on the over-enhancement than the WMSHE and ADPHE methods. Global histogram equalization on the locally threshold implemented histogram provides an extra limitation for enhancement between the parts of image with different characteristics and improves image integrity.

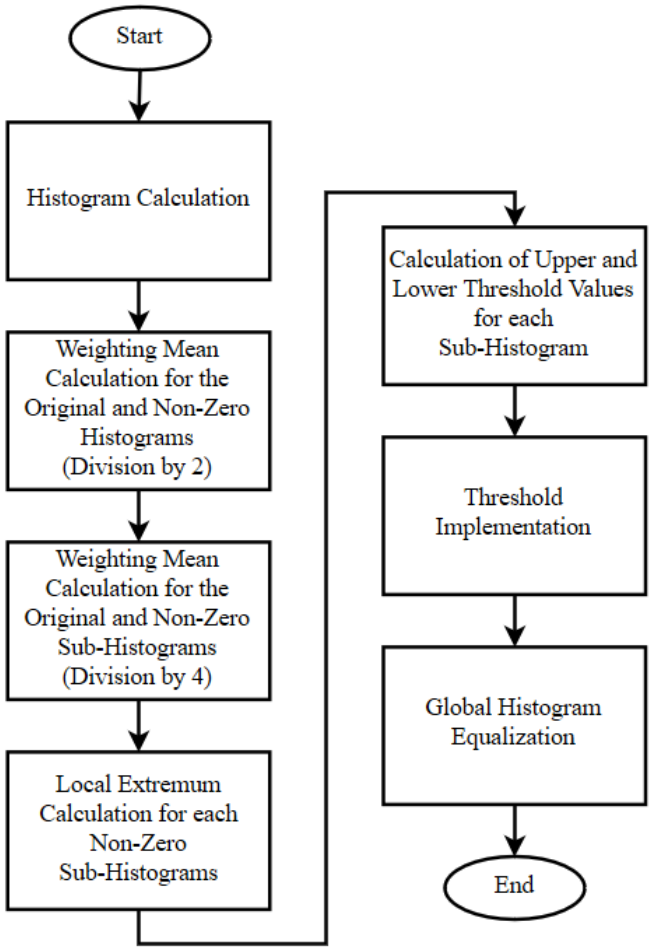

Figure 3.1. Block diagram of the proposed method for histogram equalization of low-contrast infrared images

Procedure of the WMDPHE method is shown in Figure 3.1. First of all, histogram of the input image is calculated. The histogram will be examined as two parts in subsequent calculations as original and non-zero histogram. As the name implies, non-zero histogram is the non-zero values of the original histogram that are leaned against the minimum gray-level as shown in Figure 3.2. Secondly, weighting mean calculation is performed on the gray level values of original and non-zero histograms. First weighting mean values of the both histograms are used for dividing the histograms into two parts. Similarly, weighing mean calculation is performed again on these two parts, and then non-zero and original histograms are divided into four parts with using upper and lower weighting mean values as shown in Figure 3.3. Summations of occurrence values for each sub-histogram are also calculated for using in threshold calculation in the following steps.

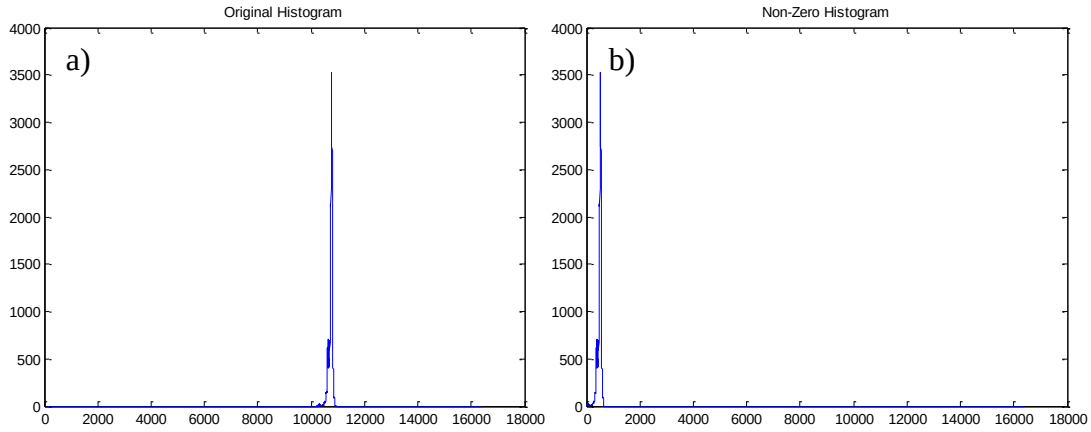

Figure 3.2. a) Original and b) non-zero histograms

Non-zero histogram is used for local extremum calculation. Local extremum points represent the hot and cold details in the image. In the original histogram, there may be pixels that are not in the image within the narrow field representing the detailed information of the histogram. Omitting these zero values ensures that these values are not taken into account in the local extremum calculation and the details are preserved better. Since the meaningful part of the original histogram in Figure 3.3 does not have a large number of zero-valued pixels, the weighting mean values of the original and

non-zero histograms were calculated in similar values as expected. On the other hand, the effect of zero-valued pixels on the histogram can be better seen in the cumulative distribution.

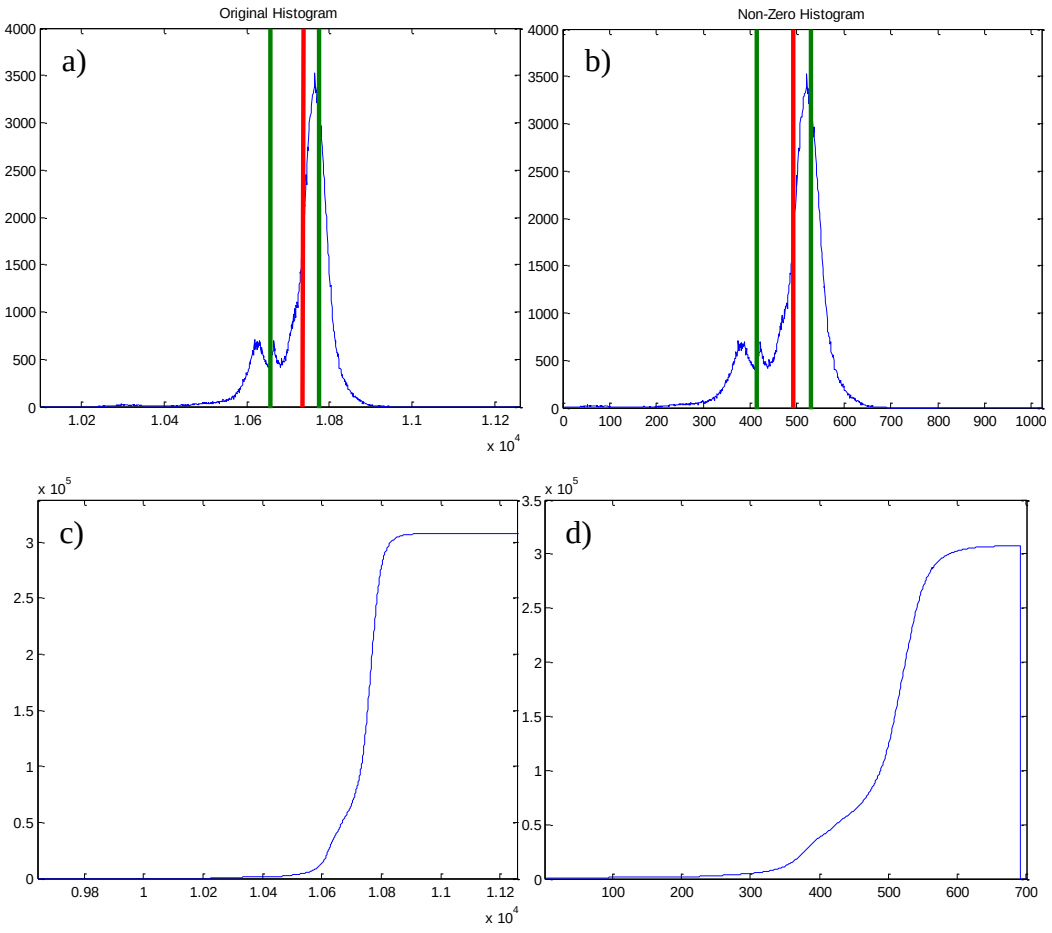

Figure 3.3. Separation of the a) original and b) non-zero histograms into the sub-histograms by weighting mean values. Firstly, the histograms divided into two parts by red lines and secondly, partitions divided again by green lines into four sub-histograms. Cumulative distribution of the c) original and d) non-zero histograms shows the effect of zero-valued elements on the histogram

In the next step, local maximum and minimum values and their summations for each sub-histogram are calculated in order to use in threshold calculation. For discrete sequences, elements that are larger or smaller than their neighbors can be taken as local maximum or minimum. A one-dimensional window can be used for finding the local extremum values of the histogram [19]. Figure 3.4 shows the steps of searching local extremum values.

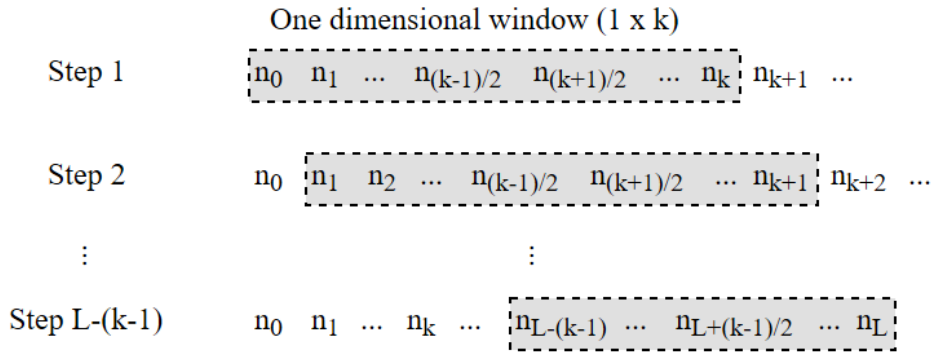

Figure 3.4. Local extremum searching steps

where n_i is the number of pixels in i^{th} gray intensity level, k is the one-dimensional window length (must be an odd number) and L is the number of gray levels in the non-zero histogram. Local maximums and minimums are searched by shifting the (1×k) window step by step. By comparing the values other than middle value in the window, the minimum and maximum values between these elements are found. Then these values are compared with the value in middle of the window to determine whether the local minimum or local maximum. For example, in the second step of Figure 3.4, histogram value of $n_{(k+1)/2}{}^{th}$ gray level will be compared with maximum and minimum of the other elements in window. If it is bigger than the maximum of the others, it will be used as local maximum. If it is smaller than the minimum value of the other values in window, then it will be used as local minimum.

Upper, middle and lower weighting mean values of the original and non-zero histograms, summation of local maximum and local minimum values of the non-zero sub-histograms and summation values of the original sub-histograms are used to generate the upper and lower threshold values for each sub-histogram. Similar with ADPHE, lower threshold is used for protecting the detailed information and upper threshold is used for preventing the background noise. If the upper threshold value is too large, over-enhancement of background noise may be occurred and if it is too small, details of the background will be lost. It is also important that the lower threshold value is selected correctly. Foreground details can be lost or saturated by

miscalculation of the lower threshold level. In order to find these thresholds, histogram statistics-based adaptive threshold calculations are performed in the proposed WMDPHE method. Upper and lower threshold values are calculated as

$$T_{UP[n]} = \frac{G_{dmax} \times NZSMAX_n}{\text{WMValue}_n \times SUM_n} \quad (3.1)$$

$$T_{LOW[n]} = \frac{G_{dmax} \times NZSMIN_n}{\text{WMValue}_n \times SUM_n} \quad (3.2)$$

where $T_{UP[n]}$ and $T_{LOW[n]}$ are the upper and lower threshold values of n^{th} non-zero sub-histogram, G_{dmax} is the maximum available gray level of the dynamic range, $NZSMAX_n$ is the summation of n^{th} non-zero sub-histogram's local maximum values, WMValue_n is the upper weighting mean boundary of the n^{th} non-zero sub-histogram, SUM_n is the summation of original values of the n^{th} sub-histogram and $NZSMIN_n$ is the summation of n^{th} non-zero sub-histogram's local minimum values.

Threshold implementation to original histogram is the next step of the proposed method. The upper and lower threshold values that calculated separately for each sub-histogram are applied to the respective portions of the histogram. Threshold implementation procedure can be illustrated as

$$n_{i,TH} = \begin{cases} T_{UP[n]}, & n_i \geq T_{UP[n]} \\ n_i, & T_{LOW[n]} < n_i < T_{UP[n]} \\ T_{LOW[n]}, & 0 < n_i \leq T_{LOW[n]} \\ 0, & n_i = 0 \end{cases} \quad (3.3)$$

where $n_{i,TH}$ is the threshold applied number of pixels in i^{th} gray intensity level. Threshold applied histogram for the sample image is shown in Figure 3.5.

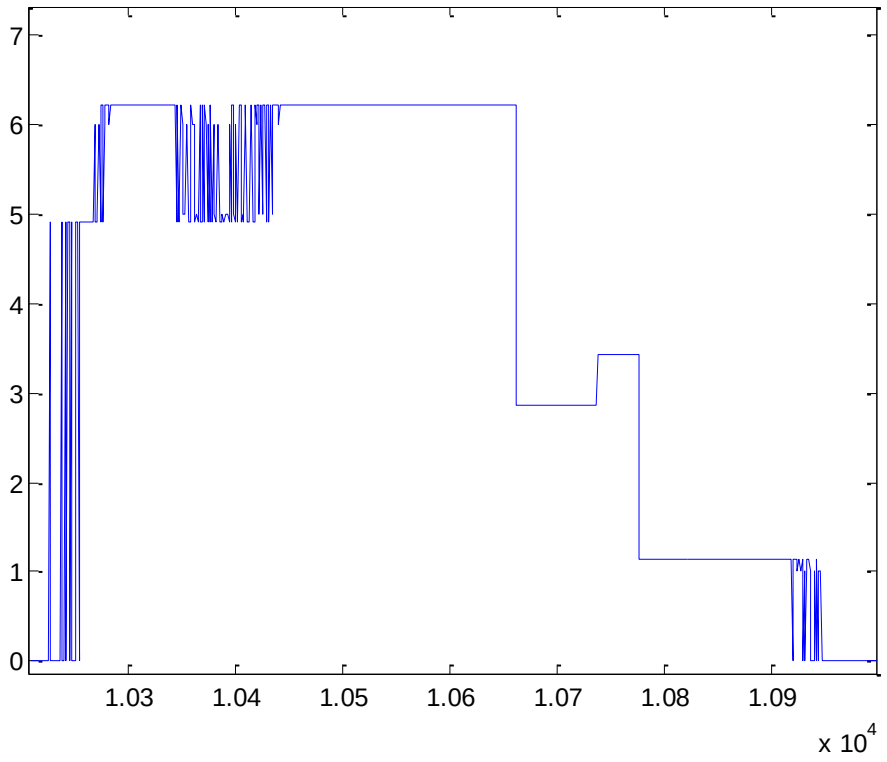

Figure 3.5. Threshold implemented histogram

As the final step, global histogram equalization is performed. This step requires recalculation of the threshold implemented histogram's statistics, since the total occurrence value of the original histogram changed with applying the thresholds. Probability density function (pdf) and cumulative distribution function (cdf) are calculated for the threshold implemented histogram before the equalization. Then histogram equalization is performed as in equation (2.4). Outputs of the WMDPHE method that applied to various raw images are given in Figure 3.6, Figure 3.8, Figure 3.10 and Figure 3.12. Raw and equalized histograms of these images shown in Figure 3.7, Figure 3.9, Figure 3.11 and Figure 3.13.

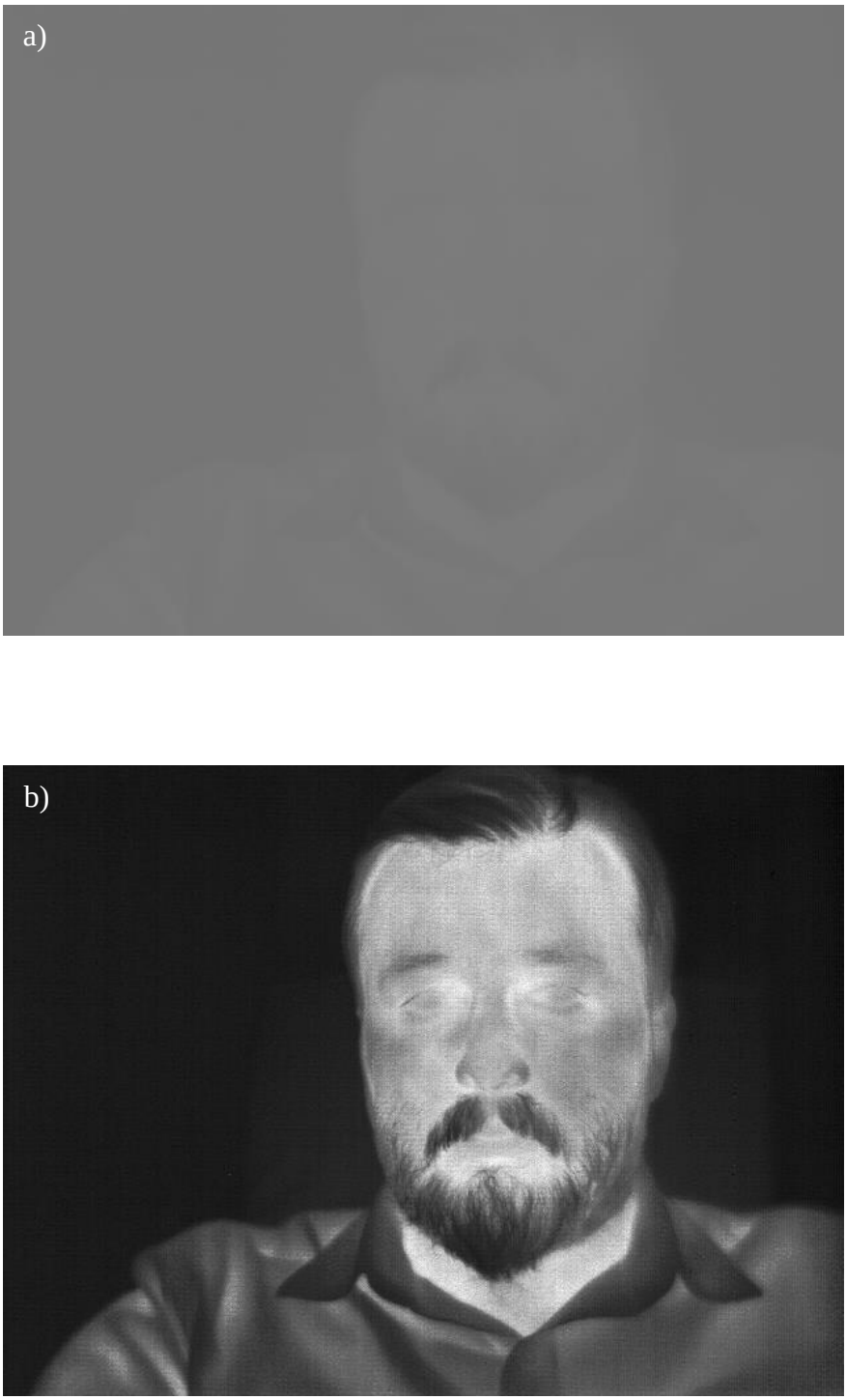

Figure 3.6. a) Raw image and b) contrast enhanced image with WMDPHE method

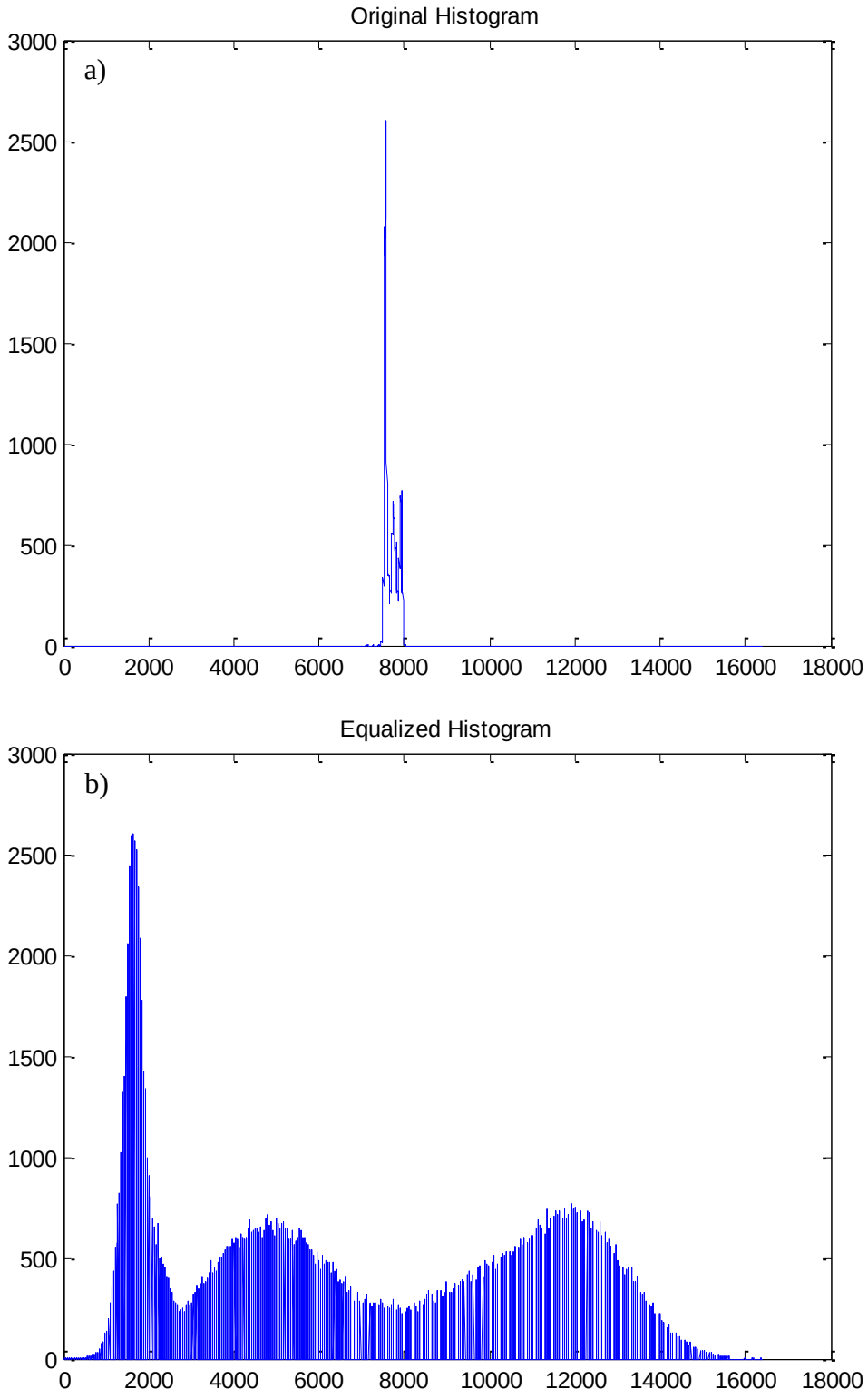

Figure 3.7. a) Raw histogram and b) contrast enhanced histogram with WMDPHE method

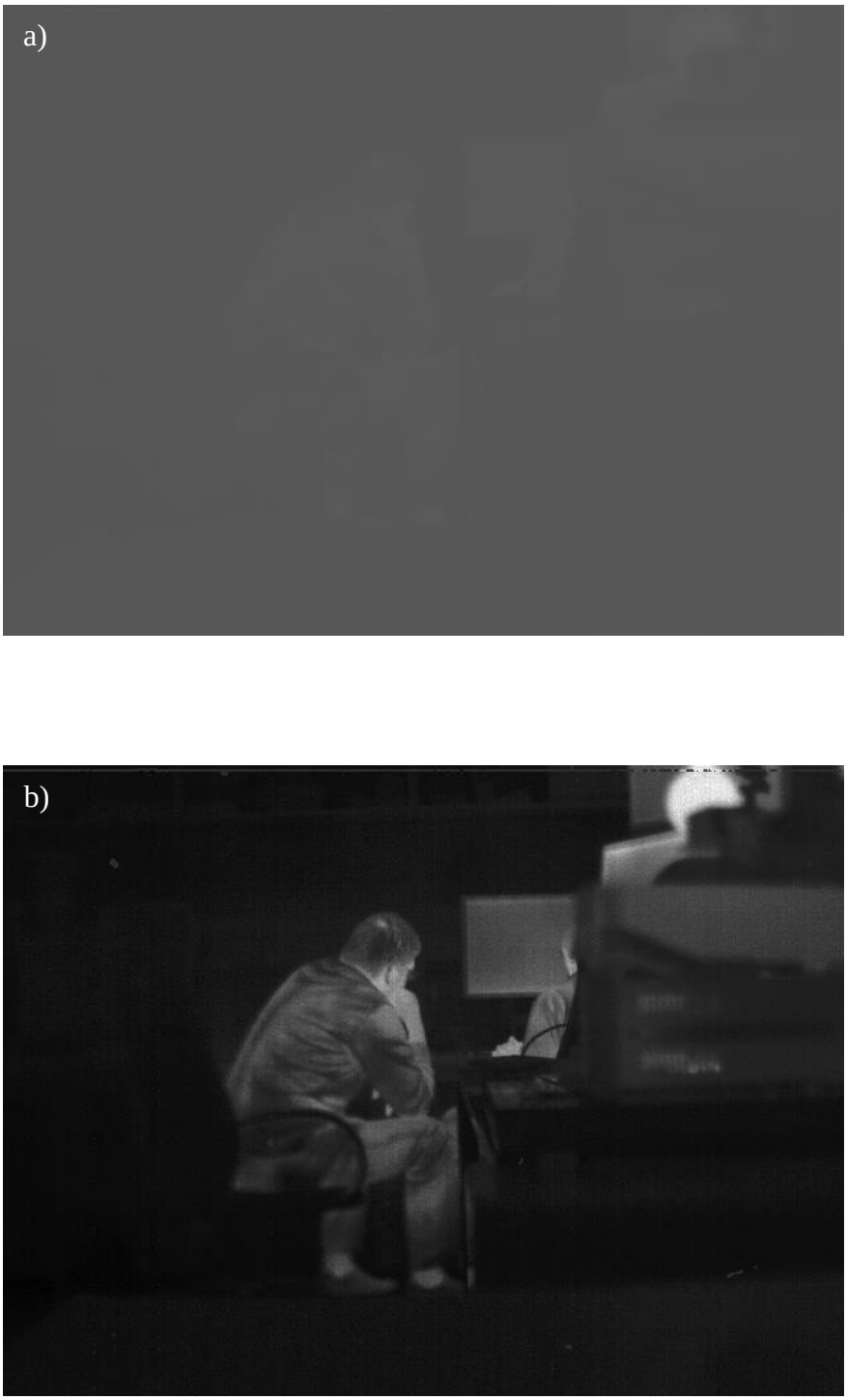

Figure 3.8. a) Raw image and b) contrast enhanced image with WMDPHE method

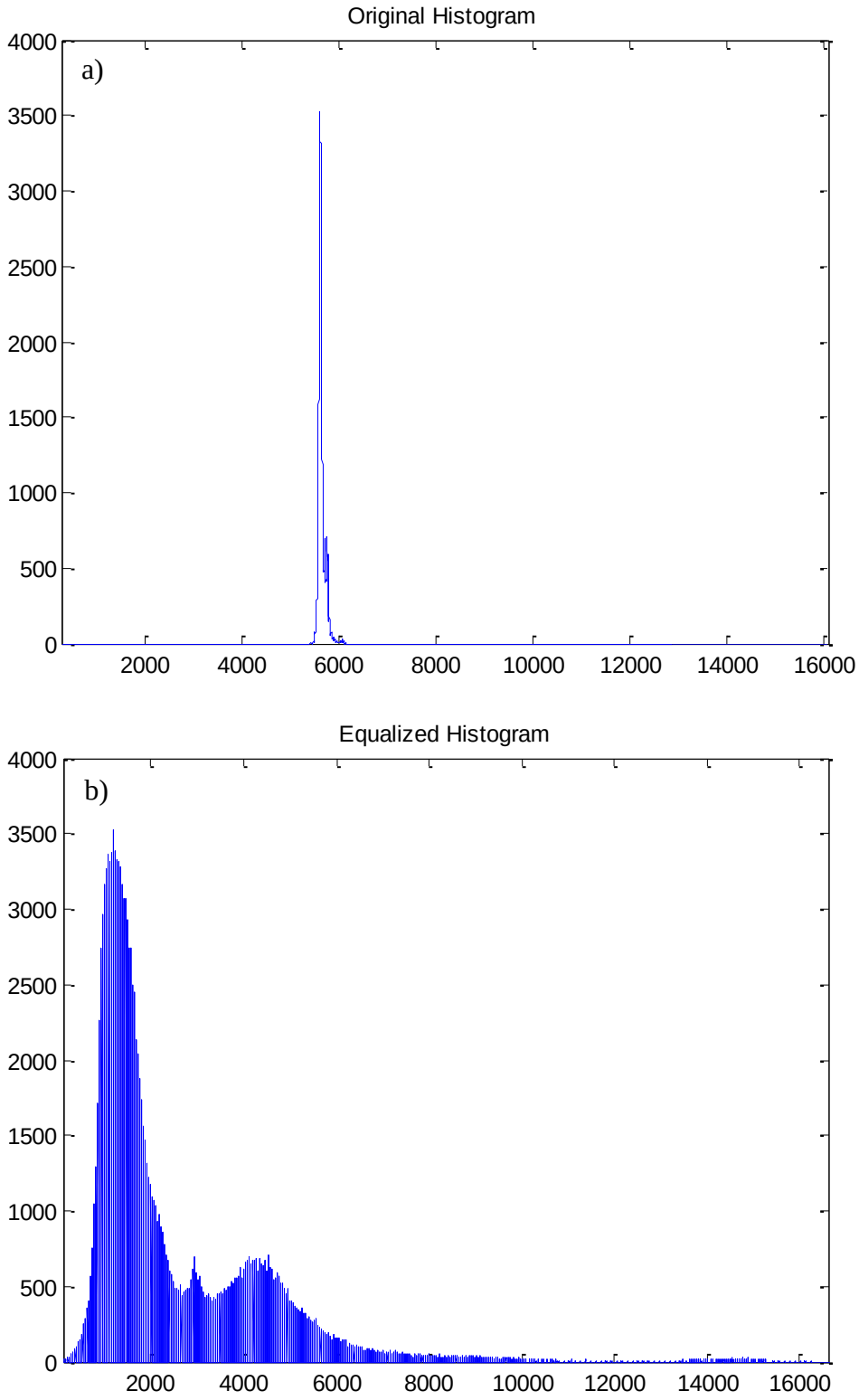

Figure 3.9. a) Raw histogram and b) contrast enhanced histogram with WMDPHE method

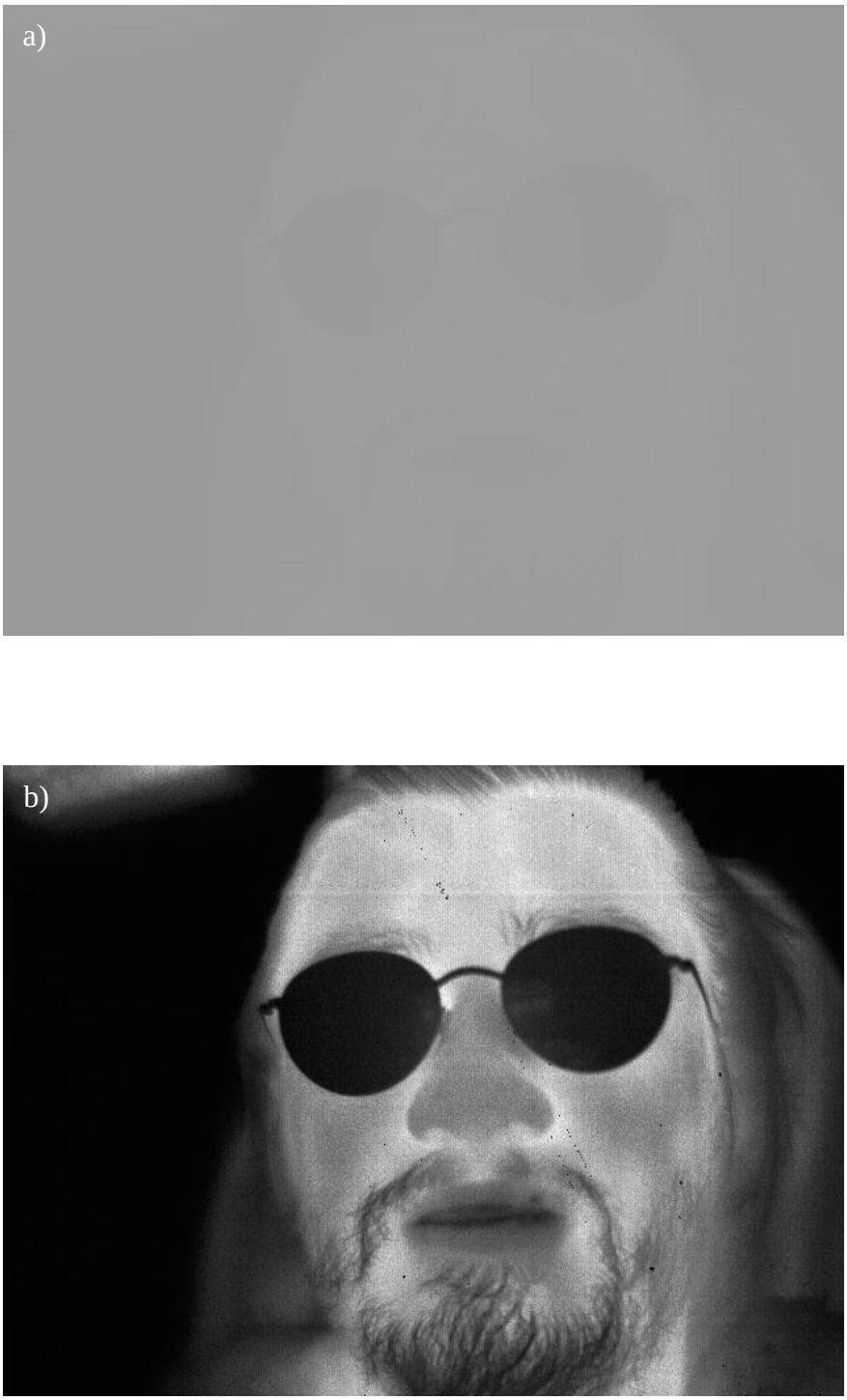

Figure 3.10. a) Raw image and b) contrast enhanced image with WMDPHE method

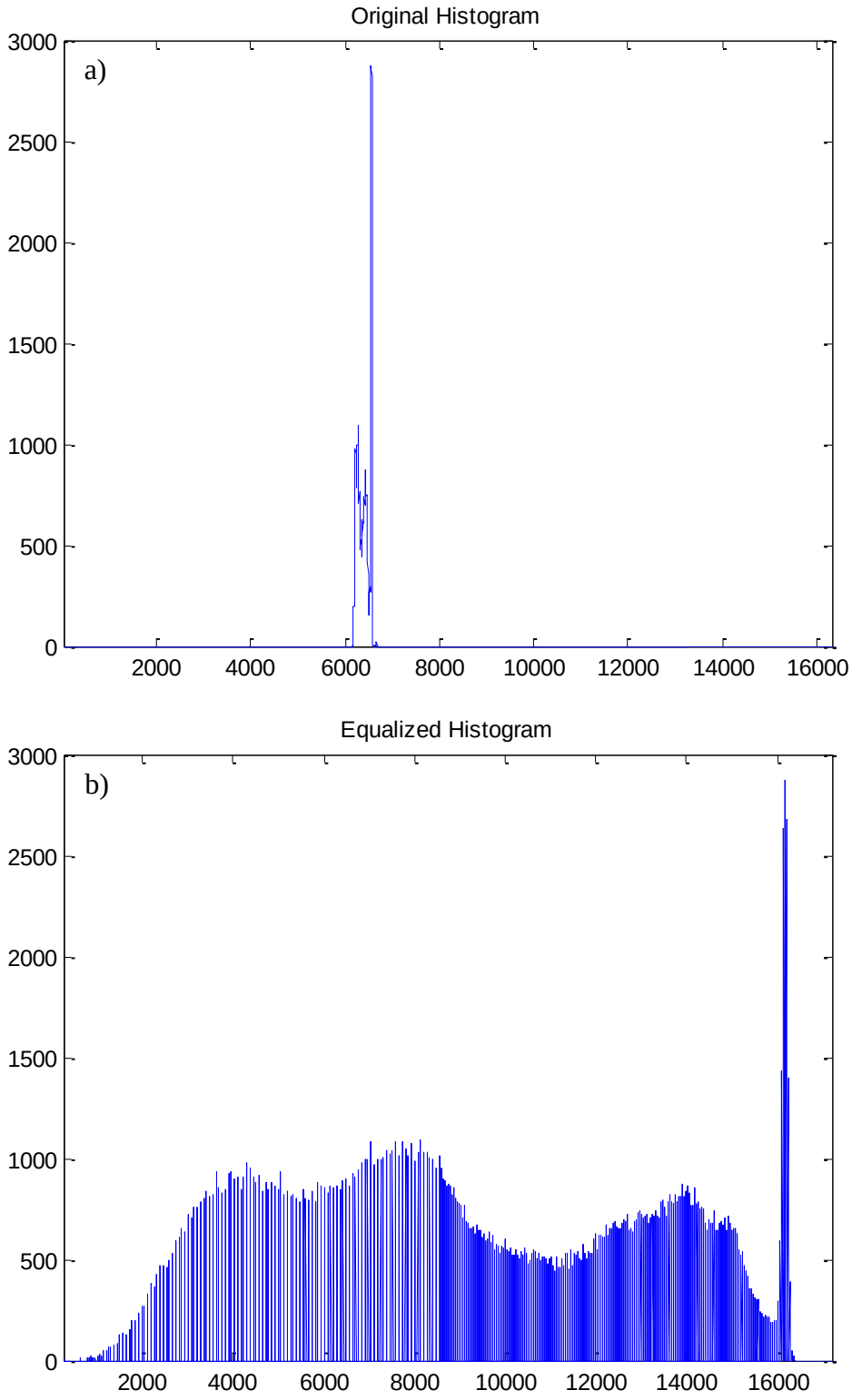

Figure 3.11. a) Raw histogram and b) contrast enhanced histogram with WMDPHE method

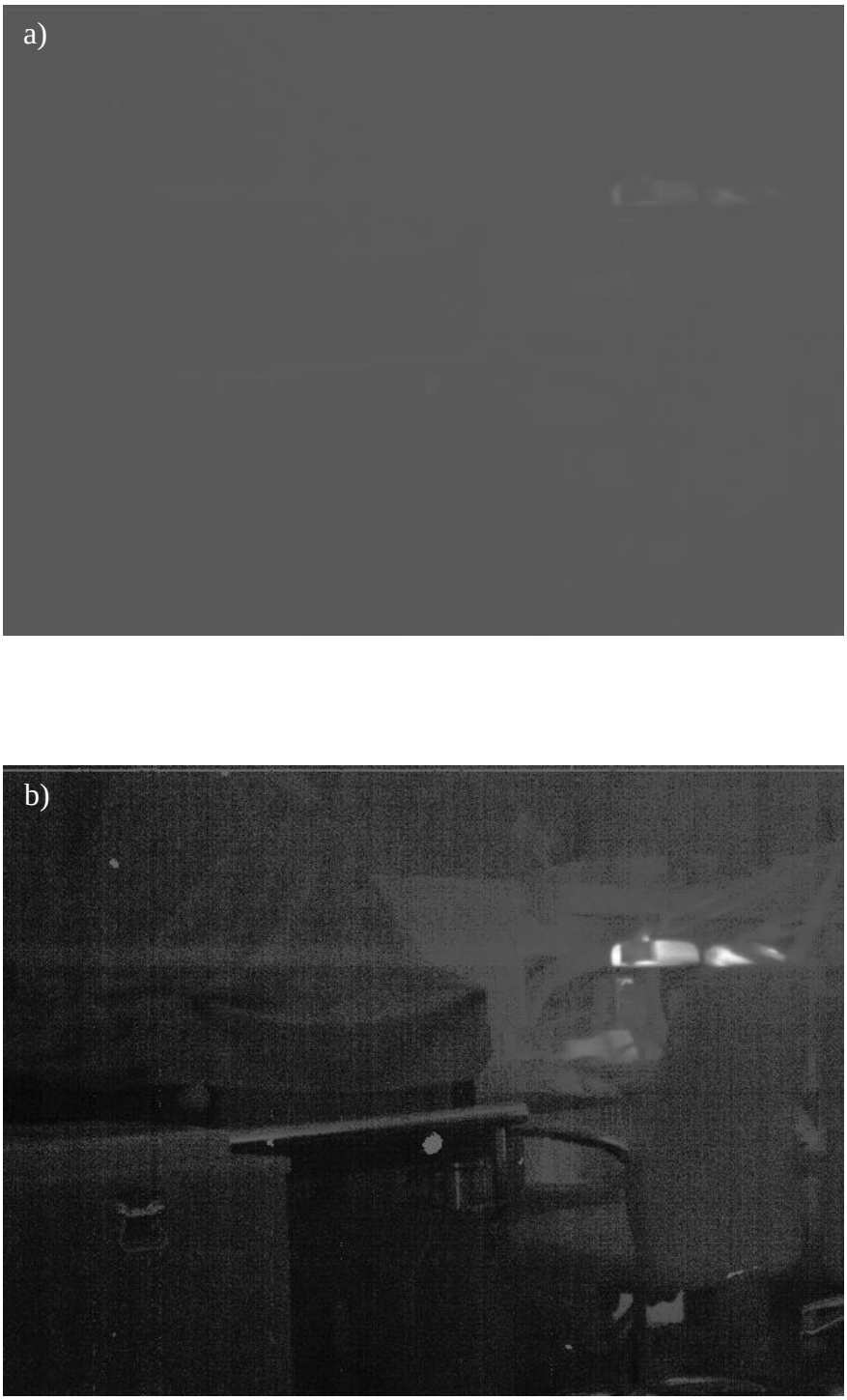

Figure 3.12. a) Raw image and b) contrast enhanced image with WMDPHE method

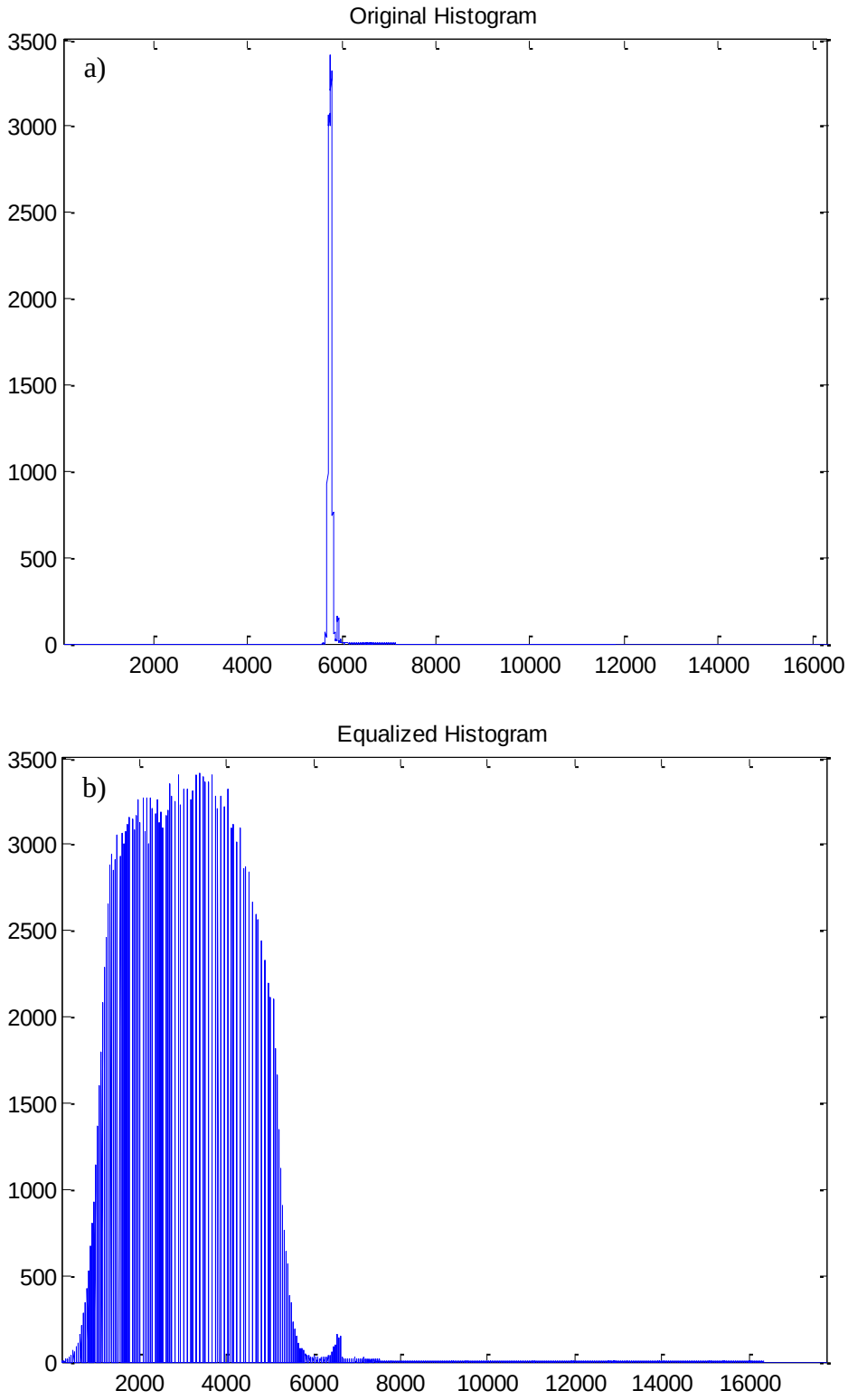

Figure 3.13. a) Raw histogram and b) contrast enhanced histogram with WMDPHE method

3.2. FPGA Implementation

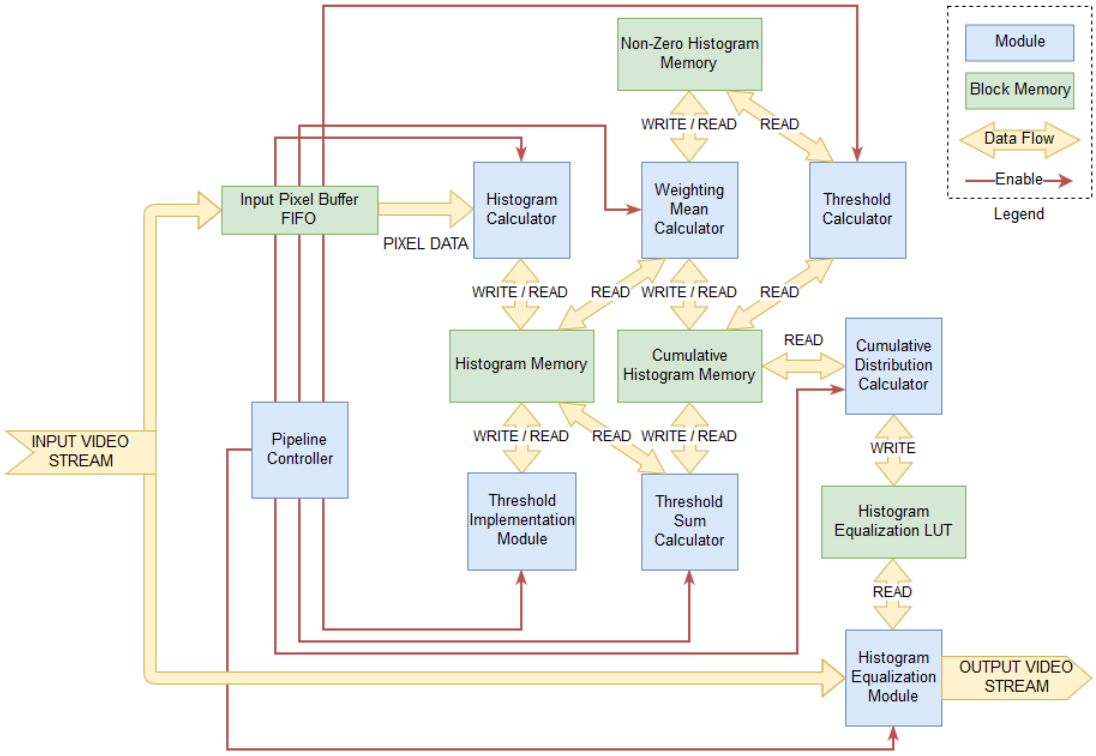

Figure 3.14. Block diagram of the FPGA implementation

Structure of the WMDPHE implementation is given in Figure 3.14. Input video stream consists of frame valid (fval), line valid (lval), data valid (dval), pixel clock and pixel data. Pixel clock is 40MHz and pixel data is 14-bit for the selected infrared camera. Effective pixel clock is 10MHz due to the limitation of the ROIC. Structure of the frame valid, line valid and data valid signals are shown in Figure 3.15.

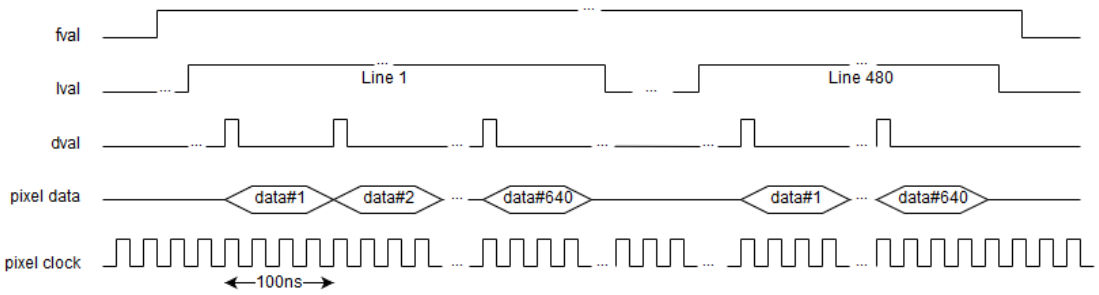

Figure 3.15. 640×480 video stream timing structure

3.2.1. Image Acquisition and Histogram Calculation

Image acquisition is the first stage of the real-time image processing pipeline. Proper image acquisition is critical, because any misses in the timing or pixel data will conclude as failure of the enhancement. Structure of the image acquisition and histogram calculation blocks is shown in Figure 3.16.

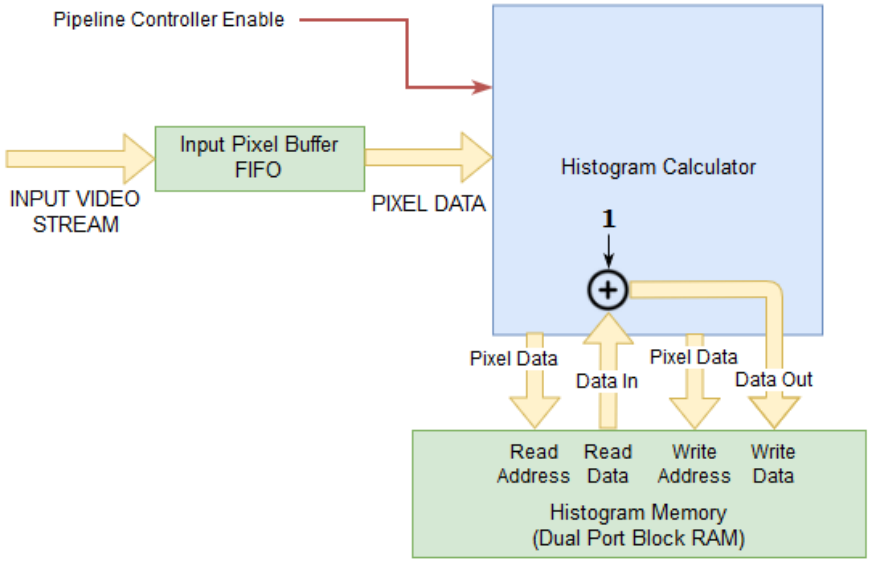

Figure 3.16. Structure of the image acquisition and histogram calculation blocks

Frame buffer is not used in the firmware and video data stream is processed by the pipeline in real-time. Input Pixel Buffer FIFO is used for receiving the incoming pixel data. This asynchronous FIFO provides both timing and data buffering and prevents any misalignments on input video stream. Timing controlling signals of the input stream are connected into FIFO enables in order to buffering the incoming data synchronously. Reading of the pixel data controlled by Histogram Calculator module with using faster internal pipeline clock. When the Pipeline Controller module enables the histogram calculation, Histogram Calculator module starts to read pixel data from the Input Pixel Buffer FIFO. Reading control is organized by counting parametrized image width and height values. Histogram Calculator uses the incoming pixel data for address of the Histogram Memory. Histogram Memory is a Dual Port Block RAM that stores the original histogram data. The data read from Histogram Memory is

incremented by one by the Histogram Calculator and increased value is saved back to the same address in the histogram.

3.2.2. Histogram Separation by Image Statistics

Division of the original histogram into four sub-histograms is performed by Weighting Mean Calculator module. In addition to histogram division, this module is responsible for generation of the non-zero and cumulative histograms. Figure 3.17 illustrates the Weighting Mean Calculator module's interaction with the histogram memories.

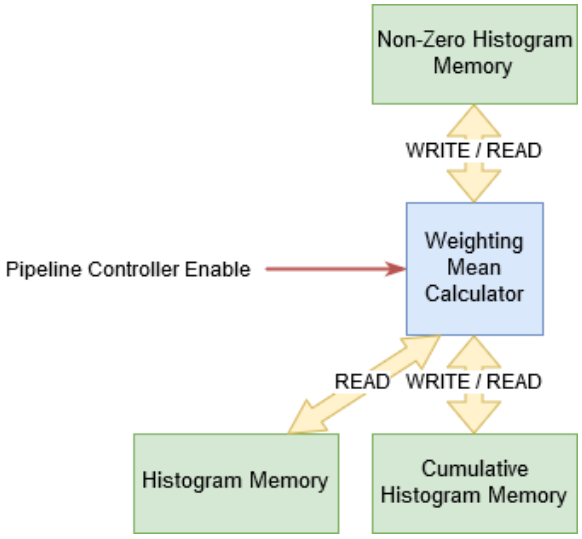

Figure 3.17. Weighting mean calculation blocks

Designed firmware consists of three main Dual Port Block Memories that are used for image statistics calculation as Histogram Memory, Non-Zero Histogram Memory and Cumulative Histogram Memory. After the histogram calculation is performed, Weighting Mean Calculator module scans the whole histogram and calculates weighting mean, non-zero histogram length and non-zero weighting mean values. Cumulative histogram and non-zero histograms are also calculated in this scanning process. Cumulative histogram is generated by consecutive addition of the read original histogram values. These values are written sequentially to the Cumulative Histogram Memory. When first scanning of the original histogram is finished, second

scanning from the beginning of the histogram to the original weighting mean value is performed. Upper and lower weighting mean values for the original and non-zero histograms are calculated in this scanning. Arithmetic operations are done in fixed-point values with using parallel multiplication and pipelined division blocks that are built-in IPs of the Xilinx Vivado Design Suite. Mathematical simplifications were also done on the paper in order to simplify the state machine structure and reduce the arithmetic blocks' logic resource utilization.

3.2.3. Threshold Calculation and Implementation

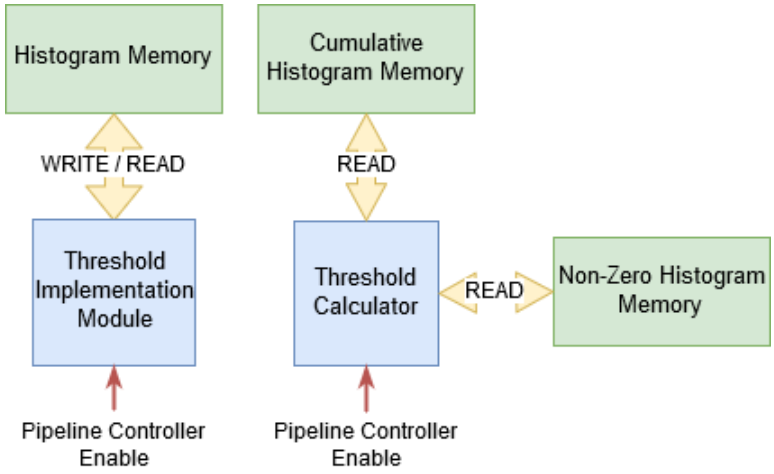

Figure 3.18. Threshold calculation and implementation modules

Local minimum and maximum calculation for non-zero histogram and threshold calculation for each original sub-histogram are done by Threshold Calculator module. Local extremum calculation is performed with shifting a (1×5) one dimensional window on the non-zero histogram. Middle value of the window is compared with the minimum and maximum of the other values in the same window to find out whether it is an extremum value. Summation of the local minimum and maximum values of the non-zero histogram is also calculated for the threshold calculation. The original histogram summation values that required for the threshold value calculation, are read from the Cumulative Histogram Memory. Proper weighting mean values are used as read address for the collecting these summation values from the memory. Upper and

lower threshold calculation for every sub-histogram is performed as equation (3.1) and equation (3.2). Fixed-point pipelined division IP from built-in Xilinx IP Catalog is used to calculate these thresholds.

Threshold Implementation Module is responsible for applying the upper and lower threshold values into relevant original sub-histograms. After the Threshold Calculator module finishes its operation, Pipeline Controller enables the Threshold Implementation Module. Equation (3.3) is implemented into a state machine in order to clip the histogram values. Last modification on the Histogram Memory is made in this module and all the histogram processing steps are finished when this module completes the implementation. Threshold Calculation and Implementation modules' operations on block memories are given in Figure 3.18.

3.2.4. Histogram Equalization

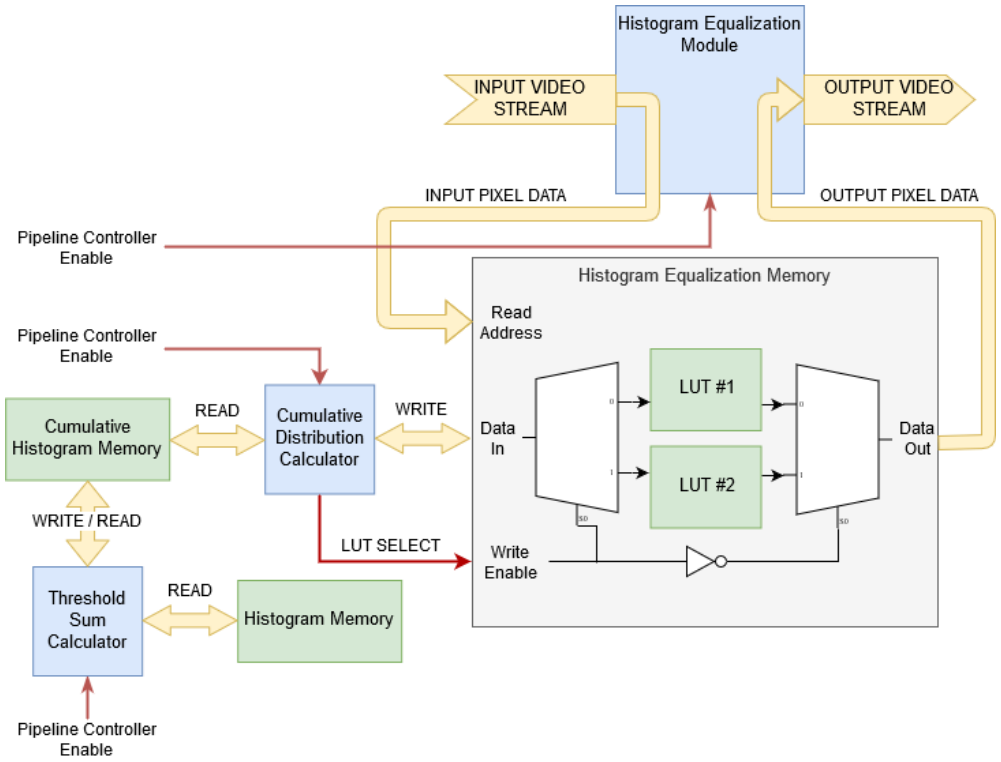

Figure 3.19. Cumulative histogram calculation and histogram equalization modules

Final stage of the designed firmware is histogram equalization. After the threshold applied histogram is ready, Pipeline Controller module enables the Threshold Sum Calculator and Cumulative Distribution Calculator modules, respectively. These modules are responsible for the generation of histogram equalization look-up table (LUT) with calculating the cumulative distribution function from the threshold implemented histogram. After the LUT is created, Histogram Equalization module simply matches the incoming pixel value with the equalized pixel value and generates output timing signals to be compatible with the pixel output values. Structure of the cumulative histogram calculation and histogram equalization modules are given in Figure 3.19.

In order to determine the cumulative distribution function, it is necessary to update the cumulative histogram consisting of consecutive sums of clipped histogram values according to the threshold values. Threshold Sum Calculator module performs this calculation and transmits the calculated total number of remnant histogram occurrences to the Cumulative Distribution Calculator module.

Cumulative Distribution module responsible for the calculation of histogram equalization as in equation (2.4) for every values of the Cumulative Histogram Memory and updating the relevant LUT with controlling the write enable of these two Block RAMs. Histogram Equalization Memory consists of two separate LUTs. The reason for using two different memories is to simplify the real-time pipelined operation. While the histogram equalization data of the new image is written to one of these two memories, the histogram equalization data of the current image is read from the other memory. This ping-pong memory organization prevents possible data collisions and provides a higher data transfer rate.

Histogram Equalization Module is directly connected into the input video stream. Incoming raw pixel values used as read address inputs of the Histogram Equalization Memory and equalized pixel value is read from the appropriate LUT. Read data

oriented to the output ports of the WMDPHE firmware with generating proper Frame Valid, Line Valid and Data Valid timing signals.

3.2.5. Real-Time Image Enhancement Pipeline Design

Pipeline Controller module is maestro of the other modules in the firmware. This module is responsible for controlling the histogram equalization operation by adjusting enable signals of the modules in proper order. Frame valid signal is monitored by this module to arrange the timing between enable signals. Timing requirements adjusted as compatible with 30 frames per second (FPS) video stream timing.

Calculation of the first histogram equalization data takes three frame time, because the design does not include any frame buffer memory. Therefore, first histogram equalized frame is generated with two frame latency. In order to prevent decreasing of the FPS due to lack of frame buffer memory, the histogram equalized image output is given from the third frame with using the statistics of the second image before itself. That means the actual histogram statistics are used with approximately 66 milliseconds latency for 30FPS video input. This latency can be negligible for many applications in thermal domain.

Operation of the modules are arranged with respect to transition of the frame valid signal as shown in Figure 3.20. In the first frame's active data input time interval, in other words, when the frame valid is high in the first frame, histogram calculation is performed. Weighting mean calculation, threshold calculation, threshold implementation, threshold summation calculation and resetting of the relevant modules and memories are performed after falling of the frame valid signal. Operation of these modules are adjusted as sequential, since the processing on these modules require low amount of time. Total calculation and resetting processes take 1/3 of the blanking between two frame valid intervals as shown in Figure 3.21.

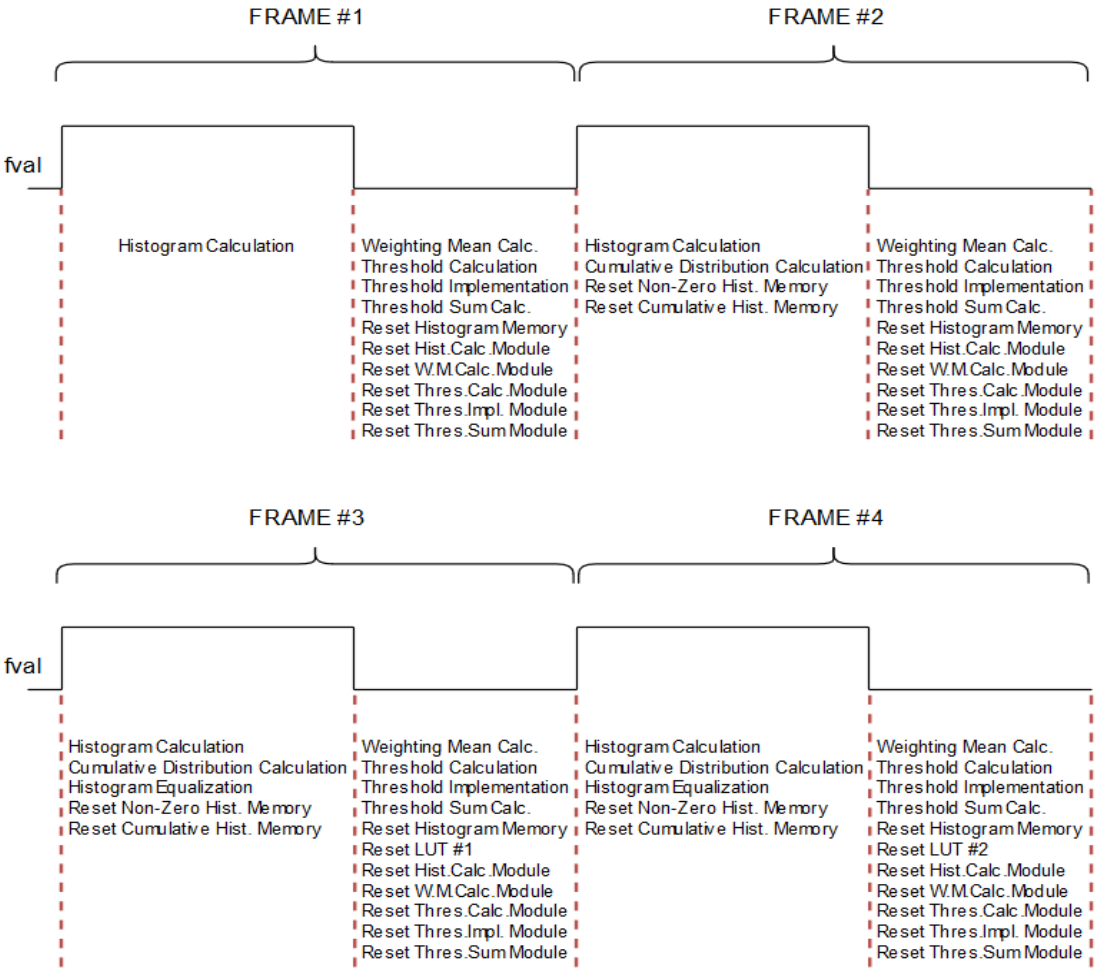

Figure 3.20. Pipeline organization of the firmware

When rising of the frame valid is captured for the second time, cumulative distribution function is operated in parallel with histogram calculation process. Cumulative distribution calculation requires the highest processing time compared to the other modules. Because of this requirement, this module placed into active frame valid interval, which is longer than the blanking part of the frame valid signal for 30 FPS video input. Histogram equalization is started parallelly with the histogram calculation and cumulative distribution calculation with the arrival of the third frame. Histogram equalization process is operated as pixel by pixel like the histogram calculation and it takes whole active frame input time. Since the first equalization data is written on the

LUT#1, Histogram Equalization module is read the equalization data from this memory first. LUT#1 is reset on the following negative edge of the frame valid signal. While LUT#1 is read by Histogram Equalization module, next frame's histogram equalization data is written to LUT#2 by the Cumulative Distribution Calculator module. Writing, reading and resetting processes of these two memories are adjusted as ping-pong buffer memory organization in the designed pipeline.

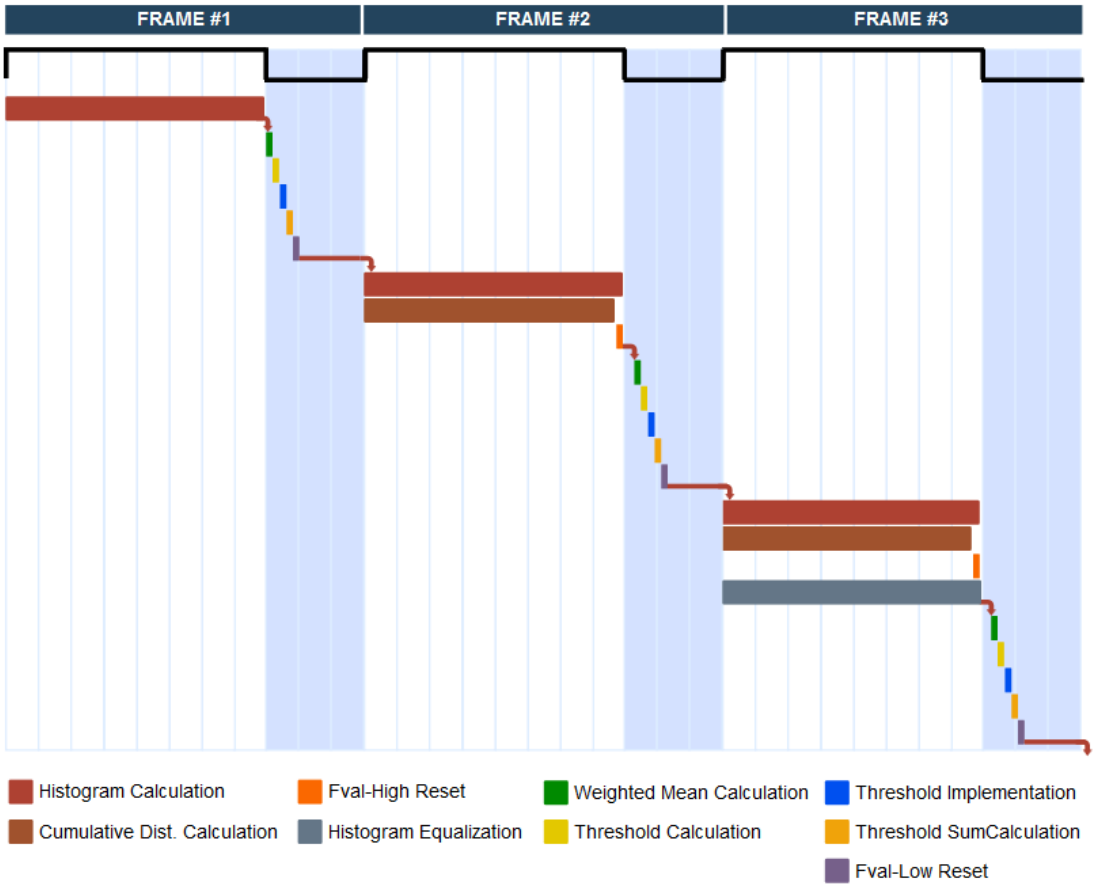

Figure 3.21. Timing requirements and parallel operation of the modules

CHAPTER 4

RESULTS

This chapter gives the results of implementation of the proposed contrast enhancement algorithm. Performance comparison of the implemented firmware includes comparison of output images of the commonly used infrared contrast enhancement algorithms and the proposed algorithm's MATLAB and FPGA implementations. In addition, deviation of gray levels, signal-to-noise ratio and linear blur index of the output images are compared in order to evaluate performance quantitatively .

This chapter organized as follows: Section 4.1 presents the output comparison of the Contrast Stretching, Linear Histogram Equalization, WMSHE, ADPHE, CLAHE and implementations of the proposed WMDPHE method. Section 4.2 discusses the performance of these contrast enhancement methods quantitatively.

4.1. Performance Comparison of the Proposed Algorithm with Investigated Contrast Enhancement Algorithms

Contrast enhancement performances of the Contrast Stretching, Linear Histogram Equalization, Weighting Mean-Separated Sub-Histogram Equalization, Adaptive Double Plateaus Histogram Equalization, Contrast Limited Adaptive Histogram Equalization and proposed Weighting Mean-Separated Double Plateaus Histogram Equalization implementations are compared with using output images in Figure 4.1, Figure 4.3, Figure 4.5 and Figure 4.7. Histograms of the output images are given in Figure 4.2, Figure 4.4, Figure 4.6 and Figure 4.8. MATLAB and FPGA implementation results of Weighting Mean-Separated Double Plateaus Histogram Equalization are used for evaluating the FPGA implementation performance. Outputs of the other investigated methods are generated from MATLAB implementations.

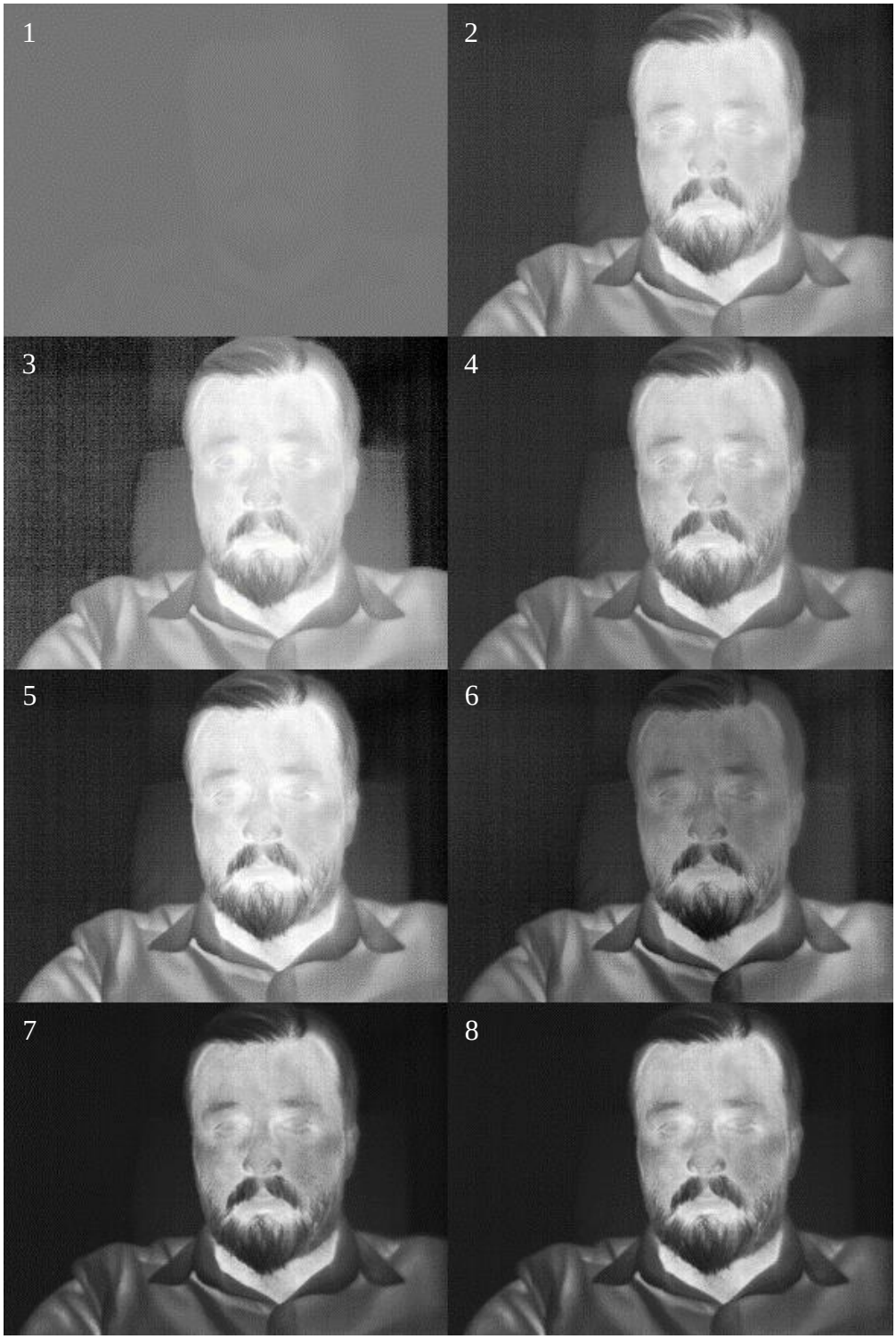

Figure 4.1. Comparison of 1) Raw image, 2) Contrast stretching, 3) Linear HE, 4) WMSHE, 5) ADPHE, 6) CLAHE, 7) MATLAB and 8) FPGA implementation of the proposed method

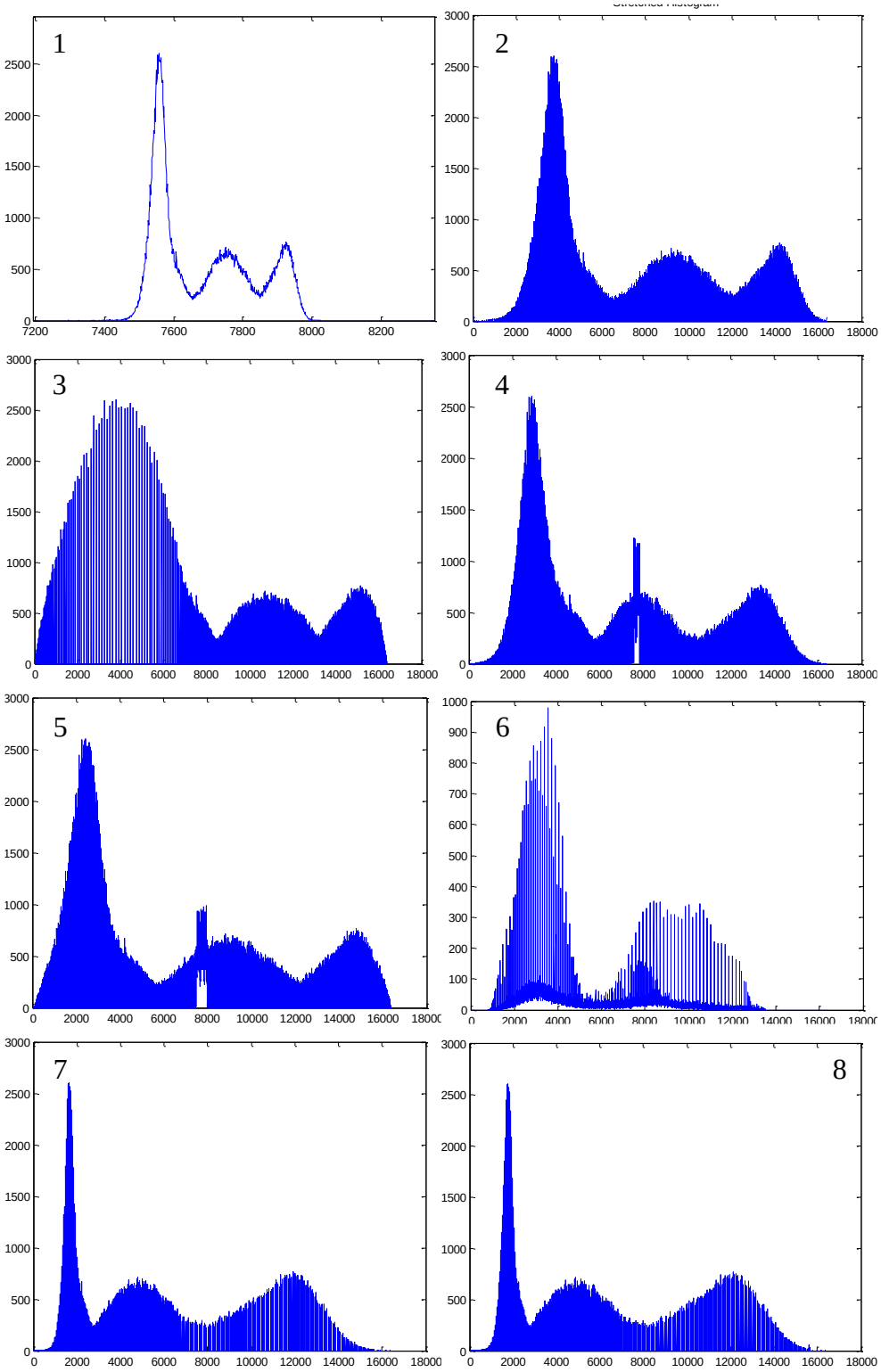

Figure 4.2. Histogram comparison of 1) Raw image (zoomed), 2) Contrast stretching, 3) Linear HE, 4) WMSHE, 5) ADPHE, 6) CLAHE, 7) MATLAB and 8) FPGA implementation of the proposed method

Figure 4.3. Comparison of 1) Raw image, 2) Contrast stretching, 3) Linear HE, 4) WMSHE, 5) ADPHE, 6) CLAHE, 7) MATLAB and 8) FPGA implementation of the proposed method

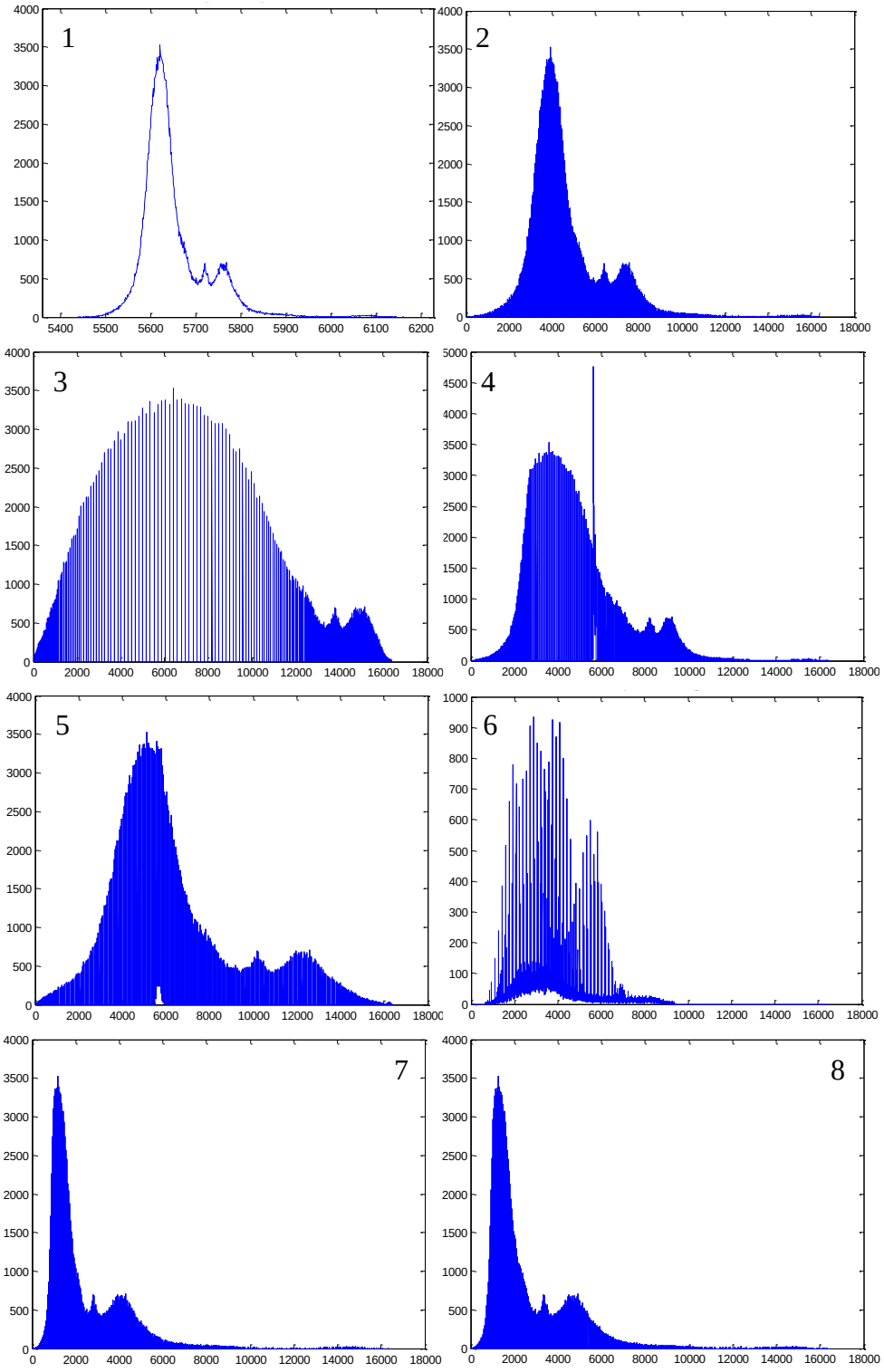

Figure 4.4. Histogram comparison of 1) Raw image (zoomed), 2) Contrast stretching, 3) Linear HE, 4) WMSHE, 5) ADPHE, 6) CLAHE, 7) MATLAB and 8) FPGA implementation of the proposed method

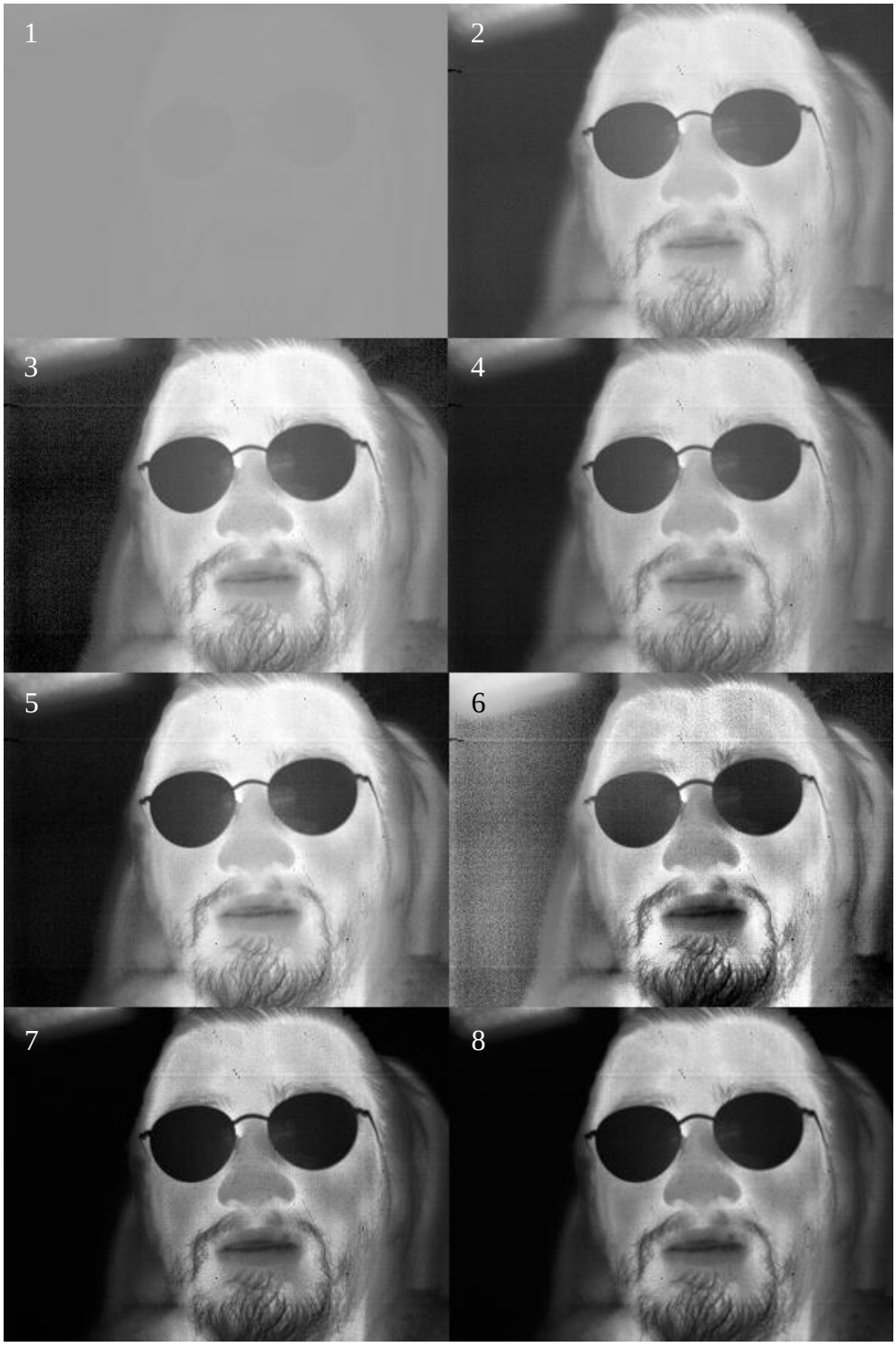

Figure 4.5. Comparison of 1) Raw image, 2) Contrast stretching, 3) Linear HE, 4) WMSHE, 5) ADPHE, 6) CLAHE, 7) MATLAB and 8) FPGA implementation of the proposed method

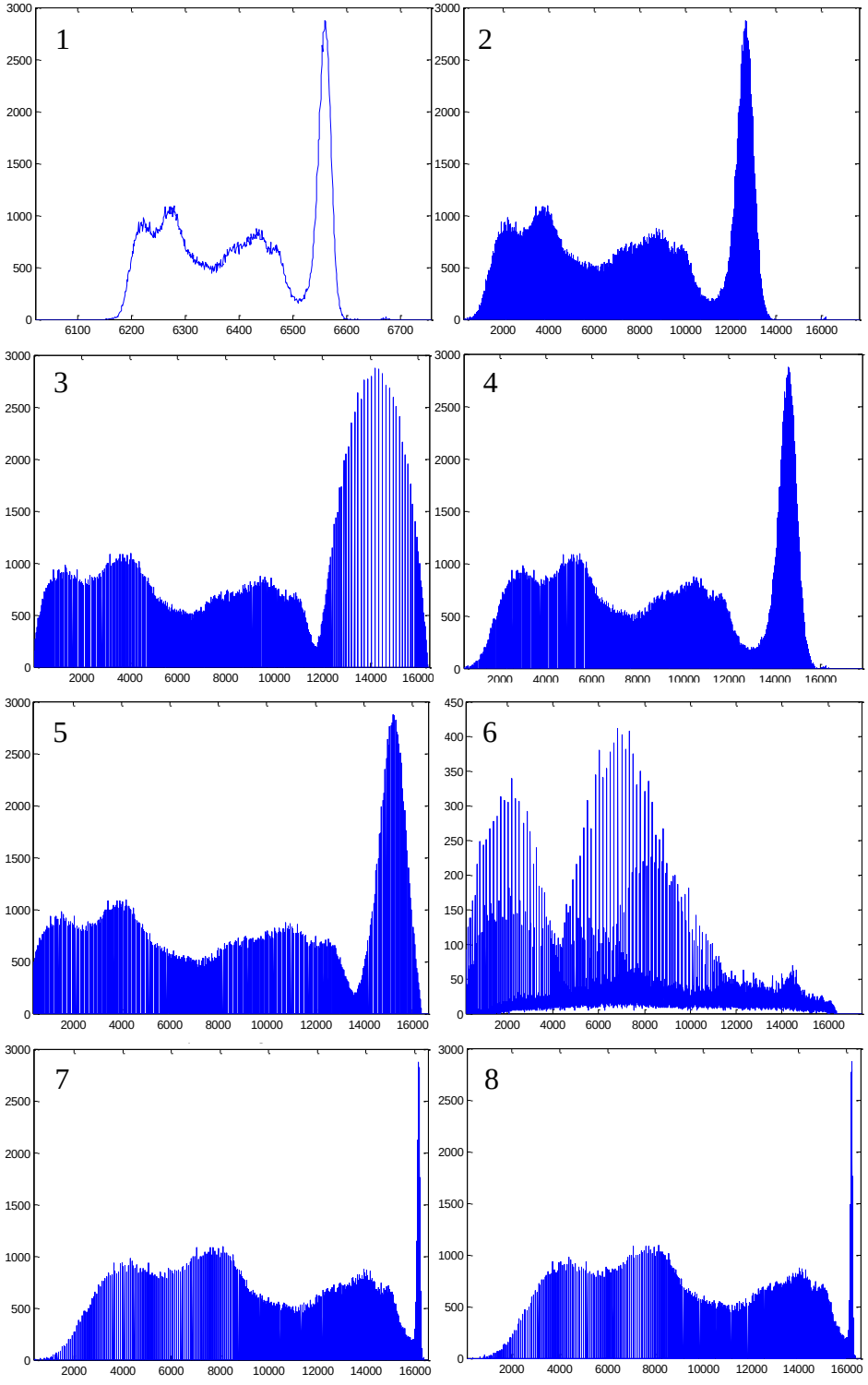

Figure 4.6. Histogram comparison of 1) Raw image (zoomed), 2) Contrast stretching, 3) Linear HE, 4) WMSHE, 5) ADPHE, 6) CLAHE, 7) MATLAB and 8) FPGA implementation of the proposed method

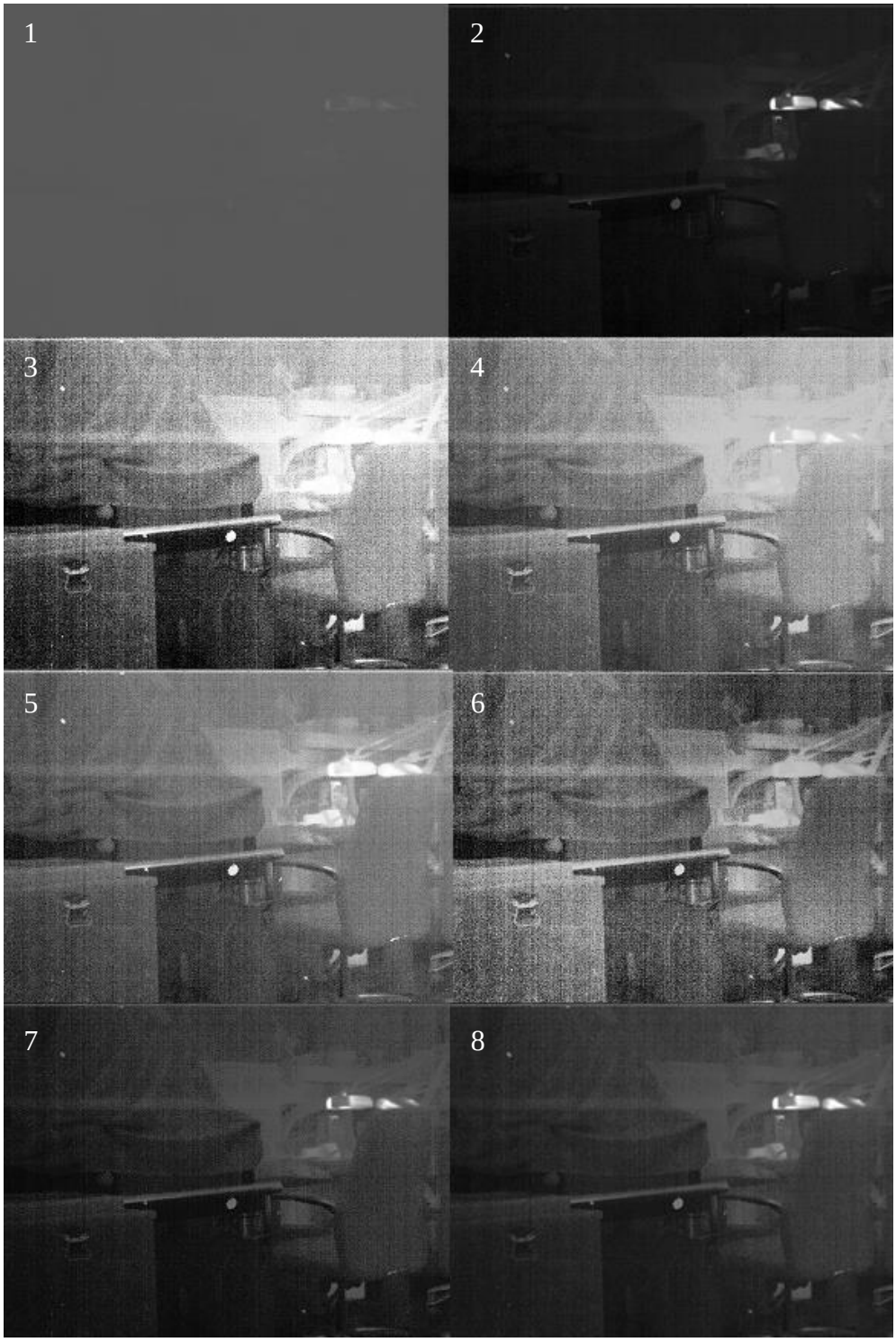

Figure 4.7. Comparison of 1) Raw image, 2) Contrast stretching, 3) Linear HE, 4) WMSHE, 5) ADPHE, 6) CLAHE, 7) MATLAB and 8) FPGA implementation of the proposed method

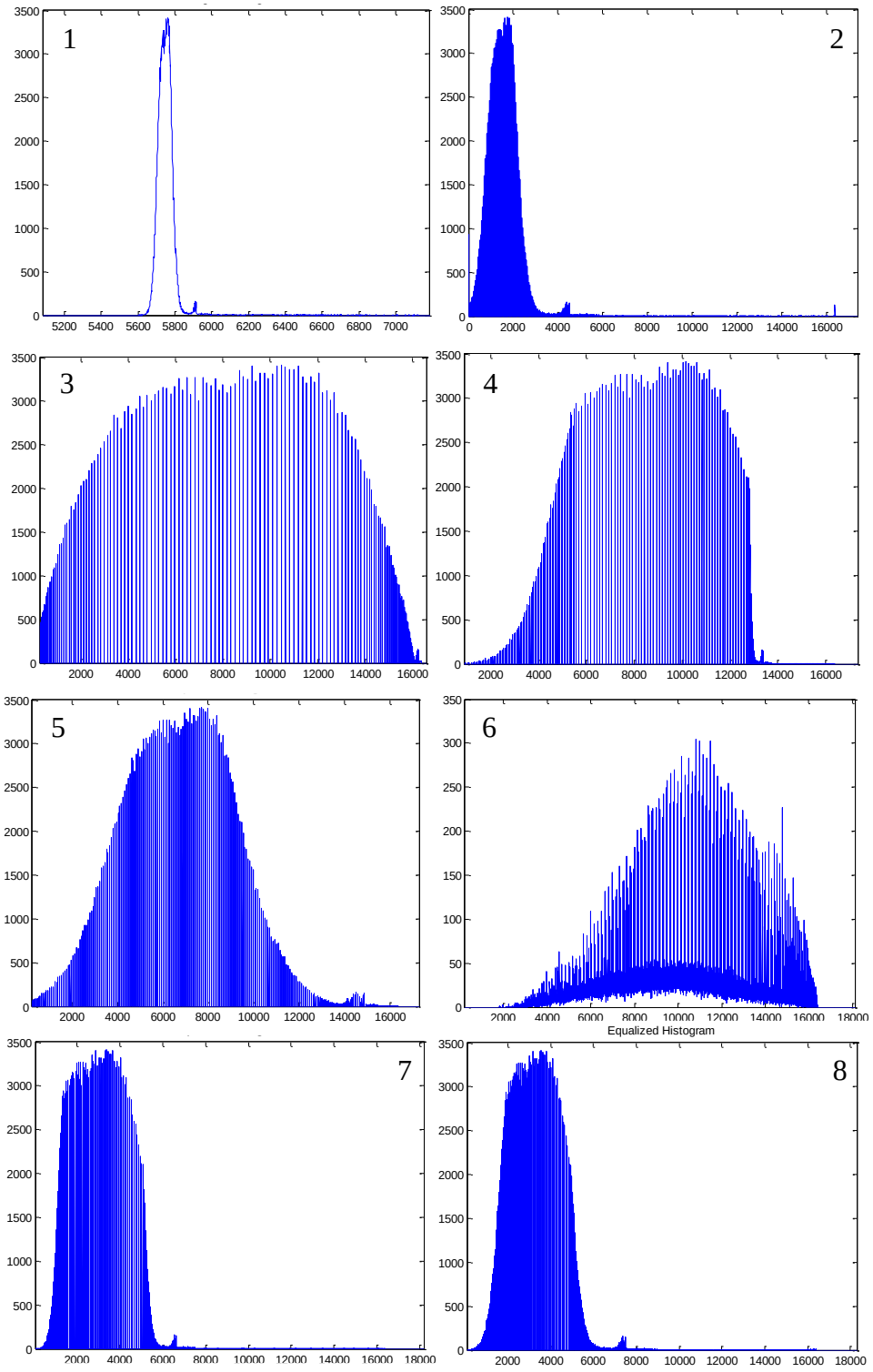

Figure 4.8. Histogram comparison of 1) Raw image (zoomed), 2) Contrast stretching, 3) Linear HE, 4) WMSHE, 5) ADPHE, 6) CLAHE, 7) MATLAB and 8) FPGA implementation of the proposed method

4.2. Quantitative Evaluation of the Contrast Enhancement

Visual comparison of the output images may indicate which method is better in overall, but good enhancement results may also vary from person to person. Therefore, an appropriate quantitative evaluation is required to objectively measure the success of the focusing enhancement type. Standard deviation is a popular evaluation method for the quantifying the dynamic range of the contrast enhanced output images. Liang et al. [19] used a standard deviation based image contrast function for the evaluation of the dynamic range which is proposed by Chang.-Jiang et al. [24] as the following equations

$$C_{contrast} = \frac{1}{m \times n} \sum_{i=0}^{m-1} \sum_{j=0}^{n-1} [g(i,j)]^2 - \left| \frac{1}{m \times n} \sum_{i=0}^{m-1} \sum_{j=0}^{n-1} g(i,j) \right|^2 \quad (4.1)$$

$$C^*_{contrast} = 10 \log_{10} C_{contrast} \quad (4.2)$$

where m is height and n is width of the image, $g(i,j)$ is the intensity level of the pixel at (i,j). Since the dynamic range of the output image can be improved with over-enhancement of the pixels, this approach alone is not enough for the correct evaluation. Appropriate method should measure both the dynamic range and level of excessive contrast enhancement. Signal-to-noise ratio (SNR) is commonly used method for the comparing the enhancement quality. However, this method requires a golden image as a reference for the calculation of the effect of the noise on output image. In practice, this method is inconvenient since there are no golden image for the comparison.

Byeong Hak Kim et al. [25] proposed subtraction signal-to-noise ratio (SSNR) method to find out the amount of amplification of the noise after contrast enhancement. This method calculates mean subtraction signal error (MSSE) with using consecutive images instead of golden image for the calculation of the SNR. MSSE and SSNR values are calculated as

$$MSSE = \frac{1}{m \times n} \sum_{i=0}^{m-1} \sum_{j=0}^{n-1} [I_t(i,j) - I_{t+1}(i,j)]^2 \qquad (4.3)$$

$$SSNR = 10 \log_{10}({G_{dmax}}^2 / MSSE) \quad (4.4)$$

where I_t and I_{t+1} are consecutive images, and G_{dmax} is the maximum gray level of the image. Preventing the amplification of noise may be cause blur in the output image. In order to measure this effect, linear blur index is used [26]. It is defined as

$$p_{ij} = \sin\left[\frac{\pi}{2} \times \left(1 - \frac{g(i,j)}{G_{dmax}}\right)\right] \quad (4.5)$$

$$\gamma(g) = \frac{2}{m \times n} \sum_{i=1}^{m} \sum_{j=1}^{n} min\{p_{ij}, (1 - p_{ij})\} \quad (4.6)$$

Excessive expansion of the dynamic range is often inefficient, as it over-amplifies noise and detailed data as seen in the LHE output images. Therefore, dynamic range evaluation must be done with respect to amplification of noise level. Similarly with dynamic range, as the signal-to-noise ratio of the enhanced image increases, detailed thermal information can be disappeared due to the blur. For this reason, these two parameters must be evaluated with taking linear blur index into account.

Quantitative evaluation of contrast enhancement of the proposed contrast enhancement method is performed in MATLAB with using image contrast function, SSNR and linear blur index values. Figure 4.9 shows the three sets of consecutive input images for the dynamic range, SSNR and linear blur index calculations. Contrast stretching, LHE, WMSHE, ADPHE, CLAHE methods are compared with MATLAB and FPGA implementations of the proposed WMDPHE method. Contrast enhancement outputs of the consecutive images are given in the figures from Figure 4.10 to Figure 4.15.

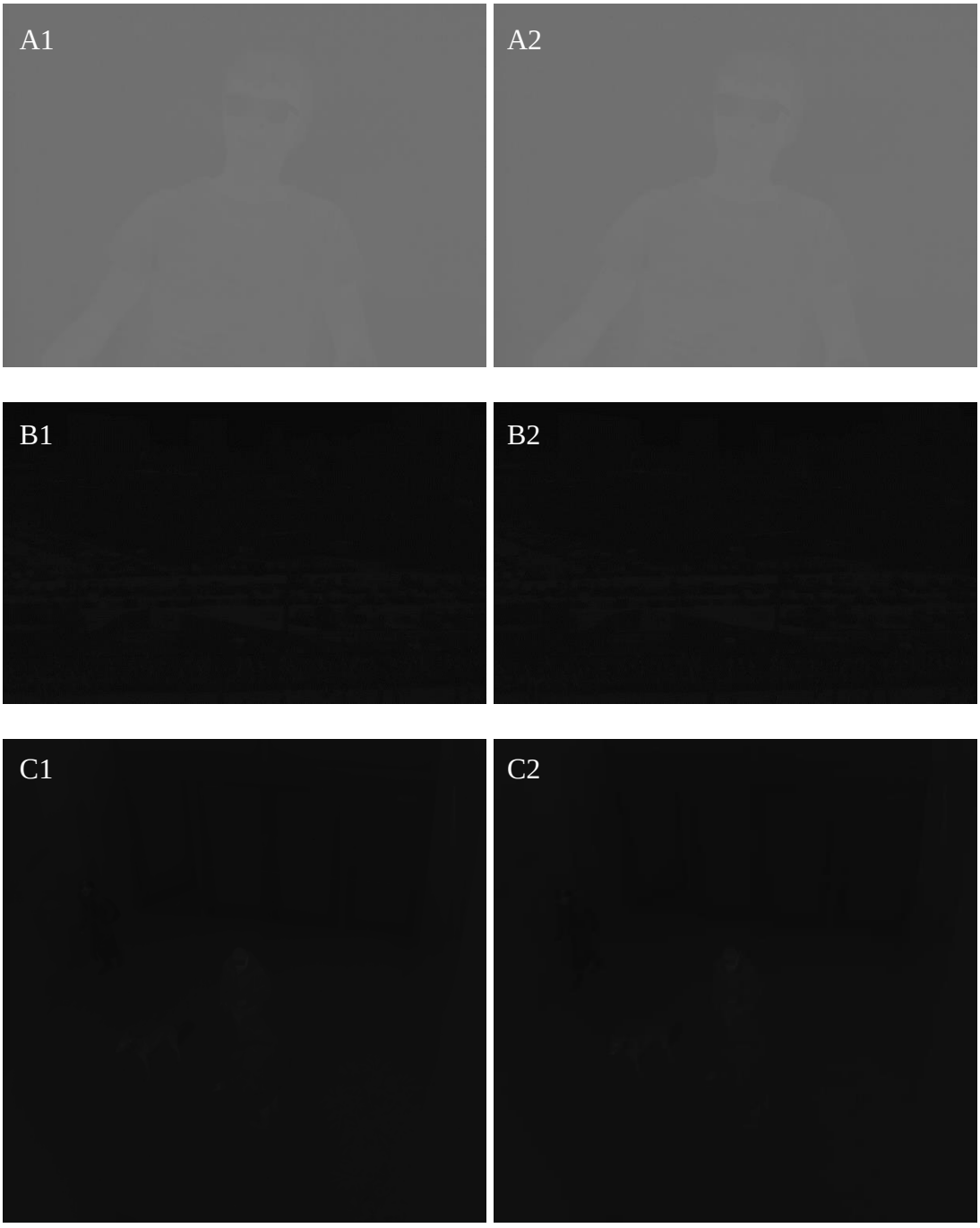

Figure 4.9. Consecutive low-contrast raw images for the quantitative performance evaluation. A1 and A2 are taken from the MT-CORE-F-B6417 LWIR Camera Core. B1, B2, C1 and C2 are taken from BU-TIV Benchmark Dataset [27].

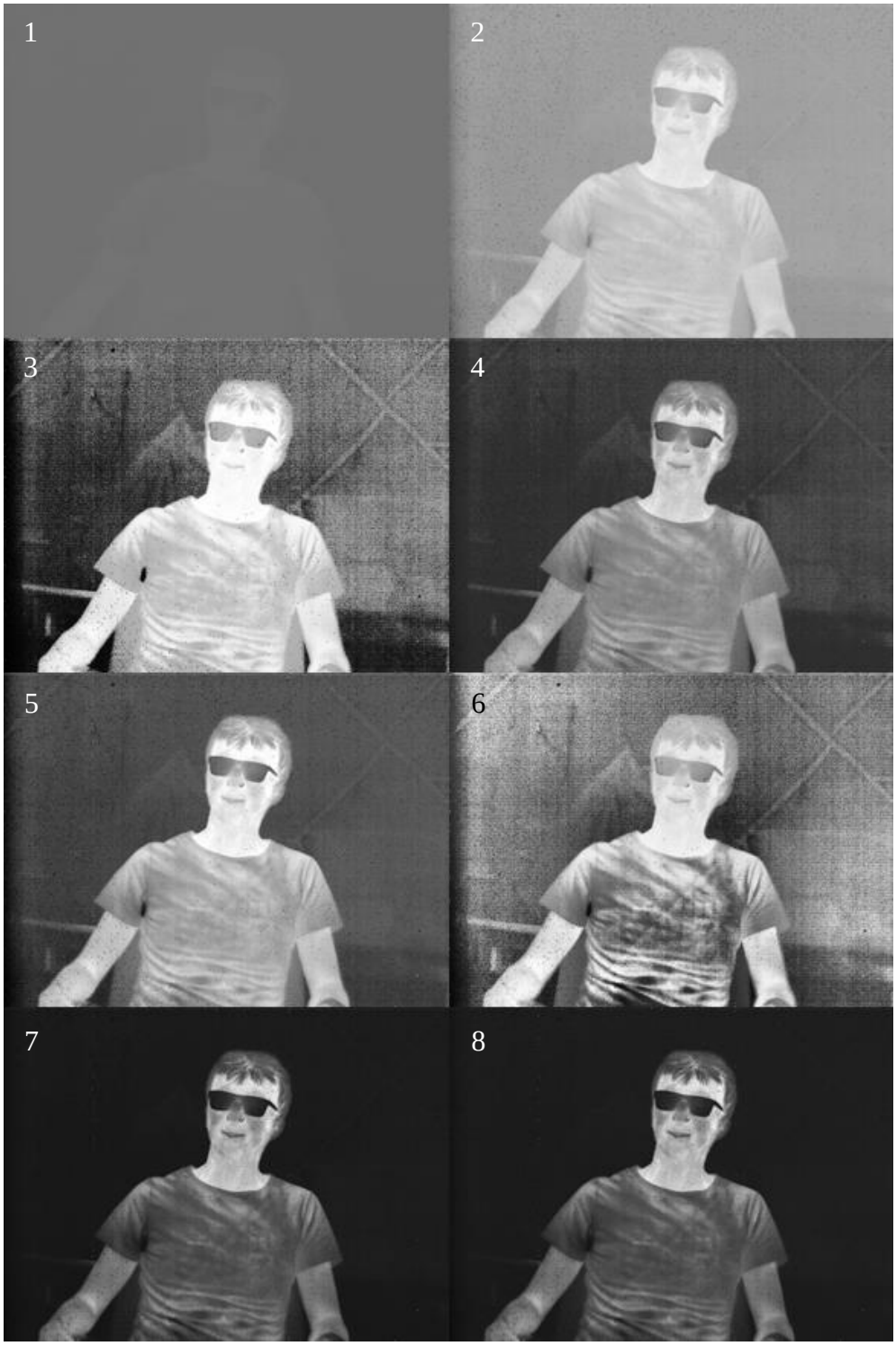

Figure 4.10. Comparison of 1) Raw image A1, 2) Contrast stretching, 3) Linear HE, 4) WMSHE, 5) ADPHE, 6) CLAHE, 7) MATLAB and 8) FPGA implementation of the proposed method

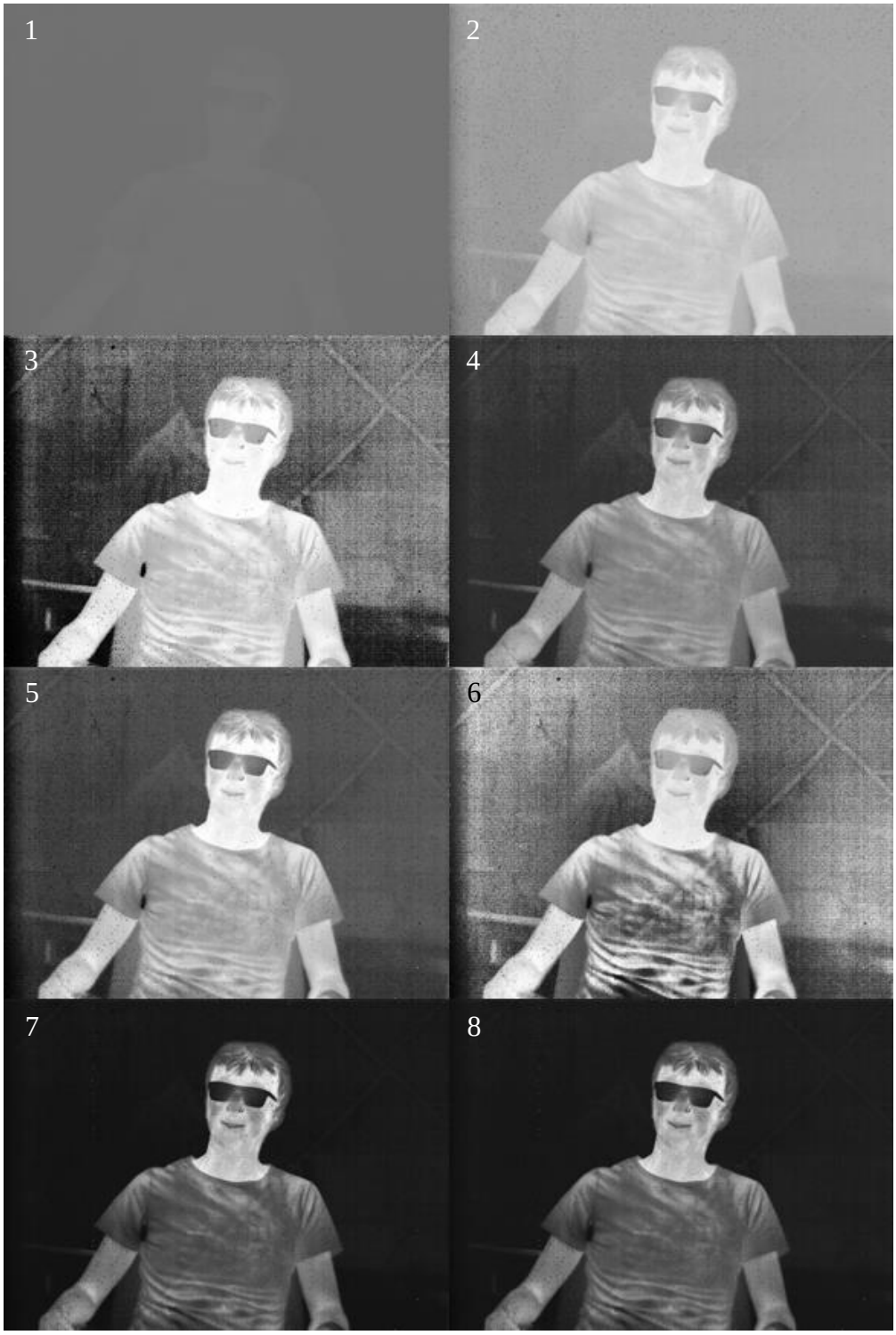

Figure 4.11. Comparison of 1) Raw image A2, 2) Contrast stretching, 3) Linear HE, 4) WMSHE, 5) ADPHE, 6) CLAHE, 7) MATLAB and 8) FPGA implementation of the proposed method

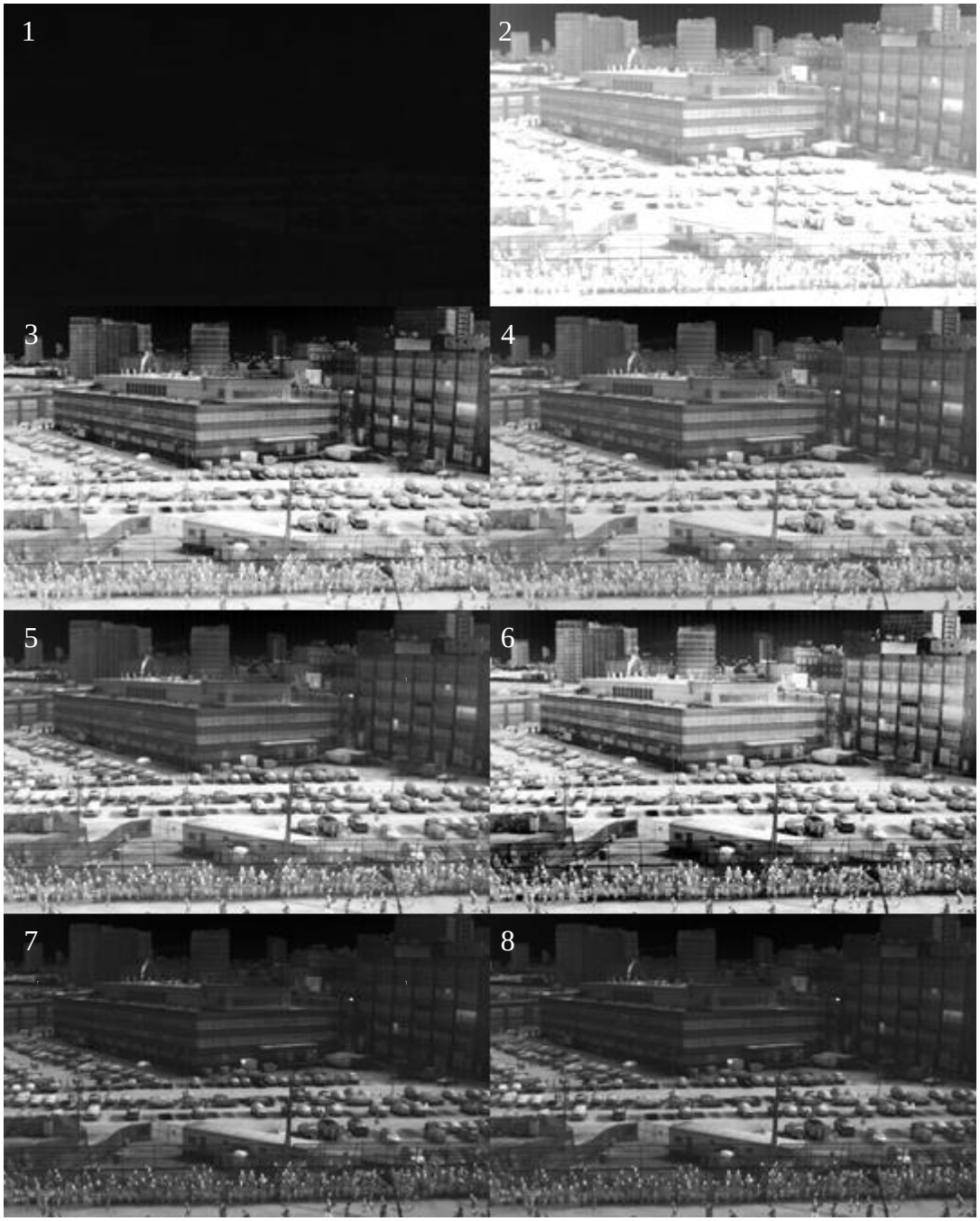

Figure 4.12. Comparison of 1) Raw image B1, 2) Contrast stretching, 3) Linear HE, 4) WMSHE, 5) ADPHE, 6) CLAHE, 7) MATLAB and 8) FPGA implementation of the proposed method

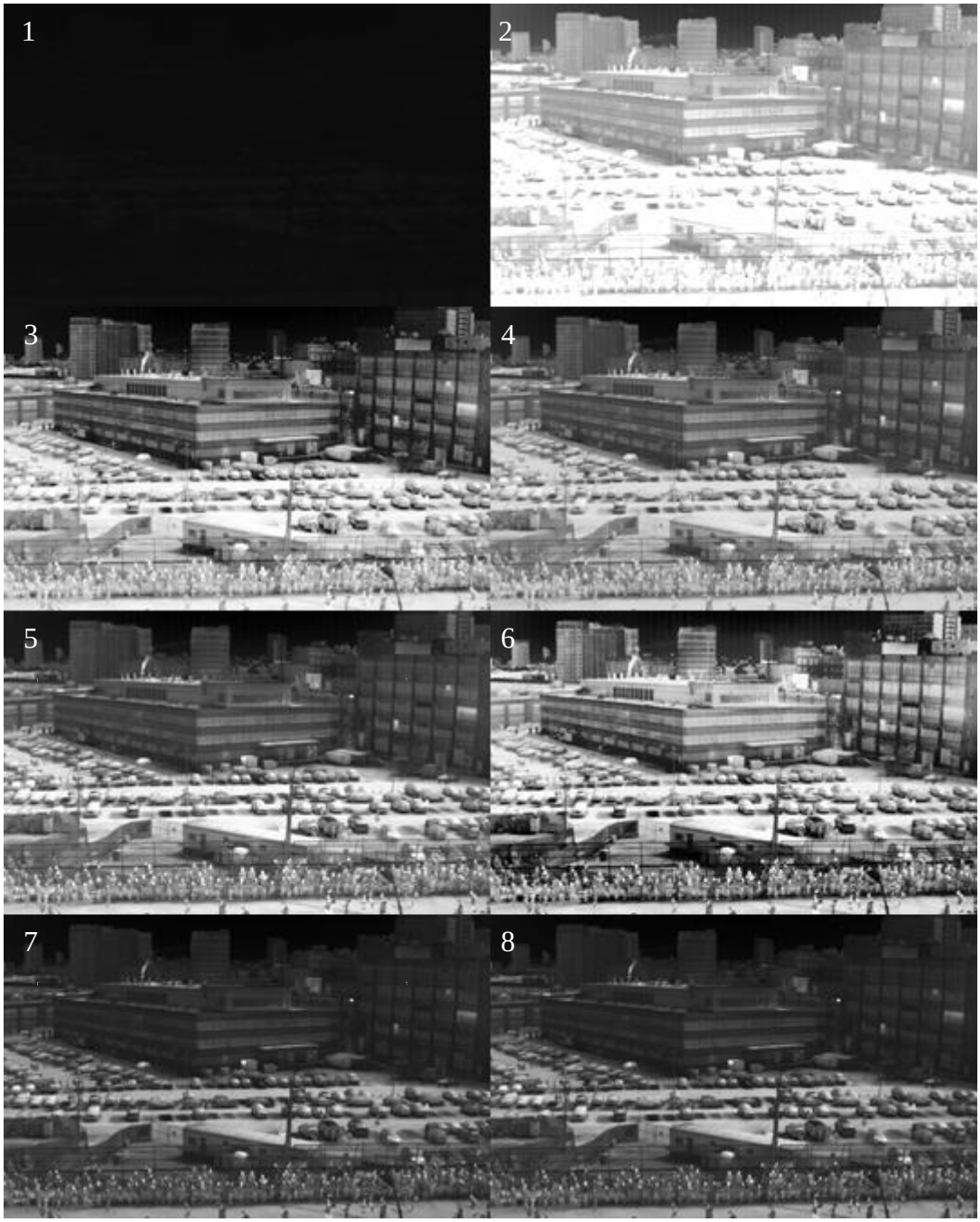

Figure 4.13. Comparison of 1) Raw image B2, 2) Contrast stretching, 3) Linear HE, 4) WMSHE, 5) ADPHE, 6) CLAHE, 7) MATLAB and 8) FPGA implementation of the proposed method

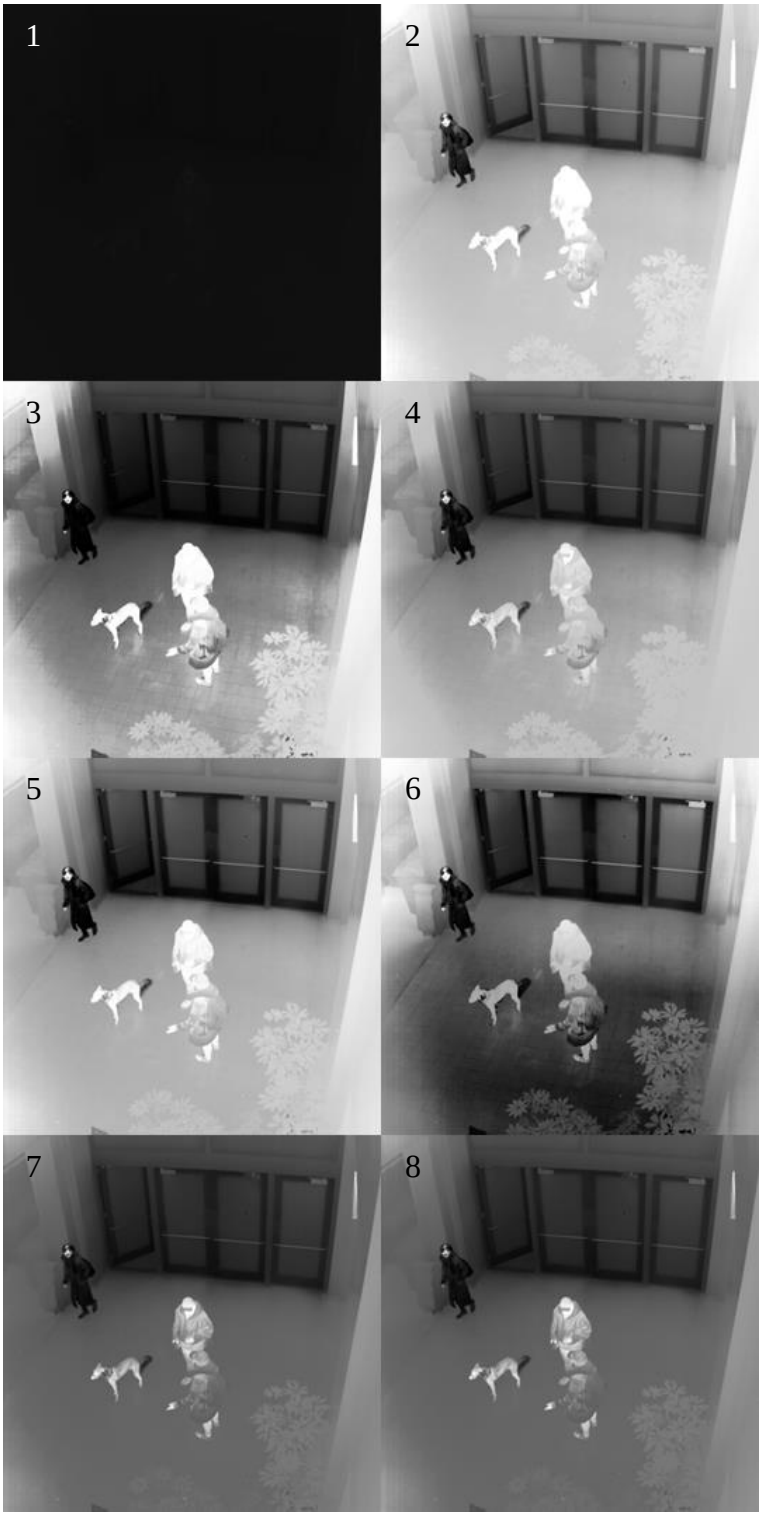

Figure 4.14. Comparison of 1) Raw image C1, 2) Contrast stretching, 3) Linear HE, 4) WMSHE, 5) ADPHE, 6) CLAHE, 7) MATLAB and 8) FPGA implementation of the proposed method

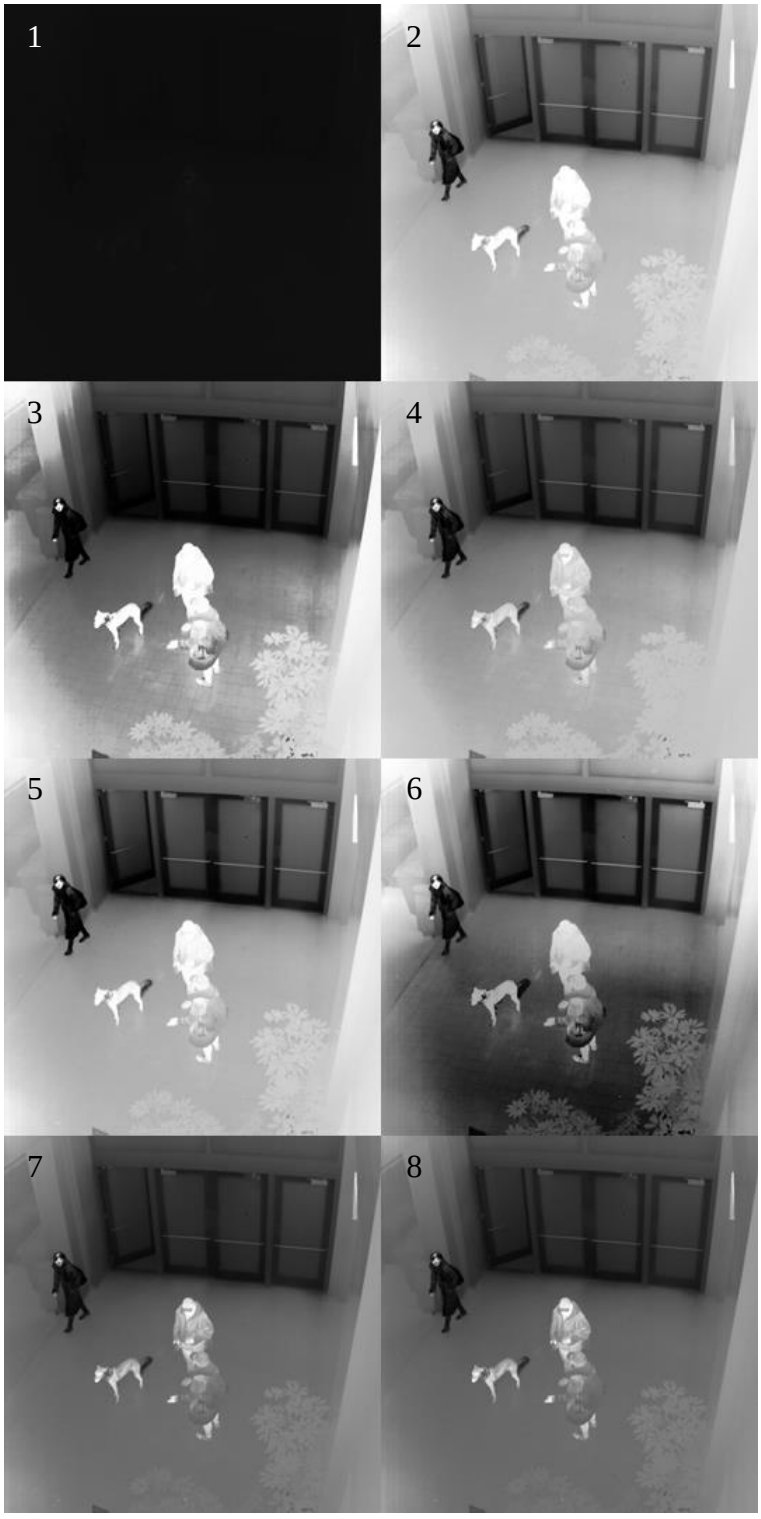

Figure 4.15. Comparison of 1) Raw image C2, 2) Contrast stretching, 3) Linear HE, 4) WMSHE, 5) ADPHE, 6) CLAHE, 7) MATLAB and 8) FPGA implementation of the proposed method

SSNR value represents the number of meaningful pixels over the number of noisy or over-enhanced pixels. Since the consecutive images are used, noise that caused by the imaging system is substantially similar. Background and foreground enhancement levels of the output images can be obtainable since the noisy parts of the consecutive images are subtracted from each other in SSNR calculation. Maximum value of the SSNR results is accepted as the optimal enhancement method in comparing reduction of the gray level over-enhancement.

Linear blur index gives the measurement of blur in the enhanced images. The performance of the enhancement method is better if the linear blur index is small.

As the result of numerical evaluation, the method which obtains the optimum result from these three measurements will be considered as the optimal contrast improvement method among the investigated methods.

Table 4.1. *Comparison of the image contrast parameters for A1 and A2*

Contrast Enhancement Method	Contrast Function of A1 (dB)	Contrast Function of A2 (dB)	SSNR (dB)	Linear Blur Index
Contrast Stretching	152.3314	152.0260	74.0593	0.7872
Histogram Equalization	171.0278	171.0277	56.2868	0.4053
WMSHE	163.2782	163.2736	74.0055	0.3792
ADPHE	165.5348	166.2634	70.4052	0.3832
CLAHE	165.7592	165.7894	56.6046	0.5106
WMDPHE (MATLAB)	161.1143	162.0807	71.5411	0.1355
WMDPHE (Firmware)	160.4952	161.7429	68.1682	0.1354

Table 4.2. *Comparison of the image contrast parameters for B1 and B2*

Contrast Enhancement Method	Contrast Function of B1 (dB)	Contrast Function of B2 (dB)	SSNR (dB)	Linear Blur Index
Contrast Stretching	165.9163	166.5685	71.3180	0.4440
Histogram Equalization	171.0673	171.0673	76.1293	0.4016
WMSHE	167.6757	167.6783	78.3208	0.4332
ADPHE	168.3274	168.3569	74.7631	0.3394
CLAHE	169.6878	169.6904	69.3335	0.4211
WMDPHE (MATLAB)	161.5676	162.0398	71.6899	0.1979
WMDPHE (Firmware)	161.7334	162.6477	71.2328	0.2041

Table 4.3. *Comparison of the image contrast parameters for C1 and C2*

Contrast Enhancement Method	Contrast Function of C1 (dB)	Contrast Function of C2 (dB)	SSNR (dB)	Linear Blur Index
Contrast Stretching	165.3939	165.3844	50.0461	0.5465
Histogram Equalization	171.0620	171.0619	58.4815	0.4008
WMSHE	166.5603	166.5734	59.5134	0.5841
ADPHE	167.0306	167.2829	55.4362	0.6052
CLAHE	167.3268	167.3248	56.1139	0.3456
WMDPHE (MATLAB)	157.2843	158.5042	60.3466	0.3330
WMDPHE (Firmware)	157.2517	157.8636	62.8844	0.3364

Table 4.1, Table 4.2 and Table 4.3 give the results of comparison of the three sets of consecutive output images in terms of dynamic range, over-enhancement and blur levels. In first image set, linear blur index of the proposed method is better than the other methods while keeping SSNR and contrast levels at acceptable levels. Histogram equalization has the higher contrast but since it over-enhances the image, SSNR value of this method is insufficient. WMSHE and ADPHE methods performed well if less attention is paid to the blur effect. For the second image set, similar results are observed with the results of the first image set. This time, histogram equalization and CLAHE performed slightly better in SSNR evaluation. In the third image set, proposed contrast enhancement method has the better performance in linear blur index and SSNR values. On the other hand, the dynamic range enhancement of the proposed method is less than the other methods. CLAHE and WMSHE also exhibited good performance.

According to these results, suitable methods varied among the image characteristics. When the linear blur index levels are compared, proposed WMDPHE method outperformed the other contrast enhancement methods in terms of preserving the detailed thermal information while adjusting the background and foreground intensity levels with preventing the excessive amplification of noise and intensity level saturation. WMSHE, CLAHE and ADPHE methods also achieved good performance in contrast enhancement and proper noise amplification. However, compared to the WMDPHE method, these methods lost more detailed thermal information while improving the dynamic range.

CHAPTER 5

CONCLUSION AND FUTURE WORK

Infrared imaging is used in many applications and infrared imaging systems require some pre-processing operations. These image enhancement requirements may vary with according to area of use. Contrast enhancement is one of the most important pre-processing requirements of the infrared imaging systems. Proper enlargement of the dynamic range affects the output image characteristics. If the visibility of the scene is important, then the correct displaying of the background and foreground temperature can be compromised. On the other hand, if the correct visibility of the temperature is critical, dynamic range and visibility may be reduced due to limited enhancement of the contrast.

In this thesis, a contrast enhancement method is proposed for achieving the proper balance between visibility of the image details and preserving the temperature characteristics of the image. Firstly, widely used contrast enhancement algorithms for infrared and gray scale images are searched and analyzed. Then a contrast enhancement method based on histogram equalization is designed. Proposed contrast enhancement method is derived from ADPHE and WMSHE, which are well known methods for infrared and grayscale histogram equalization. ADPHE algorithm is modified from the WMSHE perspective and threshold or plateau calculation of the ADPHE is rearranged. Investigated and proposed methods are implemented in MATLAB to compare their performance. Since the FPGA implementation will be used in an imaging system, coding of the MATLAB prototype is done similar to digital designing structure with using HDL. Secondly, firmware architecture of the proposed method is designed and FPGA implementation is performed with using Verilog HDL on Xilinx Vivado Design Suite. Functional and post-implementation timing simulations are performed with using various low-contrast thermal test images for

evaluating the contrast enhancement performance and testing the real-time image processing pipeline. Implementation of the proposed algorithm is integrated into a FPGA-based infrared imaging system and real-time contrast enhancement is achieved with desired performance. XC7A100T-1CSG324C FPGA from the Xilinx Artix-7 family is used in the infrared imaging system due to its low-cost and high performance-per-watt advantages. FPGA resource utilization of implementation of the proposed algorithm is shown in Table 5.1. Note that, the selected FPGA is used for not only the contrast enhancement, but also for receiving and transmitting the image data, communicating with the ROIC and operating offset and gain corrections. Therefore, size of the FPGA is selected by considering these operations.

Table 5.1. *Utilization of FPGA resources after the implementation*

Resource	*Utilization*	*Available*	*Utilization %*
LUT	6485	63400	10.23
LUTRAM	17	19000	0.09
FF	12581	126800	9.92
BRAM	34.50	135	25.56
DSP	7	240	2.92
IO	40	210	19.05
BUFG	4	32	12.50
MMCM	1	6	16.67

FPGA implementation is designed with the arithmetic modules that are using fixed-point operations for simplicity and reducing the logic resource utilization. Output images of the FPGA implementation has negligible intensity level differences comparing with MATLAB prototype, since the latter can perform floating point operations. This can be solved in the firmware with replacing fixed-point operations with floating point operations.

Calculation of the raw image statistics and histogram equalization operations are designed to require minimal memory usage. Memory addressing and arbitration of the memory usage by the modules are also adjusted for the proper real-time operation. Contrast enhanced output frame is transmitted with two frame latency since there is no frame buffer used in the design. External memory can be used for preventing this latency, but since it is a real-time operation, high-speed external memory is required and this may be a problem for low-cost imaging systems.

Memory and data bus organizations are implemented as parametrically with according to the input image resolution from the infrared detector. These parameters can also be adjusted for resolutions except the VGA resolution and real-time contrast enhancement can be achieved for the other detectors with higher or lower resolutions.

Contrast enhancement is performed by using histogram statistics in the proposed method. Spatial methods, tile separation and neighborhood properties can also be used for obtaining the thermal characteristics and enhancing the contrast of infrared images.

Temperature accuracy of the contrast enhanced output images by the proposed method can be analyzed with controlled infrared radiation source like blackbody. Calibration mechanisms can be added to the firmware for achieving more accurate temperature representation in the output image with providing a higher dynamic range.

Proposed contrast enhancement algorithm is essentially designed for enhancing the low-contrast raw LWIR images. On the other hand, test result of the proposed algorithm on SWIR image looks promising and can be also used in SWIR imaging systems with some modifications to the algorithm if necessary. Figure 5.1 shows the low-contrast raw SWIR image and contrast enhancement result of it.

In conclusion, the FPGA implementation and test results show that the proposed contrast enhancement algorithm is capable and applicable to be used in FPGA-based real-time infrared imaging systems for adaptively improving the dynamic range of the low-contrast frames.

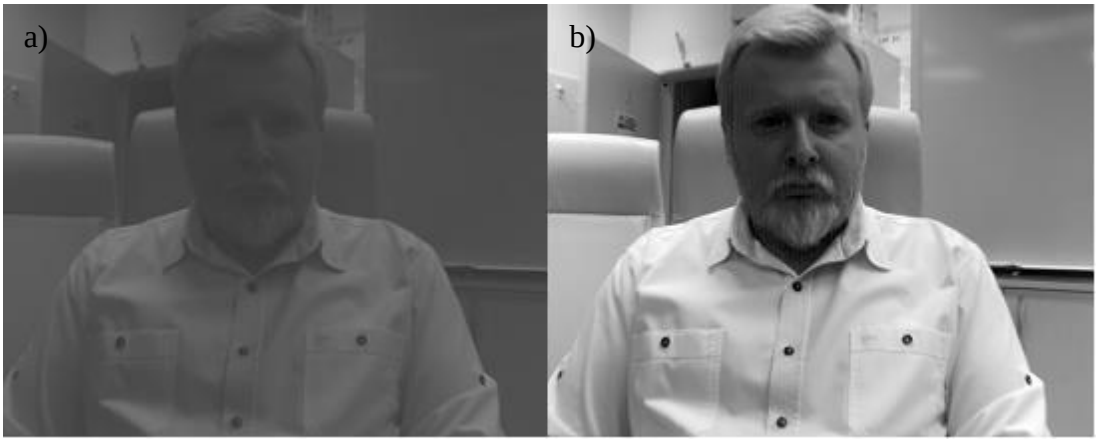

Figure 5.1. a) Low-contrast SWIR image b) Contrast enhanced image with the proposed method

REFERENCES

[1] Ibarra-Castanedo, Clemente. (2005). Quantitative subsurface defect evaluation by pulsed phase thermography: depth retrieval with the phase [ressource électronique]

[2] A. A. Richards, "Infrared and Ultraviolet: The Edges of the Rainbow," *Alien Vis. Explor. Electromagn. Spectr. with Imaging Technol. Second Ed.*, pp. 1–40, 2011.

[3] FLIR and ITC, "Thermal imaging guidebook for industrial applications," *FLIR Syst.*, p. 48, 2011.

[4] A. Rogalski, "Infrared detectors: An overview," *Infrared Physics and Technology*. 2002.

[5] Bhan, R & Saxena, Raghvendra & Jalwania, C.R. & Lomash, S.K.. (2009). Uncooled Infrared Microbolometer Arrays and their Characterisation Techniques. Defence Science Journal. 59. 580. 10.14429/dsj.59.1562.

[6] D. S. Tezcan, S. Eminoğlu, and T. Akın, "A Low Cost Uncooled Infrared Microbolometer Detector in Standard CMOS Technology," IEEE Transactions on Electron Devices, Vol. 50, No. 2, pp. 494-502, 2003.

[7] E. Alpman, "Development of Low-Cost Uncooled Infrared Detector Arrays in Standard CMOS and SOI-CMOS Processes," M.S. Thesis, Department of Electrical and Electronics Engineering, Middle East Technical University, 2005.

[8] K. S. Demirci, "A Low-Cost 16x16 Uncooled Infrared Detector FPA Using Standard CMOS and Wafer Level MEMS Processes," M.S. Thesis, Department of Electrical and Electronics Engineering, Middle East Technical University, 2005.

[9] D. S. Tezcan, S. Eminoğlu, O. Akar, and T. Akın, "An Uncooled Microbolometer Infrared Focal Plane Array in Standard CMOS," Proceedings of SPIE, Vol. 4288, pp. 112-121, 2001.

[10] S. Eminoğlu, M. Y. Tanrıkulu, and T. Akın, “Low-Cost 64x64 Uncooled Infrared Detector Arrays in Standard CMOS,” The 12th Int. Conf. on Solid-State Sensors and Actuators (TRANSDUCERS’03), pp. 316-319, 2003.

[11] S. Eminoğlu, “Uncooled Infrared Focal Plane Arrays with Integrated Readout Circuitry Using MEMS and Standard CMOS Technologies,” Ph. D. Dissertation, Department of Electrical and Electronics Engineering, Middle East Technical University, 2003.

[12] S. Eminoğlu, M. Y. Tanrıkulu, and T. Akın, “Low-Cost Uncooled Infrared Detector Arrays in Standard CMOS,” Proceedings of SPIE, Vol. 5074, pp. 425-436, 2003.

[13] Rodriguez-Andina, J.J. & de la Torre, E & Valdés, María. (2017). FPGAs: Fundamentals, advanced features, and applications in Industrial Electronics. 10.1201/9781315162133.

[14] P. M. Arabi, G. Joshi, T. Bhat, and H. L. Singh, “Identifying suitable enhancement technique for thermal and non-thermal diabetic foot images,” pp. 335–338.

[15] Narasimhan, S.G. & Nayar, S.K.. (2003). Contrast restoration of weather degraded images. Pattern Analysis and Machine Intelligence, IEEE Transactions on. 25. 713- 724. 10.1109/TPAMI.2003.1201821.

[16] Virgil E. Vickers "Plateau equalization algorithm for real-time display of high-quality infrared imagery," Optical Engineering 35(7), (1 July 1996). https://doi.org/10.1117/1.601006

[17] B. J. Wang, S. Q. Liu, Q. Li, and H. X. Zhou, “A real-time contrast enhancement algorithm for infrared images based on plateau histogram,” *Infrared Phys. Technol.*, 2006.

[18] R. Lai, Y. T. Yang, B. J. Wang, and H. X. Zhou, “A quantitative measure based infrared image enhancement algorithm using plateau histogram,” *Opt. Commun.*, vol. 283, no. 21, pp. 4283–4288, 2010.

[19] K. Liang, Y. Ma, Y. Xie, B. Zhou, and R. Wang, “A new adaptive contrast enhancement algorithm for infrared images based on double plateaus histogram equalization,” *Infrared Phys. Technol.*, vol. 55, pp. 309–315, 2012.

[20] P. C. Wu, F. C. Cheng, and Y. K. Chen, “A weighting mean-separated sub-histogram equalization for contrast enhancement,” in *2010 International Conference on Biomedical Engineering and Computer Science, ICBECS 2010*, 2010.

[21] S. A. Hariprasad, A. K. S, and V. Ahmed, “Novel Weighted Mean Separated Histogram Equalization for Contrast Enhancement of Underwater Images,” *Int. J. Sci. Eng. Res.*, vol. 4, no. 12, 2013.

[22] A. Rogalski, "Next decade in infrared detectors," Proc. SPIE 10433, Electro-Optical and Infrared Systems: Technology and Applications XIV, 104330L (9 October 2017); doi: 10.1117/12.2300779

[23] V. Schatz, “Low-latency histogram equalization for infrared image sequences: A hardware implementation,” *J. Real-Time Image Process.*, vol. 8, no. 2, pp. 193–206, 2013.

[24] Chang.-Jiang. Zhang, Fu. Meng-Yin, Mei. Jin, Qi-Hong Zhang, Approach to enhance contrast of infrared image based on wavelet transform, Journal of Infrared and Millimeter Waves 23 (2) (2004) 119–124.

[25] B. H. Kim, M. Y. Kim, and Y. S. Chae, “Background registration-based adaptive noise filtering of LWIR/MWIR imaging sensors for UAV applications,” *Sensors (Switzerland)*, vol. 18, no. 1, 2018.

[26] Bai, X. Morphological infrared image enhancement based on multi-scale sequential toggle operator using opening and closing as primitives. Infrared Phys. Technol. 2015, 68, 143–151.

[27] Zheng Wu, Nathan Fuller, Diane Theriault, Margrit Betke, "A Thermal Infrared Video Benchmark for Visual Analysis", in Proceeding of 10th IEEE Workshop on Perception Beyond the Visible Spectrum (PBVS), Columbus, Ohio, USA, 2014.